

Quantum Geometric Origin of the Intrinsic Nonlinear Hall Effect

Yannis Ulrich,^{1,2,*} Johannes Mitscherling,³ Laura Classen,^{1,4} and Andreas P. Schnyder¹

¹Max Planck Institute for Solid State Research, D-70569 Stuttgart, Germany

²Department of Physics, Technical University of Munich, D-85748 Garching, Germany

³Max Planck Institute for the Physics of Complex Systems, Nöthnitzer Strasse 38, D-01187 Dresden, Germany

⁴School of Natural Sciences, Technische Universität München, 85748 Garching, Germany

(Dated: June 24, 2025)

We analyze the quantum geometric contribution to the intrinsic second-order nonlinear Hall effect (NLHE) for a general multiband Hamiltonian. The nonlinear conductivity, obtained in Green's function formalism, is decomposed into its quantum geometric constituents using a projector-based approach. In addition to the previously identified Berry curvature and interband quantum metric dipoles, we obtain a third term of quantum geometric origin, given by the momentum derivative of the *intra*band quantum metric. This contribution, which we term the intraband quantum metric dipole, provides substantial corrections to the NLHE in topological magnets and becomes the dominant geometric term in topological antiferromagnets with gapped Dirac cones. Considering generalized 2D and 3D Weyl/Dirac Hamiltonians, describing a large class of topological band crossings with sizable quantum geometry, we derive analytical expressions of the NLHE, thereby revealing the individual contributions of the three quantum geometric terms. Combined with an exhaustive symmetry classification of all magnetic space groups, this analysis leads to the identification of several candidate materials expected to exhibit large intrinsic NLHE, including the antiferromagnets Yb_3Pt_4 , CuMnAs , and CoNb_3S_6 , as well as the nodal-plane material MnNb_3S_6 . Finally, our projector-based approach yields a compact expression for the NLHE in terms of momentum derivatives of the Bloch Hamiltonian matrix alone, enabling efficient numerical evaluation of each contribution in the aforementioned materials.

Introduction.— Quantum geometry, such as the Berry curvature and the quantum metric, has become an essential tool for understanding wave-function properties of materials and relating them to physical responses [1–4]. While the Berry curvature, whose integral is the Chern number, describes intrinsic linear Hall effects, the quantum metric is intimately connected to nonlinear responses, such as second-harmonic generation, bulk photovoltaic effects, and the nonlinear Hall effect [5–35]. In strongly correlated systems, on the other hand, quantum geometry can guarantee finite superfluidity [36] and stabilize fractional Chern insulators [37].

For the linear Hall effect, the Berry curvature provides a direct link between the band topology of a material and the magnitude of the Hall effect. For example, in a Weyl semimetal with just two Weyl points, the linear Hall current is proportional to the momentum-space distance between the two Weyl points, which are sources and sinks of Berry flux [38, 39]. In general, a topological material has a large network of (near) band degeneracies generating large Berry curvature [40], consisting of Weyl points, Berry curvature hotspots [41, 42] and possibly nodal planes [43–45]. From the knowledge of this network of band topologies, one can infer the size of the linear Hall current. This connection has given us a deeper understanding of the intrinsic linear Hall effect and guided the design of new materials with large intrinsic anomalous Hall responses [46].

While the relationship between band geometry and Hall response is straightforward and well-established in the linear regime, it is more involved and remains largely unexplored in the nonlinear regime. Since nonlinear responses include further virtual interband transitions, they are promising can-

didates for originating from more diverse quantum geometric invariants than just the Berry curvature [6, 47, 48]. All of these additional geometrical quantities, just like the Berry curvature, are, in general, large near (gapped) topological band crossings, where the character of the wave functions changes rapidly in momentum space. To establish the precise connection between band geometry and nonlinear Hall responses, one must derive the respective contributions for the different types of band crossings. A systematic quantum geometric decomposition of nonlinear responses has become theoretically tractable only recently within a fully gauge-invariant band projector formalism [6, 48–54].

In this work, we perform a rigorous quantum geometrical decomposition of the second-order nonlinear Hall effect (NLHE). We find that the NLHE originates from *three* distinct quantum geometrical terms: the Berry curvature dipole (BCD) and the interband quantum-metric dipole (interQMD), which have previously been discussed [55, 56], and in addition an intraband term proportional to the momentum-space derivative of the quantum metric. This third term, which we refer to as the “intraband quantum metric dipole” (intraQMD), is particularly large for topological antiferromagnets and magnetic nodal-plane materials. Moreover, it is the only quantum geometric contribution to the NLHE for antiferromagnets with threefold rotation symmetry \mathcal{C}_3 .

We present the various geometric contributions to the NLHE in the unifying projector framework [48], which allows for a straightforward numerical implementation and encompasses both non-degenerate and degenerate bands. We present closed analytic formulas for the most common types of topological band crossings, namely (gapped) Dirac/Weyl points, nodal lines, and nodal planes, thereby revealing the relevance of the three quantum geometric terms. By combining the analytical results with a comprehensive symmetry analysis for

* y.ulrich@fkf.mpg.de

all magnetic space groups (MSG), we obtain stringent search and design criteria for materials with large intrinsic NLHE. To facilitate numerical evaluation for systems with multiple bands, we provide formulas entirely in terms of derivatives of the Bloch Hamiltonian. Our results reveal and clarify the complex quantum geometric origin of the NLHE, and set the stage for a systematic exploration of the rich structure of DC nonlinear responses.

Quantum geometric expansion of the NLHE.— We start by calculating the second-order DC conductivity tensor, relating the nonlinear response of the current density to the electric fields via $j^a = \sum_{b,c} \sigma^{a;bc} E^b E^c$, with spatial indices a, b, c , for a general quadratic Hamiltonian

$$\hat{H} = \sum_{\alpha,\beta} \hat{c}_\alpha^\dagger(\mathbf{k}) H_{\alpha\beta}(\mathbf{k}) \hat{c}_\beta(\mathbf{k}). \quad (1)$$

The Hamiltonian defines the Bloch Hamiltonian matrix $\hat{H}(\mathbf{k}) = (H_{\alpha\beta}(\mathbf{k}))$ given in the “orbital” basis, which may include spin, atomic orbitals, sublattice, or other degrees of freedom within the unit cell, with corresponding creation operators for fixed lattice momentum denoted by $\hat{c}_\alpha^\dagger(\mathbf{k})$. Using Green’s function formalism, the nonlinear DC conductivity of such a non-interacting system is given by [57–59]

$$\begin{aligned} \sigma^{a;bc} = & -\frac{e^3}{\hbar} \int_{\text{BZ}} \frac{d^d \mathbf{k}}{(2\pi)^d} \int_{-\infty}^{\infty} d\epsilon \frac{\partial f(\epsilon)}{\partial \epsilon} \\ & \times \text{Re tr} \left[\hat{A}(\epsilon, \mathbf{k}) \hat{H}^a(\mathbf{k}) \frac{\partial \hat{G}^R(\epsilon, \mathbf{k})}{\partial \epsilon} \right. \\ & \left. \times \left(\hat{H}^b(\mathbf{k}) \hat{G}^R(\epsilon, \mathbf{k}) \hat{H}^c(\mathbf{k}) + \frac{1}{2} \hat{H}^{bc}(\mathbf{k}) + (b \leftrightarrow c) \right) \right], \end{aligned} \quad (2)$$

involving momentum derivatives $\hat{H}^a(\mathbf{k}) = \partial_{k^a} \hat{H}(\mathbf{k})$ and $\hat{H}^{ab}(\mathbf{k}) = \partial_{k^a} \partial_{k^b} \hat{H}(\mathbf{k})$ of the Bloch Hamiltonian, the retarded Green’s function $\hat{G}^R(\epsilon, \mathbf{k}) = [\epsilon + \mu - \hat{H}(\mathbf{k}) + i\Gamma]^{-1}$ with chemical potential μ , the Fermi function distribution $f(\epsilon)$ at temperature T , and the spectral function $\hat{A}(\epsilon, \mathbf{k}) = -\pi \text{Im} \hat{G}^R(\epsilon, \mathbf{k})$. We introduce a finite, constant phenomenological relaxation rate $\Gamma > 0$, related to the lifetime by $\tau = 1/2\Gamma$, a common approximation in the literature [60–65]. Such a scattering rate can, e.g., be derived microscopically in a self-consistent Born approximation that includes the effects of white-noise disorder [66, 67], and is necessary for ensuring a finite conductivity in the DC limit. The scattering rate is treated as band-independent. Further discussion of this approximation and its limitations is provided in the Supplemental Material (SM) [57].

The matrices within the trace in Eq. (2) generally do not commute, reflecting the nontrivial multiband nature of the system, which we characterize in terms of quantum geometry. In the following, we focus on $\sigma^{a;bb}$, which is most relevant for experiments, while the more general case $b \neq c$ is treated in the SM [57]. To reveal the relevant quantum geometric invariants for $\sigma^{a;bb}$, we diagonalize the Bloch Hamiltonian matrix, yielding

$$\hat{H}(\mathbf{k}) = \sum_{n \in \text{bands}} E_n(\mathbf{k}) \hat{P}_n(\mathbf{k}), \quad (3)$$

with dispersion $E_n(\mathbf{k})$ and orthogonal projector $\hat{P}_n(\mathbf{k})$ onto the (non-)degenerate bands. Importantly, all subsequent quantities, expressed in projectors, are immediately gauge-invariant. The nontrivial geometry arises from virtual interband transitions due to the coupling to the electric field. This can be seen by performing a “quantum geometric expansion” of $\sigma^{a;bb}$ after inserting Eq. (3) into Eq. (2). In this expansion, we separate band-dependent quantities from quantum geometric invariants—traces over projectors and their derivatives. We use $\hat{P}_n(\mathbf{k}) \partial^a \hat{H}(\mathbf{k}) \hat{P}_m(\mathbf{k}) = \delta_{nm} v_n^a(\mathbf{k}) \hat{P}_n(\mathbf{k}) + i \epsilon_{nm}(\mathbf{k}) \hat{e}_{nm}^a(\mathbf{k})$ with quasiparticle velocity $v_n^a(\mathbf{k}) = \partial^a E_n(\mathbf{k})$, direct band gap $\epsilon_{mn}(\mathbf{k}) = E_m(\mathbf{k}) - E_n(\mathbf{k})$, and transition dipole moments $\hat{e}_{nm}^a(\mathbf{k}) = i \hat{P}_n(\mathbf{k}) \partial^a \hat{P}_m(\mathbf{k}) \hat{P}_m(\mathbf{k})$ [47, 48] with short notation $\partial^a \equiv \partial_{k^a}$. A similar expression holds for $\hat{P}_n(\mathbf{k}) \partial^a \partial^b \hat{H}(\mathbf{k}) \hat{P}_m(\mathbf{k})$, including the quasiparticle mass $m_n^{ab}(\mathbf{k}) = (\partial^a \partial^b E_n(\mathbf{k}))^{-1}$, the covariant derivative of the transition dipole moment $\nabla^a \hat{e}_{nm}^b$, and three-band processes $\hat{e}_{nl}^a \hat{e}_{lm}^b$ [57].

We perform a perturbative expansion in Γ , assuming Γ is much smaller than the bandwidth, and retain the three dominant orders Γ^{-2} , Γ^{-1} , and Γ^0 . Details of the entire derivation are presented in the SM [57]. Summarizing the main findings for the zero temperature limit, we obtain the leading-order decomposition

$$\begin{aligned} \sigma^{a;bb} = & \frac{e^3}{\hbar} \sum_{n \in \text{bands}} \int \frac{d^d \mathbf{k}}{(2\pi)^d} \delta(E_n(\mathbf{k}) - \mu) \left[\sigma_{\text{NLD}}^{a;bb}(\mathbf{k}) \right. \\ & \left. + \sigma_{\text{BCD}}^{a;bb}(\mathbf{k}) + \sigma_{\text{interQMD}}^{a;bb}(\mathbf{k}) + \sigma_{\text{intraQMD}}^{a;bb}(\mathbf{k}) \right], \end{aligned} \quad (4a)$$

where the band- and momentum-resolved contributions read

$$\sigma_{\text{NLD}}^{a;bb}(\mathbf{k}) = -\frac{1}{(2\Gamma)^2} \frac{v_n^a(\mathbf{k})}{m_n^{bb}(\mathbf{k})} \text{tr}[\hat{P}_n(\mathbf{k})], \quad (4b)$$

$$\sigma_{\text{BCD}}^{a;bb}(\mathbf{k}) = \frac{1}{2\Gamma} v_n^b(\mathbf{k}) \Omega_n^{ab}(\mathbf{k}), \quad (4c)$$

$$\sigma_{\text{interQMD}}^{a;bb}(\mathbf{k}) = 2 \sum_{m \neq n} \frac{v_n^b(\mathbf{k}) g_{mn}^{ab}(\mathbf{k}) - v_n^a(\mathbf{k}) g_{mn}^{bb}(\mathbf{k})}{\epsilon_{mn}(\mathbf{k})}, \quad (4d)$$

$$\sigma_{\text{intraQMD}}^{a;bb}(\mathbf{k}) = -\frac{1}{2} \partial^a g_n^{bb}(\mathbf{k}), \quad (4e)$$

The quantum geometric invariants involved—the quantum metric, Berry curvature, and two-state quantum metric—are given in projector form as [48]

$$g_n^{ab}(\mathbf{k}) = \frac{1}{2} \text{tr}[\partial_a \hat{P}_n \partial_b \hat{P}_n], \quad (5a)$$

$$\Omega_n^{ab}(\mathbf{k}) = i \text{tr}[\hat{P}_n(\mathbf{k}) \partial^a \hat{P}_n(\mathbf{k}) \partial^b \hat{P}_n(\mathbf{k})] - (a \leftrightarrow b), \quad (5b)$$

$$g_{mn}^{ab}(\mathbf{k}) = \frac{1}{2} \text{tr}[\partial^a \hat{P}_m(\mathbf{k}) \partial^b \hat{P}_n(\mathbf{k})]. \quad (5c)$$

The terms are arranged by their order in the scattering rate Γ . It importantly only features as a prefactor and does not affect momentum integration. Band structure and quantum geometry are separated in each term, and the latter is expressed in a manifestly gauge-invariant way. Hereinafter we set $\hbar = e = 1$.

TABLE I. Symmetry conditions for all components of Eq. (4), without loss of generality for the case $\sigma^{x;yy}$. A \checkmark indicates that a term may be observed under this symmetry. A full table containing information about the nonzero tensor components of each contribution is provided in the SM [57], along with an MSG analysis. \mathcal{P} denotes inversion, \mathcal{T} time-reversal, \mathcal{C}_n n-fold rotation, and \mathcal{M} mirror symmetries.

	\mathcal{P}	\mathcal{T}	\mathcal{PT}	$\mathcal{C}_2^z, \mathcal{C}_2^x, \mathcal{M}_x$	$\mathcal{C}_2^y, \mathcal{M}_y$	\mathcal{C}_3^z
NLD	\times	\times	\checkmark	\times	\checkmark	\checkmark
BCD	\times	\checkmark	\times	\times	\checkmark	\times
interQMD	\times	\times	\checkmark	\times	\checkmark	\times
intraQMD	\times	\times	\checkmark	\times	\checkmark	\checkmark

Distinct quantum geometric origins of the NLHE.— The first term (4b) has previously been recovered in both semiclassical as well as quantum calculations referred to as the Drude weight dipole or nonlinear Drude weight (NLD) [68, 69]. The projector rank $\text{tr}[P_n]$ counts the band degeneracy.

The remaining three terms arise from virtual interband transitions, as they involve traces over projectors onto multiple distinct bands in the quantum geometric expansion. The second term (4c) is known as Berry curvature dipole (BCD) [55]. The third term (4d) involves the two-state quantum metric normalized by the direct band gap between the two involved bands. This contribution, dubbed (band-normalized) quantum metric dipole, has been identified in semiclassical and density matrix approaches [31, 56]. Alternative methods, such as the Luttinger-Kohn method or a Moyal product expansion, yield qualitatively similar terms with different coefficients [32, 70]. As it explicitly depends on the two-state quantum metric g_{nm}^{ab} , we refer to it as the interband quantum metric dipole (interQMD).

The fourth term (4e) yields the dipole of the *intra*band quantum metric g_n^{ab} . In contrast to the previous contribution, we therefore refer to this term as the intra band quantum metric dipole (intraQMD). It has not yet been identified in any aforementioned calculations [31, 32, 56, 70] to the best of our knowledge. The quantum metric dipole arises from symmetrized and band-traced two-state quantum geometric connections $\text{tr}[\hat{e}_{nm}^b \nabla^a \hat{e}_{mn}^c]$ and three-band contributions $\text{tr}[\hat{e}_{nm}^a \hat{e}_{ml}^b \hat{e}_{ln}^c]$ [48, 57], showing its nontrivial interband origin. We emphasize that in multiband systems with more than two bands, the single-band and two-state quantum metrics are generally distinct geometric quantities, related by the identity $\sum_{n \neq m} g_{nm}^{ab} = -g_n^{ab}$. Moreover, the coefficient of the intraQMD is independent of the band structure.

Numerically, the separation of quantum geometry and band structure enables efficient evaluation in many cases. As detailed in the SM [57], derivatives of the projectors can be replaced by appropriate combinations of derivatives of the Bloch Hamiltonian matrix. In this way, numerical differentiation schemes, such as finite differences, can be avoided, which is particularly advantageous for computational studies of three-dimensional (3D) multiband models.

Distinguishing contributions by symmetries.— In the linear case, longitudinal and Hall contributions are distinct by their symmetry under exchange of current and electric field direc-

TABLE II. Contributions found for the minimal (tilted) Weyl/Dirac models discussed in the main text. Here, minimal indicates that only the lowest required order in momentum k for nontrivial results is included in the model Hamiltonian.

	NLD	BCD	interQMD	intraQMD
Gapped Dirac point in 3D	\checkmark	\times	\checkmark	\checkmark
Gapless Weyl point in 3D	\checkmark	\times	\checkmark	\times
Gapped Dirac point in 2D	\checkmark	\checkmark	\checkmark	\checkmark
Gapless Dirac point in 2D	\checkmark	\times	\checkmark	\checkmark
Nodal line in 3D	\checkmark	\checkmark	\checkmark	\checkmark
Nodal plane in 3D	\checkmark	\times	\checkmark	\checkmark

tions, i.e., the symmetric and antisymmetric parts of the conductivity tensor σ^{ab} with $j^a = \sigma^{ab} E^b$. In the nonlinear case, this separation is more subtle and requires knowledge of the full conductivity tensor $\sigma^{a;bc}$. It was shown that the conductivity tensor can be separated into a fully symmetric Ohmic (dissipative) part and a non-dissipative Hall part containing the remaining components [71]. Using the expression for the full conductivity tensor [57], we identify the NLD contribution as purely Ohmic, the BCD and interQMD contributions as purely Hall, and the intraQMD contribution as mixed.

The different contributions can, to some extent, be distinguished by their transformation properties under common symmetries [32, 57, 72], as summarized in Tab. I. In the SM [57], we provide the list of nonzero tensor components for each contribution. In particular, for antiferromagnetic order with the magnetic \mathcal{PT} symmetry, all terms except the BCD contribute. Similarly, higher-order multipolar orderings can be characterized by their behavior under inversion (\mathcal{P}), time-reversal (\mathcal{T}), and rotation symmetries, which restrict allowed contributions [57, 73]. Certain symmetries, such as \mathcal{C}_3 , also relate different components of the tensor $\sigma^{a;bc}$ among themselves. We extend the magnetic symmetry analysis when identifying material candidates.

To quantify the relevance of the various contributions beyond the symmetry analysis, we analytically calculate the contributions to the NLHE for several topological band models. We focus on non-centrosymmetric systems with broken time-reversal symmetry, thereby allowing for contributions beyond the BCD (see Table I). The zero-, one-, or two-dimensional degeneracies in momentum space can be locally approximated by low-energy Hamiltonians. In the following, we discuss the \mathcal{PT} -symmetric 3D tilted Dirac point, the related 3D Weyl point, and a nodal plane. Further examples for the two-dimensional (2D) tilted Dirac point and a 3D nodal line are given in the SM [57], along with a description of the analytic methods employed. An overview of the discussed models is given in Tab. II.

3D tilted Dirac point.— To elucidate the behavior of QMD-driven contributions (inter- and intraQMD), we begin by investigating a four-band \mathcal{PT} symmetric 3D tilted Dirac point with uniform velocity v described by the Hamiltonian

$$H = tk_y \sigma_0 \tau_0 + v(k_x \sigma_z \tau_x + k_y \sigma_0 \tau_y + k_z \sigma_x \tau_x) + m \sigma_y \tau_x, \quad (6)$$

with tensor product of Pauli matrices τ and σ . Antiferromag-

netic systems with \mathcal{PT} symmetry have recently been studied to identify contributions to the NLHE beyond the BCD [74–76]. A mass term proportional to m is introduced, which breaks \mathcal{P} and \mathcal{T} individually, while preserving \mathcal{PT} . The tilt parameter $t \propto 1$ also breaks inversion symmetry, affecting the Fermi surface but not the quantum geometry. Thus, to obtain contributions to the NLHE, we effectively compute skewed averages of the underlying quantum geometry of a Dirac point. This is illustrated in Fig. 1(a,b), where we plot the inter- and intraQMD contributions prior to integration in a cross-section of k -space, along with the skewed Fermi surfaces. The model also possesses mirror symmetries $\mathcal{M}_x, \mathcal{M}_z$, which, as indicated in Table I, imply that the only nonzero Hall conductivities are $\sigma^{y;xx} = \sigma^{y;zz}$, and that the BCD contribution vanishes. The material CuMnAs realizes such Dirac points near the Fermi energy and has previously been connected to the NLHE [74, 77]. Under pressure, Bi₂CuO₄ may also exhibit Dirac points near the Fermi surface in an antiferromagnetic phase [78].

Note that the model consists of two doubly degenerate bands. The projector formalism is particularly convenient in this case, as it effectively reduces the system to a two-band model with projectors $\hat{P}_1(\mathbf{k})$ and $\hat{P}_2(\mathbf{k})$ projecting onto the entire degenerate eigenspaces of each band. Analytic expressions of the conductivities are obtained and presented in the SM [57]. All contributions except for the BCD are nonzero. The results are plotted in Fig. 1(c,d) as functions of m and μ . We see that for fixed chemical potential $\mu = 0.2$, the intraQMD contribution dominates at larger gap sizes. For fixed gap $m = 0.1$, the intraQMD and interQMD contributions are of equal importance when approaching the band edge. Particle-hole symmetry enforces that all contributions are odd functions of μ [57], which is confirmed by the analytic expressions. When the mass m is set to 0, the Hamiltonian can be block-diagonalized into two gapless 3D Weyl points, with nonzero NLD and interQMD contributions. The latter is proportional to $1/\mu$, diverging at the band crossing point [57].

Nodal plane.— Eq. (4d) suggests that the interQMD contribution is enhanced when two bands are close in energy and near quantum metric hot spots. Both of these features are present in a (gapped) nodal plane, which is a two-dimensional band degeneracy [40, 43–45, 79–96]. Indeed, when a perturbative symmetry-breaking term gaps the nodal plane, the two-state quantum metric increases significantly within the gap, while the band gap remains perturbatively small. We give a low-energy model for such a nodal plane, located at $k_z = 0$,

$$H = \epsilon k_y \sigma_0 + v k_z \sigma_z + a k_z k_x (\sigma_y + \sigma_z) + m (\sigma_x + \sigma_z). \quad (7)$$

Here ϵ represents a tilting of the nodal plane, v is a velocity in the z direction, and m controls the symmetry-breaking gap. The term proportional to a is required for nonvanishing quantum geometric invariants. The model is minimally constructed to yield nonzero contributions to $\sigma^{z;xx}$. In the following, the results are independent of the chemical potential, since it can be absorbed into the tilt term by a momentum shift.

Required by the open Fermi surface, we restrict the integration in k_z within Eq. (4) to the interval $[-L, L]$ and keep only the leading order behavior for $L \rightarrow \infty$. In real systems,

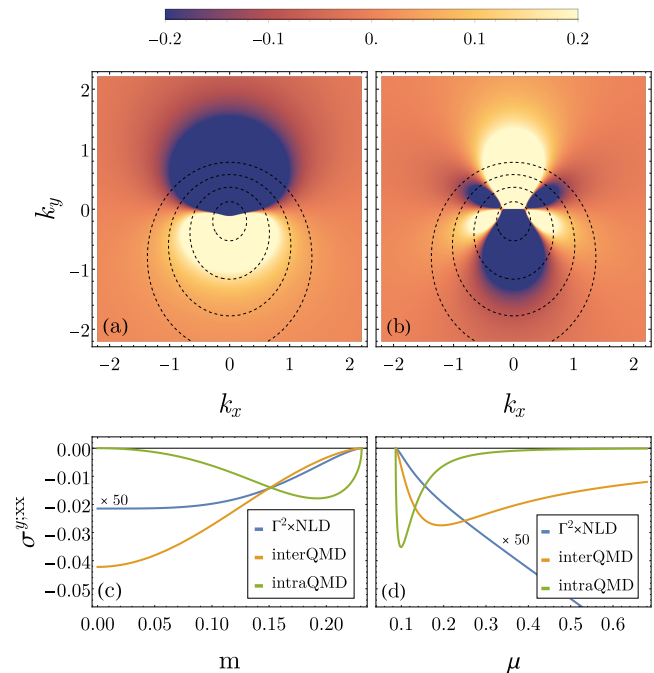


FIG. 1. The (a) inter- and (b) intraQMD contributions before k -integration along the cut of momentum space $k_z = 0$ for the 3D Dirac model defined in Eq. (6) with velocity $v = 1$, tilt $t = 0.5$, and mass m . We give the dependence of the three nonzero contributions on (c) the gap m for $\mu = 0.2$ and (d) the chemical potential μ for $m = 0.1$ of $\sigma^{y;xx}$. In both cases, the chemical potential lies within the upper band.

such a cutoff arises naturally from the dispersion of the nodal plane. The resulting conductivities are

$$\begin{aligned} \sigma_{\text{NLD}}^{z;xx} &= -\frac{agL}{16\pi^2\epsilon\Gamma^2}, & \sigma_{\text{interQMD}}^{z;xx} &= \frac{a \log(2 + \sqrt{3})}{16\pi^2\epsilon v}, \\ \sigma_{\text{BCD}}^{z;xx} &= 0, & \sigma_{\text{intraQMD}}^{z;xx} &= \frac{ag}{16\pi^2\epsilon Lv^2}. \end{aligned} \quad (8)$$

The BCD is not symmetry-forbidden but vanishes in this minimal model; including higher-order corrections to the Hamiltonian would restore a finite contribution. The nonzero contributions are inversely proportional to the tilt of the nodal plane ϵ , indicating that flatter nodal planes yield stronger contributions, which we attribute to the increased density of states. The NLD and intraQMD contributions are proportional to the gap m , whereas the interQMD term is independent (to leading order in L). We see that nodal planes are promising candidates for large, QMD-driven NHLE. A clear separation from intra- and interQMD contributions requires a more detailed analysis beyond low-energy models. Note that for degenerate nodal planes ($m = 0$), the system recovers $\mathcal{C}_2\mathcal{T}$ symmetry, forcing all contributions to $\sigma^{z;xx}$ to be zero [57].

Other models.— In the SM [57], we present further analytic results for a tilted 2D Dirac point and a 3D nodal line. For the former, we find that the components $\sigma^{x;yy}$ and $\sigma^{y;xx}$ originate from different quantum geometric invariants, arising from a symmetry combining time-reversal and mirror reflection. Specifically, $\sigma^{x;yy}$ receives contributions exclusively

from the BCD, while $\sigma^{y;xx}$ consists of NLD, interQMD, and intraQMD contributions. In contrast to $\sigma^{x;yy}$, these contributions do not vanish when the mass gap is closed. We close by 3D nodal lines, thereby completing the treatment of 0-, 1-, and 2-dimensional band degeneracies. The QMD-driven contributions to the NLHE increase for flatter nodal lines, and are strongly enhanced for a vanishing mass gap [57, 97].

Candidate materials.— To identify materials exhibiting an NLHE driven by quantum geometric invariants beyond the BCD, we derive stringent constraints by accounting for all symmetries of the material’s magnetic space group (MSG). We describe four specific choices of constraints, along with material candidates from the MAGNDATA database [98, 99] that are known to have a non-vanishing Fermi surface. Complete MSG listings for each case, as well as additional material candidates, are provided in the SM [57].

First, 208 MSGs prohibit the BCD while permitting nonzero NLD, inter-, or intraQMD contributions. Of the 429 materials in the MAGNDATA database [98, 99] with a nonzero nonlinear conductivity tensor (solely inferred from symmetry arguments), 175 possess a phase belonging to one of these MSGs, suggesting that these effects may be prevalent in magnetic materials. Examples include CuMnAs [74], CoNb₃S₆ [100], and Mn₂Au [101].

Second, we impose conditions such that the BCD and interQMD contributions vanish along a crystallographic plane (e.g., xy), whereas the NLD and intraQMD remain finite. We note that NLD and intraQMD cannot be distinguished by magnetic symmetry. We find 15 such MSGs, that enable separating NLD and intraQMD from interQMD contributions. A representative material satisfying this condition is Yb₃Pt₄ [102].

Finally, since nodal planes can enhance QMD-driven NLHE, we identify MSGs that enforce nodal planes while selectively suppressing only the BCD, where we find 15 MSGs with MnNb₃S₆ as metallic, ferromagnetic candidate material [103].

Discussion.— Within a fully gauge-invariant approach, we identified three quantum geometric contributions to the second-order nonlinear Hall effect (NLHE), including a previously unrecognized contribution proportional to the intraband quantum metric dipole (intraQMD). A magnetic symmetry analysis revealed nodal-plane materials and antiferromagnetic Dirac systems as promising candidates for quantum-metric-dipole-driven NLHE, complementing the Berry-curvature-driven response.

Whereas our result agrees with previous semiclassical results predicting the Berry curvature dipole (BCD) and (band-normalized) interband quantum metric dipole (interQMD) contributions, the intraQMD contribution has not been obtained within a semiclassical description to the best of our knowledge. Finding similar but not identical formulas by different approaches is commonly observed in the nonlinear regime [3]. It seems reasonable that the discrepancy arises from a distinct treatment of virtual interband effects and relaxation processes. Indeed, assuming an infinite lifetime of remote states using a phenomenological two-lifetime approach

[3, 5, 69] within our derivation, we find a vanishing intraQMD and strongly modified interQMD [57]. The Boltzmann equation can be derived from the Green’s function formalism by assuming that quasiparticles have an infinite lifetime (i.e., a delta-function spectral function) [104], suggesting that the additional intraQMD term may arise in a semiclassical theory by lifting this assumption within a multiband setting. Recent progress has been made here by employing Wigner-Moyal approaches [70, 105], where the intraQMD contribution may arise after including a suitable collision integral. The theory of DC response functions in dispersive multiband systems would greatly benefit from a careful reevaluation of both semiclassical and fully quantum approaches, systematically investigating the implications of nontrivial quantum geometry within a fully gauge-invariant framework, as presented here. It may also provide further insights on unconventional transport in flatband systems, where similar discrepancies have been discussed recently [53, 106–108].

The diverse quantum geometric origins of the intrinsic NLHE suggest that novel disorder- and interaction-induced nonlinear Hall responses may arise from combining microscopic impurity or electron-phonon scattering with nontrivial quantum geometry. While numerical progress has been made for minimal models, such as the 2D Dirac point [58], a complete understanding remains an open challenge. The presented quantum geometric expansion provides a suitable framework, starting from a perturbative Green’s function approach, enabling studies of how contributions are modified and whether additional geometric invariants emerge. Temperature-dependent experiments may help separate contributions via the distinct scattering rate scaling, such as the nonlinear Drude and quantum metric dipole contributions, or new extrinsic effects [34, 35].

The presented techniques, built around a quantum geometric decomposition of Green’s function-based response functions via band projectors [6, 48–50, 53], can be straightforwardly extended to further DC responses, such as the spin Hall, Nernst, and DC Kerr effects in the nonlinear regime. In particular, our scattering rate expansion [57] also enables access to higher-order effects such as third-order or magneto-nonlinear Hall responses [56]. A systematic understanding of the quantum geometric structure of nonlinear responses may reveal unexpected links between observables, clarify the role of emerging geometric invariants [6, 47, 48, 52, 54, 109], and guide the design of nonlinear phenomena in quantum materials.

Acknowledgments.— We thank Pavel Ostrovsky for deriving Eq. (2) and for enlightening us about the role of disorder on the NLHE. The authors are also grateful to Tobias Holder, Moritz Hirschmann, and Raymond Wiedmann for helpful discussions. Y.U., L.C. and A.P.S. are funded by the Deutsche Forschungsgemeinschaft (DFG, German Research Foundation) – TRR 360 – 492547816. J.M. was, in part, supported by the Deutsche Forschungsgemeinschaft under Grant cluster of excellence ct.qmat (EXC 2147, Project No. 390858490).

- [1] P. Törmä, Essay: Where can quantum geometry lead us?, *Phys. Rev. Lett.* **131**, 240001 (2023).
- [2] J. Yu, B. A. Bernevig, R. Queiroz, E. Rossi, P. Törmä, and B.-J. Yang, Quantum geometry in quantum materials, [arXiv:2501.00098](https://arxiv.org/abs/2501.00098).
- [3] Y. Jiang, T. Holder, and B. Yan, Revealing quantum geometry in nonlinear quantum materials, [arXiv:2503.04943](https://arxiv.org/abs/2503.04943).
- [4] N. Verma, P. J. W. Moll, T. Holder, and R. Queiroz, Quantum geometry: Revisiting electronic scales in quantum matter, [arXiv:2504.07173](https://arxiv.org/abs/2504.07173).
- [5] T. Holder, D. Kaplan, and B. Yan, Consequences of time-reversal-symmetry breaking in the light-matter interaction: Berry curvature, quantum metric, and diabatic motion, *Physical Review Research* **2**, 033100 (2020).
- [6] A. Avdoshkin, J. Mitscherling, and J. E. Moore, The multi-state geometry of shift current and polarization, [arXiv:2409.16358](https://arxiv.org/abs/2409.16358).
- [7] J. Ahn, G.-Y. Guo, and N. Nagaosa, Low-frequency divergence and quantum geometry of the bulk photovoltaic effect in topological semimetals, *Physical Review X* **10**, 041041 (2020).
- [8] P. Zhu and A. Alexandradinata, Anomalous shift and optical vorticity in the steady photovoltaic current, *Phys. Rev. B* **110**, 115108 (2024).
- [9] P. Bhalla, K. Das, D. Culcer, and A. Agarwal, Resonant second-harmonic generation as a probe of quantum geometry, *Phys. Rev. Lett.* **129**, 227401 (2022).
- [10] L. Wu, S. Patankar, T. Morimoto, N. L. Nair, E. The-walt, A. Little, J. G. Analytis, J. E. Moore, and J. Orenstein, Giant anisotropic nonlinear optical response in transition metal monpnictide Weyl semimetals, *Nature Physics* **13**, 350 (2017).
- [11] A. M. Cook, B. M. Fregoso, F. de Juan, S. Coh, and J. E. Moore, Design principles for shift current photovoltaics, *Nature Communications* **8**, 14176 (2017).
- [12] F. de Juan, A. G. Grushin, T. Morimoto, and J. E. Moore, Quantized circular photogalvanic effect in Weyl semimetals, *Nature Communications* **8**, 15995 (2017).
- [13] J. E. Sipe and A. I. Shkrebti, Second-order optical response in semiconductors, *Phys. Rev. B* **61**, 5337 (2000).
- [14] Y. Zhang, J. van den Brink, C. Felser, and B. Yan, Electrically tuneable nonlinear anomalous Hall effect in two-dimensional transition-metal dichalcogenides WTe_2 and MoTe_2 , *2D Materials* **5**, 044001 (2018).
- [15] T. Low, Y. Jiang, and F. Guinea, Topological currents in black phosphorus with broken inversion symmetry, *Physical Review B* **92**, 235447 (2015).
- [16] Q. Ma, S.-Y. Xu, H. Shen, D. MacNeill, V. Fatemi, T.-R. Chang, A. M. Mier Valdivia, S. Wu, Z. Du, C.-H. Hsu, S. Fang, Q. D. Gibson, K. Watanabe, T. Taniguchi, R. J. Cava, E. Kaxiras, H.-Z. Lu, H. Lin, L. Fu, N. Gedik, and P. Jarillo-Herrero, Observation of the nonlinear Hall effect under time-reversal-symmetric conditions, *Nature* **565**, 337 (2019).
- [17] J. I. Facio, D. Efremov, K. Koepnik, J.-S. You, I. Sodemann, and J. van den Brink, Strongly Enhanced Berry Dipole at Topological Phase Transitions in BiTeI , *Physical Review Letters* **121**, 246403 (2018).
- [18] O. O. Shvetsov, V. D. Esin, A. V. Timonina, N. N. Kolesnikov, and E. V. Deviatov, Nonlinear Hall Effect in Three-Dimensional Weyl and Dirac Semimetals, *JETP Letters* **109**, 715 (2019).
- [19] S. Dzsaber, X. Yan, M. Taupin, G. Eguchi, A. Prokofiev, T. Shiroka, P. Blaha, O. Rubel, S. E. Grefe, H.-H. Lai, Q. Si, and S. Paschen, Giant spontaneous Hall effect in a nonmagnetic Weyl-Kondo semimetal, *Proceedings of the National Academy of Sciences* **118**, e2013386118 (2021).
- [20] D. Kumar, C.-H. Hsu, R. Sharma, T.-R. Chang, P. Yu, J. Wang, G. Eda, G. Liang, and H. Yang, Room-temperature nonlinear Hall effect and wireless radiofrequency rectification in Weyl semimetal TaIrTe_4 , *Nature Nanotechnology* **16**, 421 (2021).
- [21] S. Singh, J. Kim, K. M. Rabe, and D. Vanderbilt, Engineering Weyl Phases and Nonlinear Hall Effects in T_d - MoTe_2 , *Physical Review Letters* **125**, 046402 (2020).
- [22] C. Zeng, S. Nandy, and S. Tewari, Nonlinear transport in Weyl semimetals induced by Berry curvature dipole, *Physical Review B* **103**, 245119 (2021).
- [23] Z. Du, C. Wang, H.-Z. Lu, and X. Xie, Band Signatures for Strong Nonlinear Hall Effect in Bilayer WTe_2 , *Physical Review Letters* **121**, 266601 (2018).
- [24] J.-S. You, S. Fang, S.-Y. Xu, E. Kaxiras, and T. Low, Berry curvature dipole current in the transition metal dichalcogenides family, *Physical Review B* **98**, 121109 (2018).
- [25] C. Xiao, Z. Z. Du, and Q. Niu, Theory of nonlinear Hall effects: Modified semiclassics from quantum kinetics, *Physical Review B* **100**, 165422 (2019).
- [26] J. Son, K.-H. Kim, Y. Ahn, H.-W. Lee, and J. Lee, Strain Engineering of the Berry Curvature Dipole and Valley Magnetization in Monolayer MoS_2 , *Physical Review Letters* **123**, 036806 (2019).
- [27] B. T. Zhou, C.-P. Zhang, and K. Law, Highly Tunable Nonlinear Hall Effects Induced by Spin-Orbit Couplings in Strained Polar Transition-Metal Dichalcogenides, *Physical Review Applied* **13**, 024053 (2020).
- [28] H. Rostami and V. Juričić, Probing quantum criticality using nonlinear Hall effect in a metallic Dirac system, *Physical Review Research* **2**, 013069 (2020).
- [29] D.-F. Shao, S.-H. Zhang, G. Gurung, W. Yang, and E. Tsymbal, Nonlinear Anomalous Hall Effect for Néel Vector Detection, *Physical Review Letters* **124**, 067203 (2020).
- [30] L. Zhao, C. A. Belvin, R. Liang, D. A. Bonn, W. N. Hardy, N. P. Armitage, and D. Hsieh, A global inversion-symmetry-broken phase inside the pseudogap region of $\text{YBa}_2\text{Cu}_3\text{O}_y$, *Nature Physics* **13**, 250 (2017).
- [31] K. Das, S. Lahiri, R. B. Atencia, D. Culcer, and A. Agarwal, Intrinsic nonlinear conductivities induced by the quantum metric, *Physical Review B* **108**, L201405 (2023).
- [32] D. Kaplan, T. Holder, and B. Yan, Unification of nonlinear anomalous hall effect and nonreciprocal magnetoresistance in metals by the quantum geometry, *Physical Review Letters* **132**, 026301 (2024).
- [33] T. Xi, H. Jiang, J. Li, Y. He, Y. Gu, C. Fox, L. Primeau, Y. Mao, J. Rollins, T. Taniguchi, K. Watanabe, D. van der Weide, D. Rhodes, Y. Zhang, Y. Wang, and J. Xiao, Terahertz sensing based on the nonlinear electrodynamics of the two-dimensional correlated topological semimetal TaIrTe_4 , *Nature Electronics* (2025).
- [34] J. Duan, Y. Jian, Y. Gao, H. Peng, J. Zhong, Q. Feng, J. Mao, and Y. Yao, Giant second-order nonlinear hall effect in twisted bilayer graphene, *Phys. Rev. Lett.* **129**, 186801 (2022).
- [35] N. Wang, D. Kaplan, Z. Zhang, T. Holder, N. Cao, A. Wang, X. Zhou, F. Zhou, Z. Jiang, C. Zhang, S. Ru, H. Cai, K. Watanabe, T. Taniguchi, B. Yan, and W. Gao, Quantum-metric-

- induced nonlinear transport in a topological antiferromagnet, *Nature* **621**, 487 (2023).
- [36] P. Törmä, S. Peotta, and B. A. Bernevig, Superconductivity, superfluidity and quantum geometry in twisted multilayer systems, *Nature Reviews Physics* **4**, 528 (2022).
- [37] Z. Liu and E. J. Bergholtz, Recent developments in fractional chern insulators, in *Encyclopedia of Condensed Matter Physics (Second Edition)*, edited by T. Chakraborty (Academic Press, Oxford, 2024) second edition ed., pp. 515–538.
- [38] A. Burkov, Weyl metals, *Annual Review of Condensed Matter Physics* **9**, 359 (2018).
- [39] N. P. Armitage, E. J. Mele, and A. Vishwanath, Weyl and dirac semimetals in three-dimensional solids, *Rev. Mod. Phys.* **90**, 015001 (2018).
- [40] N. Huber, K. Alpin, G. L. Causer, L. Worch, A. Bauer, G. Benka, M. M. Hirschmann, A. P. Schnyder, C. Pfleiderer, and M. A. Wilde, Network of Topological Nodal Planes, Multifold Degeneracies, and Weyl Points in CoSi, *Phys. Rev. Lett.* **129**, 026401 (2022).
- [41] C. Guo, L. Hu, C. Putzke, J. Diaz, X. Huang, K. Manna, F.-R. Fan, C. Shekhar, Y. Sun, C. Felser, C. Liu, B. A. Bernevig, and P. J. W. Moll, Quasi-symmetry-protected topology in a semimetal, *Nature Physics* **18**, 813 (2022).
- [42] M. A. Wilde and C. Pfleiderer, Large curvature near a small gap, *Nature Physics* **18**, 731 (2022).
- [43] C. Zhong, Y. Chen, Y. Xie, S. A. Yang, M. L. Cohen, and S. Zhang, Towards three-dimensional Weyl-surface semimetals in graphene networks, *Nanoscale* **8**, 7232 (2016).
- [44] Q.-F. Liang, J. Zhou, R. Yu, Z. Wang, and H. Weng, Node-surface and node-line fermions from nonsymmorphic lattice symmetries, *Phys. Rev. B* **93**, 085427 (2016).
- [45] M. A. Wilde, M. Dodenhöft, A. Niedermayr, A. Bauer, M. M. Hirschmann, K. Alpin, A. P. Schnyder, and C. Pfleiderer, Symmetry-enforced topological nodal planes at the Fermi surface of a chiral magnet, *Nature* **594**, 374 (2021).
- [46] H. Tanaka, S. Okazaki, K. Kuroda, R. Noguchi, Y. Arai, S. Minami, S. Ideta, K. Tanaka, D. Lu, M. Hashimoto, V. Kandyba, M. Cattelan, A. Barinov, T. Muro, T. Sasagawa, and T. Kondo, Large anomalous hall effect induced by weak ferromagnetism in the noncentrosymmetric antiferromagnet CoNb_3S_6 , *Phys. Rev. B* **105**, L121102 (2022).
- [47] J. Ahn, G.-Y. Guo, N. Nagaosa, and A. Vishwanath, Riemannian geometry of resonant optical responses, *Nature Physics* **18**, 290 (2022).
- [48] J. Mitscherling, A. Avdoshkin, and J. E. Moore, Gauge-invariant projector calculus for quantum state geometry and applications to observables in crystals (), [arXiv:2412.03637](https://arxiv.org/abs/2412.03637).
- [49] O. Pozo and F. de Juan, Computing observables without eigenstates: Applications to bloch hamiltonians, *Phys. Rev. B* **102**, 115138 (2020).
- [50] A. Graf and F. Piéchon, Berry curvature and quantum metric in N -band systems: An eigenprojector approach, *Phys. Rev. B* **104**, 085114 (2021).
- [51] B. Mera and J. Mitscherling, Nontrivial quantum geometry of degenerate flat bands, *Phys. Rev. B* **106**, 165133 (2022).
- [52] A. Avdoshkin and F. K. Popov, Extrinsic geometry of quantum states, *Physical Review B* **107**, 245136 (2023).
- [53] O. Antebi, J. Mitscherling, and T. Holder, Drude weight of an interacting flat-band metal, *Phys. Rev. B* **110**, L241111 (2024).
- [54] A. Avdoshkin, Geometry of degenerate quantum states, configurations of m -planes and invariants on complex grassmannians, [arXiv:2404.03234](https://arxiv.org/abs/2404.03234).
- [55] I. Sodemann and L. Fu, Quantum nonlinear hall effect induced by berry curvature dipole in time-reversal invariant materials, *Phys. Rev. Lett.* **115**, 216806 (2015).
- [56] Y. Gao, S. A. Yang, and Q. Niu, Field induced positional shift of bloch electrons and its dynamical implications, *Physical Review Letters* **112**, 166601 (2014).
- [57] See the Supplemental Material, for details on Eq. (2) and a discussion on how scattering was modeled, the derivation of Eq. (4), a (magnetic) symmetry analysis of the different geometric contributions to the NLHE accompanied by corresponding material candidates, details on the model calculations presented in the main text as well as two further examples, and the derivation of an alternative expression of the NLHE which is suitable for numerical calculations.
- [58] Z. Z. Du, C. M. Wang, H.-P. Sun, H.-Z. Lu, and X. C. Xie, Quantum theory of the nonlinear hall effect, *Nature Communications* **12**, 1 (2025).
- [59] Y. Michishita and R. Peters, Effects of renormalization and non-hermiticity on nonlinear responses in strongly correlated electron systems, *Phys. Rev. B* **103**, 195133 (2021).
- [60] A. Eberlein, W. Metzner, S. Sachdev, and H. Yamase, Fermi surface reconstruction and drop in the hall number due to spiral antiferromagnetism in High- T_c cuprates, *Phys. Rev. Lett.* **117**, 187001 (2016).
- [61] S. Verret, O. Simard, M. Charlebois, D. Sénéchal, and A.-M. S. Tremblay, Phenomenological theories of the low-temperature pseudogap: Hall number, specific heat, and Seebeck coefficient, *Phys. Rev. B* **96**, 125139 (2017).
- [62] H. Kontani, T. Tanaka, and K. Yamada, Intrinsic anomalous hall effect in ferromagnetic metals studied by the multi-d-orbital tight-binding model, *Phys. Rev. B* **75**, 184416 (2007).
- [63] T. Tanaka, H. Kontani, M. Naito, T. Naito, D. S. Hirashima, K. Yamada, and J. Inoue, Intrinsic spin hall effect and orbital hall effect in 4d and 5d transition metals, *Phys. Rev. B* **77**, 165117 (2008).
- [64] J. Mitscherling, Longitudinal and anomalous hall conductivity of a general two-band model, *Phys. Rev. B* **102**, 165151 (2020).
- [65] Y. Michishita and N. Nagaosa, Dissipation and geometry in nonlinear quantum transports of multiband electronic systems, *Phys. Rev. B* **106**, 125114 (2022).
- [66] G. Rickayzen, *Green's functions and condensed matter*, Techniques of physics No. 5 (Academic Press, 1980).
- [67] A. Altland and B. D. Simons, *Condensed Matter Field Theory*, 2nd ed. (Cambridge University Press, 2010).
- [68] D. E. Parker, T. Morimoto, J. Orenstein, and J. E. Moore, Diagrammatic approach to nonlinear optical response with application to weyl semimetals, *Phys. Rev. B* **99**, 045121 (2019).
- [69] D. Kaplan, T. Holder, and B. Yan, Unifying semiclassics and quantum perturbation theory at nonlinear order, *SciPost Physics* **14**, 082 (2023).
- [70] T. Park, X. Huang, L. Savary, and L. Balents, Quantum geometry from the moyal product: quantum kinetic equation and non-linear response, [arXiv:2504.10447](https://arxiv.org/abs/2504.10447).
- [71] S. S. Tsirkin and I. Souza, On the separation of Hall and Ohmic nonlinear responses, *SciPost Phys. Core* **5**, 039 (2022).
- [72] H. Zhu, J. Li, X. Chen, Y. Yu, and Q. Liu, Magnetic geometry induced quantum geometry and nonlinear transports, *Nature Communications* **16**, 4882 (2025).
- [73] H. Watanabe and Y. Yanase, Nonlinear electric transport in odd-parity magnetic multipole systems: Application to mn-based compounds, *Physical Review Research* **2**, 043081 (2020).
- [74] C. Wang, Y. Gao, and D. Xiao, Intrinsic nonlinear hall effect in antiferromagnetic tetragonal cumnas, *Phys. Rev. Lett.* **127**,

- 277201 (2021).
- [75] H. Liu, J. Zhao, Y.-X. Huang, W. Wu, X.-L. Sheng, C. Xiao, and S. A. Yang, Intrinsic second-order anomalous hall effect and its application in compensated antiferromagnets, *Phys. Rev. Lett.* **127**, 277202 (2021).
- [76] A. Gao, Y.-F. Liu, J.-X. Qiu, B. Ghosh, T. V. Trevisan, Y. Onishi, C. Hu, T. Qian, H.-J. Tien, S.-W. Chen, M. Huang, D. Bérubé, H. Li, C. Tzschaschel, T. Dinh, Z. Sun, S.-C. Ho, S.-W. Lien, B. Singh, K. Watanabe, T. Taniguchi, D. C. Bell, H. Lin, T.-R. Chang, C. R. Du, A. Bansil, L. Fu, N. Ni, P. P. Orth, Q. Ma, and S.-Y. Xu, Quantum metric nonlinear hall effect in a topological antiferromagnetic heterostructure, *Science* **381**, 181 (2023).
- [77] P. Tang, Q. Zhou, G. Xu, and S.-C. Zhang, Dirac fermions in an antiferromagnetic semimetal, *Nature Physics* **12**, 1100 (2016).
- [78] D. Di Sante, A. Hausoel, P. Barone, J. M. Tomczak, G. Sangiovanni, and R. Thomale, Realizing double dirac particles in the presence of electronic interactions, *Phys. Rev. B* **96**, 121106 (2017).
- [79] T. Bzdušek and M. Sigrist, Robust doubly charged nodal lines and nodal surfaces in centrosymmetric systems, *Phys. Rev. B* **96**, 155105 (2017).
- [80] W. Wu, Y. Liu, S. Li, C. Zhong, Z.-M. Yu, X.-L. Sheng, Y. X. Zhao, and S. A. Yang, Nodal surface semimetals: Theory and material realization, *Phys. Rev. B* **97**, 115125 (2018).
- [81] O. Türker and S. Moroz, Weyl nodal surfaces, *Phys. Rev. B* **97** (2018).
- [82] X. Zhang, Z.-M. Yu, Z. Zhu, W. Wu, S.-S. Wang, X.-L. Sheng, and S. A. Yang, Nodal loop and nodal surface states in the Ti_3Al family of materials, *Phys. Rev. B* **97**, 235150 (2018).
- [83] Z.-M. Yu, W. Wu, Y. Zhao, and S. A. Yang, Circumventing the no-go theorem: A single Weyl point without surface Fermi arcs, *Phys. Rev. B* **100**, 041118 (2019).
- [84] B.-B. Fu, C.-J. Yi, T.-T. Zhang, M. Caputo, J.-Z. Ma, X. Gao, B. Q. Lv, L.-Y. Kong, Y.-B. Huang, P. Richard, M. Shi, V. N. Strocov, C. Fang, H.-M. Weng, Y.-G. Shi, T. Qian, and H. Ding, Dirac nodal surfaces and nodal lines in ZrSiS , *Science Advances* **5**, eaau6459 (2019).
- [85] G. Chang, B. J. Wieder, F. Schindler, D. S. Sanchez, I. Belopolski, S.-M. Huang, B. Singh, D. Wu, T.-R. Chang, T. Neupert, S.-Y. Xu, H. Lin, and M. Z. Hasan, Topological quantum properties of chiral crystals, *Nature Materials* **17**, 978 (2018).
- [86] J.-Z. Ma, Q.-S. Wu, M. Song, S.-N. Zhang, E. B. Guedes, S. A. Ekahana, M. Krivenkov, M. Y. Yao, S.-Y. Gao, W.-H. Fan, T. Qian, H. Ding, N. C. Plumb, M. Radovic, J. H. Dil, Y.-M. Xiong, K. Manna, C. Felser, O. V. Yazyev, and M. Shi, Observation of a singular Weyl point surrounded by charged nodal walls in PtGa , *Nature Communications* **12**, 3994 (2021).
- [87] F. Tang and X. Wan, Complete classification of band nodal structures and massless excitations, *Phys. Rev. B* **105**, 155156 (2022).
- [88] K. Alpin, M. M. Hirschmann, N. Heinsdorf, A. Leonhardt, W. Y. Yau, X. Wu, and A. P. Schnyder, Fundamental laws of chiral band crossings: Local constraints, global constraints, and topological phase diagrams, *Phys. Rev. Res.* **5**, 043165 (2023).
- [89] G. Frank, D. Varjas, G. Pintér, and A. Pályi, Weyl-point teleportation, *Phys. Rev. B* **109**, 205415 (2024).
- [90] T. Chen, S. Minami, A. Sakai, Y. Wang, Z. Feng, T. Nomoto, M. Hirayama, R. Ishii, T. Koretsune, R. Arita, and S. Nakatsuji, Large anomalous nernst effect and nodal plane in an iron-based kagome ferromagnet, *Science Advances* **8**, eabk1480 (2022).
- [91] S.-X. Li, W. Wang, S. Xu, T. Li, Z. Li, J. Wang, J.-J. Mi, Q. Tao, F. Tang, X. Wan, and Z.-A. Xu, Giant Anomalous Hall Effect in Kagome Nodal Surface Semimetal Fe_3Ge , [arXiv:2501.15424](https://arxiv.org/abs/2501.15424).
- [92] R. Yamada, M. T. Birch, P. R. Baral, S. Okumura, R. Nakano, S. Gao, Y. Ishihara, K. K. Kolincio, I. Belopolski, H. Sagayama, H. Nakao, K. Ohishi, T. Nakajima, Y. Tokura, T. hisa Arima, Y. Motome, M. M. Hirschmann, and M. Hirschberger, Gapping the spin-nodal planes of an anisotropic p-wave magnet to induce a large anomalous Hall effect (2025), [arXiv:2502.10386](https://arxiv.org/abs/2502.10386).
- [93] L.-H. Hu, C. Guo, Y. Sun, C. Felser, L. Elcoro, P. J. Moll, C.-X. Liu, and B. A. Bernevig, Hierarchy of quasisymmetries and degeneracies in the CoSi family of chiral crystal materials, *Phys. Rev. B* **107**, 125145 (2023).
- [94] C. Xie, H. Yuan, Y. Liu, X. Wang, and G. Zhang, Three-nodal surface phonons in solid-state materials: Theory and material realization, *Phys. Rev. B* **104**, 134303 (2021).
- [95] M. Xiao, L. Ye, C. Qiu, H. He, Z. Liu, and S. Fan, Experimental demonstration of acoustic semimetal with topologically charged nodal surface, *Science Advances* **6**, eaav2360 (2020).
- [96] A. Scheie, P. Laurell, P. A. McClarty, G. E. Granroth, M. B. Stone, R. Moessner, and S. E. Nagler, Dirac magnons, nodal lines, and nodal plane in elemental gadolinium, *Phys. Rev. Lett.* **128**, 097201 (2022).
- [97] Y. Zhang, H. Zeng, and H. Huang, Logarithmically enhanced intrinsic nonlinear hall effects in \mathcal{PT} -symmetric antiferromagnetic nodal-line semimetals, *Phys. Rev. B* **111**, L081115 (2025).
- [98] S. V. Gallego, J. M. Perez-Mato, L. Elcoro, E. S. Tasci, R. M. Hanson, K. Momma, M. I. Aroyo, and G. Madariaga, *MAGN-DATA* : towards a database of magnetic structures. i. the commensurate case, *Journal of Applied Crystallography* **49**, 1750 (2016).
- [99] S. V. Gallego, J. M. Perez-Mato, L. Elcoro, E. S. Tasci, R. M. Hanson, M. I. Aroyo, and G. Madariaga, *MAGN-DATA* : towards a database of magnetic structures. II. the incommensurate case, *Journal of Applied Crystallography* **49**, 1941 (2016).
- [100] N. D. Khanh, S. Minami, M. M. Hirschmann, T. Nomoto, M.-C. Jiang, R. Yamada, N. Heinsdorf, D. Yamaguchi, Y. Hayashi, Y. Okamura, H. Watanabe, G.-Y. Guo, Y. Takahashi, S. Seki, Y. Taguchi, Y. Tokura, R. Arita, and M. Hirschberger, Gapped nodal planes and large topological Nernst effect in the chiral lattice antiferromagnet CoNb_3S_6 , *Nature Communications* **16**, 2654 (2025).
- [101] S. P. Bommanaboyena, D. Backes, L. S. I. Veiga, S. S. Dhesi, Y. R. Niu, B. Sarpi, T. Denneulin, A. Kovács, T. Mashoff, O. Gomonay, J. Sinova, K. Everschor-Sitte, D. Schönke, R. M. Reeve, M. Kläui, H.-J. Elmers, and M. Jourdan, Readout of an antiferromagnetic spintronics system by strong exchange coupling of Mn_2Au and Permalloy, *Nature Communications* **12**, 6539 (2021).
- [102] L. S. Wu, Y. Janssen, M. C. Bennett, and M. C. Aronson, Localized moments and the stability of antiferromagnetic order in Yb_3Pt_4 , *Phys. Rev. B* **86**, 054401 (2012).
- [103] A. L. Blanc-Soreau, J. Rouxel, M.-F. Gardette, and O. Gorochov, Propriétés électriques et magnétiques de $\text{Mn}_{0,25}\text{NbS}_2$ et $\text{Mn}_{0,33}\text{NbS}_2$, *Materials Research Bulletin* **11**, 1061 (1976).
- [104] J. Rammer and H. Smith, Quantum field-theoretical methods in transport theory of metals, *Rev. Mod. Phys.* **58**, 323 (1986).
- [105] J. Mitscherling, D. S. Borgnia, S. Ahuja, J. E. Moore, and V. B. Bulchandani, Orbital Wigner functions and quantum transport in multiband systems (), [arXiv:2502.14026](https://arxiv.org/abs/2502.14026).

- [106] J. Mitscherling and T. Holder, Bound on resistivity in flat-band materials due to the quantum metric, *Phys. Rev. B* **105**, 085154 (2022).
- [107] K.-E. Huhtinen and P. Törmä, Conductivity in flat bands from the Kubo-Greenwood formula, *Phys. Rev. B* **108**, 155108 (2023).
- [108] S. A. Chen, R. Moessner, and T. K. Ng, Generalized Peierls substitution for Wannier obstructions: response to disorder and interactions (2025), [arXiv:2503.09709 \[cond-mat.str-el\]](https://arxiv.org/abs/2503.09709).
- [109] W. J. Jankowski, A. S. Morris, Z. Davoyan, A. Bouhon, F. N. Ünal, and R.-J. Slager, Non-Abelian Hopf-Euler insulators, *Phys. Rev. B* **110**, 075135 (2024).
- [110] R. Oiwa and H. Kusunose, Systematic analysis method for nonlinear response tensors, *Journal of the Physical Society of Japan* **91**, 014701 (2022).
- [111] I. A. Ado, I. A. Dmitriev, P. M. Ostrovsky, and M. Titov, Anomalous hall effect with massive dirac fermions, *Europhysics Letters* **111**, 37004 (2015).
- [112] J. Mitscherling, *Electrical conductivity in quantum materials*, PhD thesis, Universität Stuttgart (2021).
- [113] W. R. Inc., *Mathematica*, Version 14.0.
- [114] D. Varjas, F. de Juan, and Y.-M. Lu, Bulk invariants and topological response in insulators and superconductors with non-symmorphic symmetries, *Phys. Rev. B* **92**, 195116 (2015).
- [115] D. Vanderbilt, *Berry Phases in Electronic Structure Theory: Electric Polarization, Orbital Magnetization and Topological Insulators* (Cambridge University Press, 2018).
- [116] H. T. Stokes, D. M. Hatch, and B. J. Campbell, *Iso-mag, isotropy software suite*.
- [117] J. Li, Y. Li, S. Du, Z. Wang, B.-L. Gu, S.-C. Zhang, K. He, W. Duan, and Y. Xu, Intrinsic magnetic topological insulators in van der waals layered mnbi_2te_4 -family materials, *Science Advances* **5**, eaaw5685 (2019).
- [118] A. Rich, P. Scheibe, and N. Abbasi, Rule-based integration: An extensive system of symbolic integration rules, *Journal of Open Source Software* **3**, 1073 (2018).
- [119] D. J. Thouless, M. Kohmoto, M. P. Nightingale, and M. den Nijs, Quantized hall conductance in a two-dimensional periodic potential, *Phys. Rev. Lett.* **49**, 405 (1982).
-

Supplemental Material

CONTENTS

S1. NLHE in Keldysh formalism and the scattering rate	1
S2. Geometric decomposition of the nonlinear conductivity tensor	1
A. Introduction of band projectors and quantum geometric decomposition	1
1. Insertion of band projectors	1
2. Summary of quantum geometric invariants	2
3. Quantum geometric decomposition	3
B. Collecting contributions to quantum geometric quantities	5
1. Contribution A: trivial geometry $\text{tr}[\hat{P}_n]$	6
2. Contribution B: quantum geometric tensors Q_{nm}^{ab} and Q_{nm}^{ac}	6
3. Contribution C: quantum geometric tensor Q_{nm}^{bc}	7
4. Contribution D: connections $C_{nm}^{b;ac}$, $C_{nm}^{c;ab}$	8
5. Contribution E: three-band traces $\text{tr}[e_{mn}^a e_{nl}^b e_{lm}^c]$, $\text{tr}[e_{mn}^a e_{nl}^c e_{lm}^b]$	8
C. How to perform the Γ expansion	9
D. Performing the Γ expansion	10
1. Contribution \bar{A} : trivial geometry $\text{tr}[\hat{P}_n]$	10
2. Contribution \bar{B} : quantum geometric tensors Q_{nm}^{ab} and Q_{nm}^{ac}	10
3. Contribution \bar{C} : quantum geometric tensor Q_{nm}^{bc}	10
4. Contribution \bar{D} : connections $C_{nm}^{b;ac}$, $C_{nm}^{c;ab}$	11
5. Contribution \bar{E} : to three-band traces $\text{tr}[e_{mn}^a e_{nl}^b e_{lm}^c]$, $\text{tr}[e_{mn}^a e_{nl}^c e_{lm}^b]$	11
E. Combining all contributions	12
S3. Symmetry decomposition of the nonlinear conductivity tensor	15
A. Symmetry transformation of band projectors and quantum geometric invariants	15
B. Symmetry transformation of nonlinear conductivity tensor	16
C. Magnetic space groups with no BCD	18
D. Magnetic space groups with no BCD and no interQMD	18
E. Magnetic space groups with no BCD and no interQMD in a plane	18
F. Nodal planes and QMD-driven NLHE	19
S4. Particle-hole and \mathcal{CPT} Symmetry	19
A. PH Symmetry	19
B. \mathcal{CPT} Symmetry	20
S5. Analytic results for low-energy models	20
A. Calculating the NLHE analytically for low-energy models	20
B. NLHE of a 3D tilted Dirac and Weyl point	21
C. Gapless limit of the nodal plane	22
D. NLHE of a 2D Dirac point	23
E. NLHE of a nodal line	23
S6. A note on band-dependent scattering rates	25
S7. Efficient numerical evaluation of NLHE	25

S1. NLHE IN KELDYSH FORMALISM AND THE SCATTERING RATE

The nonlinear Hall conductivity can be calculated using the Keldysh formalism; the corresponding result was provided to us by Pavel Ostrovsky (Eq. (2) in the main text). This result is consistent with previous literature results [58], and also with Ref. [59] up to a prefactor of 2. We attribute this discrepancy to a missing factor of $1/2$ in their derivation. In both cases, the Fermi sea contribution vanishes, as can be confirmed by explicit calculation. In our convention, $e > 0$.

The conductivity of a material is rendered finite by various scattering processes (arising from impurities, disorder, etc.). The constant phenomenological scattering rate that we include in our Green's functions accounts for these, and is comparable but not equivalent to the relaxation-time approximation employed in semiclassical calculations [69]. Indeed, as discussed in the main text, they do not capture the intraQMD contribution [31, 32, 56, 70]. Previously, some Green's function calculations began with expressions for the conductivity at optical frequencies ω_i in clean systems and introduced lifetimes via the substitution $\omega_i \rightarrow \omega_i + i\Gamma$ [5, 110]. As we now show, this procedure yields different results. For example, for Green's functions that depend on two frequencies,

$$\mathcal{G}_n^R(\epsilon + \omega_1 + \omega_2, \mathbf{k}) = \frac{1}{\epsilon + \omega_1 + \omega_2 - E_n(\mathbf{k}) + i0^+} \rightarrow \frac{1}{\epsilon + \omega_1 + \omega_2 - E_n(\mathbf{k}) + 2i\Gamma}, \quad (\text{S1})$$

while a Green's function of the form $\mathcal{G}_n^R(\epsilon + \omega_1, \mathbf{k})$ would only be assigned a self-energy of $i\Gamma$. In the DC limit, the substitution $\omega \rightarrow \omega + i\Gamma$ thus leads to retarded and advanced Green's functions $\mathcal{G}_n^{R/A}(\epsilon, \mathbf{k})$ evaluated at the same energy ϵ and momentum \mathbf{k} but with different self-energies. In our formalism, both become $(\epsilon - E_n(\mathbf{k}) + i\Gamma)^{-1}$ at $\omega_i = 0$. Rather than introducing self-energies via frequency substitutions, we assume that the system possesses an intrinsic scattering rate, which we approximate to be constant.

As mentioned in the main text, the constant scattering rate we use can be derived microscopically in a self-consistent Born approximation that includes the effects of white-noise disorder [66, 67]. The perturbative expansion to obtain this result is controlled by Γ being much smaller than the Fermi momentum k_F [66, 67]. In a complete treatment of disorder for a specific system, one would need to calculate a generally momentum-dependent self-energy as well as vertex corrections by explicitly including interactions with scattering potentials. Crossing diagrams—generally higher-order in Γ than their non-crossing counterparts—may also play a role, as in the linear-response case [66, 111]. The constant Γ we consider corresponds to calculating only the non-interacting diagrams, but with a self-energy included in the Green's functions. Our approach is designed to remain as agnostic as possible to the microscopic details of the system, isolating quantum geometric contributions to the intrinsic nonlinear Hall conductivity. The incorporation of aforementioned corrections is left for future work.

We discuss the perturbative expansion in the scattering rate Γ in Sec. S2 C and the implications of a band-dependent Γ in Sec. S6.

S2. GEOMETRIC DECOMPOSITION OF THE NONLINEAR CONDUCTIVITY TENSOR

In this section, we demonstrate how the nonlinear conductivity given in Eq. (2) is decomposed into its quantum geometric components. The summary of steps performed is as follows: We begin by expressing the Hamiltonian (and thus also the Green's functions) in terms of band projectors [48]. The obtained traces of projectors and their derivatives are then simplified into a minimal number of independent quantum geometric invariants, such as quantum metric and Berry curvature. The coefficients in front of each of these components are simplified and expanded in the scattering rate Γ . Finally, we combine all contributions and use integration by parts to streamline the result.

A. Introduction of band projectors and quantum geometric decomposition

1. Insertion of band projectors

We employ the fact that the Bloch Hamiltonian can be decomposed in terms of its band dispersion $E_n(\mathbf{k})$ and the corresponding projection $\hat{P}_n(\mathbf{k})$ to the eigenspace,

$$\hat{H}(\mathbf{k}) = \sum_n E_n(\mathbf{k}) \hat{P}_n(\mathbf{k}), \quad (\text{S2})$$

where we consider orthogonal projectors $\hat{P}_n(\mathbf{k})\hat{P}_m(\mathbf{k}) = \delta_{nm}\hat{P}_n(\mathbf{k})$. To be concrete, the projectors take the form $\hat{P}_n(\mathbf{k}) = \sum_\alpha |u_n^\alpha(\mathbf{k})\rangle\langle u_n^\alpha(\mathbf{k})|$ with Bloch functions $|u_n^\alpha(\mathbf{k})\rangle$, where α spans the possibly degenerate eigenspace of eigenvalue E_n . Note

that the band projector is explicitly $U(N)$ invariant for N -degenerate bands [51]. Due to the form of \hat{P}_n all subsequent decompositions are explicitly gauge-invariant by construction. The retarded and advanced Green's function yield the form

$$G^{R/A}(\epsilon, \mathbf{k}) = \frac{1}{\epsilon - \hat{H}(\mathbf{k}) \pm i\Gamma} = \sum_n \frac{\hat{P}_n(\mathbf{k})}{\epsilon - E_n(\mathbf{k}) \pm i\Gamma}. \quad (\text{S3})$$

Inserting the projector expansion for the Green's functions into Eq. (2) results in

$$\begin{aligned} \sigma^{a;bc} = & -\frac{e^3}{\hbar} \int \frac{d^d \mathbf{k}}{(2\pi)^d} \int d\epsilon \frac{\partial f(\epsilon)}{\partial \epsilon} \left[\sum_{m,n} w^{nm}(\epsilon) \text{tr}[\hat{P}_m(\partial^a \hat{H}) \hat{P}_n(\partial^b \partial^c \hat{H})] \right. \\ & \left. + \frac{1}{2} \sum_{l,m,n} u^{lmn}(\epsilon) \left(\text{tr}[\hat{P}_l(\partial^a \hat{H}) \hat{P}_m(\partial^b \hat{H}) \hat{P}_n(\partial^c \hat{H})] + \text{tr}[\hat{P}_l(\partial^a \hat{H}) \hat{P}_m(\partial^c \hat{H}) \hat{P}_n(\partial^b \hat{H})] \right) \right], \quad (\text{S4}) \end{aligned}$$

where we drop the explicit reference to the momentum dependence for shorter notation. Note the explicit $b \leftrightarrow c$ symmetry. We keep the momentum derivatives of the Bloch Hamiltonian explicit at that point. The functions $w^{nm}(\epsilon)$ and $u^{lmn}(\epsilon)$, which also depend on the energies of the bands, are given by

$$\begin{aligned} w^{nm}(\epsilon) &= -\frac{1}{2} (A_n(\epsilon) G_m^A(\epsilon)^2 + A_m(\epsilon) G_n^R(\epsilon)^2) \\ &= -\frac{\Gamma}{2\pi(E_m + i\Gamma)^2(\Gamma^2 + E_n^2)} - \frac{\Gamma}{2\pi(\Gamma^2 + E_m^2)(E_n - i\Gamma)^2}, \quad (\text{S5}) \end{aligned}$$

$$\begin{aligned} u^{lmn}(\epsilon) &= -A_m(\epsilon) G_l^A(\epsilon)^2 G_n^A(\epsilon) - A_l(\epsilon) G_m^R(\epsilon)^2 G_n^R(\epsilon) \\ &= \frac{\Gamma}{\pi(\Gamma^2 + E_l^2)(E_m - i\Gamma)^2(E_n - i\Gamma)} + \frac{\Gamma}{\pi(E_l + i\Gamma)^2(\Gamma^2 + E_m^2)(E_n + i\Gamma)}, \quad (\text{S6}) \end{aligned}$$

where we used the spectral function

$$A_n(\epsilon) = -\frac{1}{2\pi i} (G^R(\epsilon) - G^A(\epsilon)) = \frac{\Gamma}{\pi(\Gamma^2 + (\epsilon - E_n)^2)}. \quad (\text{S7})$$

At zero temperature $\frac{\partial f(\epsilon)}{\partial \epsilon} = -\delta(\epsilon)$ such that

$$\begin{aligned} \sigma^{a;bc} = & \frac{e^3}{\hbar} \int \frac{d^d \mathbf{k}}{(2\pi)^d} \left[\sum_{m,n} w^{nm} \text{tr}[\hat{P}_m(\partial^a \hat{H}) \hat{P}_n(\partial^b \partial^c \hat{H})] \right. \\ & \left. + \frac{1}{2} \sum_{l,m,n} u^{lmn} \left(\text{tr}[\hat{P}_l(\partial^a \hat{H}) \hat{P}_m(\partial^b \hat{H}) \hat{P}_n(\partial^c \hat{H})] + \text{tr}[\hat{P}_l(\partial^a \hat{H}) \hat{P}_m(\partial^c \hat{H}) \hat{P}_n(\partial^b \hat{H})] \right) \right], \quad (\text{S8}) \end{aligned}$$

where $w^{nm} = w^{nm}(0)$ and $u^{lmn} = u^{lmn}(0)$.

2. Summary of quantum geometric invariants

We briefly summarize and set the notation for the quantum geometric quantities in their projector form that we will use hereafter [6, 48]. The single- and multi-band quantum geometric tensor are defined as

$$Q_n^{ab} = \text{tr}[\hat{P}_n(\partial^a \hat{P}_n)(\partial^b \hat{P}_n)], \quad (\text{S9})$$

$$Q_{mn}^{ab} = \text{tr}[\hat{P}_n(\partial^a \hat{P}_m)(\partial^b \hat{P}_n)]. \quad (\text{S10})$$

The (two-band) quantum geometric connection $C_{mn}^{a;bc}$ is defined as

$$C_{mn}^{a;bc} = \text{tr} \left[P_n(\partial^b \hat{P}_m) ((\partial^a \partial^c \hat{P}_n) + (\partial^a \hat{P}_m)(\partial^c \hat{P}_n)) \right]. \quad (\text{S11})$$

There is also a single-band connection, or skewness tensor $Q_n^{a;bc}$

$$Q_n^{a;bc} = \text{tr}[\hat{P}_n(\partial^a \hat{P}_n)(\partial^b \partial^c \hat{P}_n)] = Q_n^{a;cb}. \quad (\text{S12})$$

3. Quantum geometric decomposition

We now turn to decomposing the two types of traces appearing in Eq. (S8). The first derivative of the Bloch Hamiltonian decomposes as [48]

$$\hat{P}_m(\partial^a \hat{H}) \hat{P}_n = \delta_{mn} E_n^a \hat{P}_n - \epsilon_{mn} \hat{P}_m(\partial^a \hat{P}_n) \hat{P}_n \quad (\text{S13})$$

with $E_n^a = \partial^a E_n$ and $\epsilon_{mn} = E_m - E_n$. Moreover, $\hat{P}_m(\partial^a \hat{P}_n) \hat{P}_n = -\hat{P}_m(\partial^a \hat{P}_m) \hat{P}_n$. Using this decomposition, the trace involving three first derivatives of the Bloch Hamiltonian is expanded into

$$\text{tr}[\hat{P}_l(\partial^a \hat{H}) \hat{P}_m(\partial^b \hat{H}) \hat{P}_n(\partial^c \hat{H})] = \text{tr}[\hat{P}_l(\partial^a \hat{H}) \hat{P}_m \hat{P}_m(\partial^b \hat{H}) \hat{P}_n \hat{P}_n(\partial^c \hat{H}) \hat{P}_l] \quad (\text{S14})$$

$$\begin{aligned} &= \delta_{lm} \delta_{mn} \delta_{nl} E_m^a E_n^b E_l^c \text{tr}[\hat{P}_n \hat{P}_m \hat{P}_l] \\ &\quad + \delta_{lm} \epsilon_{mn} \epsilon_{nl} E_m^a \text{tr}[\hat{P}_m \hat{P}_m(\partial^b \hat{P}_n) \hat{P}_n \hat{P}_n(\partial^c \hat{P}_l) \hat{P}_l] \\ &\quad + \delta_{mn} \epsilon_{lm} \epsilon_{nl} E_n^b \text{tr}[\hat{P}_l(\partial^a \hat{P}_m) \hat{P}_m \hat{P}_n \hat{P}_n(\partial^c \hat{P}_l) \hat{P}_l] \\ &\quad + \delta_{nl} \epsilon_{lm} \epsilon_{mn} E_l^c \text{tr}[\hat{P}_l(\partial^a \hat{P}_m) \hat{P}_m \hat{P}_m(\partial^b \hat{P}_n) \hat{P}_n \hat{P}_l] \\ &\quad - \epsilon_{lm} \epsilon_{mn} \epsilon_{nl} \text{tr}[\hat{P}_l(\partial^a \hat{P}_m) \hat{P}_m \hat{P}_m(\partial^b \hat{P}_n) \hat{P}_n \hat{P}_n(\partial^c \hat{P}_l) \hat{P}_l] \end{aligned} \quad (\text{S15})$$

$$\begin{aligned} &= \delta_{lm} \delta_{mn} \delta_{nl} E_m^a E_n^b E_l^c \text{tr}[\hat{P}_m] \\ &\quad - \delta_{lm} \epsilon_{mn}^2 E_m^a \text{tr}[\hat{P}_m(\partial^b \hat{P}_n) \hat{P}_n(\partial^c \hat{P}_l)] \\ &\quad - \delta_{mn} \epsilon_{nl}^2 E_n^b \text{tr}[\hat{P}_l(\partial^a \hat{P}_m) \hat{P}_m(\partial^c \hat{P}_l)] \\ &\quad - \delta_{nl} \epsilon_{lm}^2 E_l^c \text{tr}[\hat{P}_l(\partial^a \hat{P}_m) \hat{P}_m(\partial^b \hat{P}_n)] \\ &\quad - \epsilon_{lm} \epsilon_{mn} \epsilon_{nl} \text{tr}[\hat{P}_l(\partial^a \hat{P}_m) \hat{P}_m(\partial^b \hat{P}_n) \hat{P}_n(\partial^c \hat{P}_l)]. \end{aligned} \quad (\text{S16})$$

Terms with two velocities, such as $E_m^a E_n^b$, vanish due to $\epsilon_{nn} = 0$. Using that $\epsilon_{nm} \neq 0 \Rightarrow n \neq m$ and $\hat{P}_n(\partial^a \hat{P}_m) \hat{P}_m = \hat{P}_n(\partial^a \hat{P}_m)$ for $n \neq m$, we obtain

$$\begin{aligned} &\text{tr}[\hat{P}_l(\partial^a \hat{H}) \hat{P}_m(\partial^b \hat{H}) \hat{P}_n(\partial^c \hat{H})] \\ &= \delta_{lm} \delta_{mn} \delta_{nl} E_m^a E_n^b E_l^c \text{tr}[\hat{P}_l] \\ &\quad - \delta_{lm} \epsilon_{mn}^2 E_m^a \text{tr}[\hat{P}_m(\partial^b \hat{P}_n)(\partial^c \hat{P}_m)] - \delta_{mn} \epsilon_{nl}^2 E_n^b \text{tr}[\hat{P}_l(\partial^a \hat{P}_m)(\partial^c \hat{P}_l)] - \delta_{nl} \epsilon_{lm}^2 E_l^c \text{tr}[\hat{P}_n(\partial^a \hat{P}_m)(\partial^b \hat{P}_n)] \\ &\quad - \epsilon_{lm} \epsilon_{mn} \epsilon_{nl} \text{tr}[\hat{P}_l(\partial^a \hat{P}_m)(\partial^b \hat{P}_n)(\partial^c \hat{P}_l)]. \end{aligned} \quad (\text{S17})$$

We can now identify the two-state quantum geometric tensor given in Eq. (S10) in the second line, arriving at

$$\begin{aligned} \text{tr}[\hat{P}_l(\partial^a \hat{H}) \hat{P}_m(\partial^b \hat{H}) \hat{P}_n(\partial^c \hat{H})] &= \delta_{lm} \delta_{mn} \delta_{nl} E_m^a E_n^b E_l^c \text{tr}[\hat{P}_l] \\ &\quad - \delta_{lm} \epsilon_{nm}^2 E_m^a Q_{nm}^{bc} - \delta_{mn} \epsilon_{ml}^2 E_m^b Q_{ml}^{ac} - \delta_{nl} \epsilon_{ln}^2 E_l^c Q_{ln}^{ab} \\ &\quad - \epsilon_{lm} \epsilon_{mn} \epsilon_{nl} \text{tr}[\hat{P}_l(\partial^a \hat{P}_m)(\partial^b \hat{P}_n)(\partial^c \hat{P}_l)]. \end{aligned} \quad (\text{S18})$$

The second trace in Eq. (S8) is more elaborate as it involves the second derivative of the Bloch Hamiltonian. To simplify the expression, we use the (hermitian) gauge-invariant interband transition rate in projector form [47, 48]

$$\hat{e}_{mn}^a = i \hat{P}_m(\partial^a \hat{P}_n) \hat{P}_n, \quad (\text{S19})$$

such that the first derivative of the Bloch Hamiltonian yields the form

$$\hat{P}_m(\partial^a \hat{H}) \hat{P}_n = \delta_{mn} E_n^a \hat{P}_n + i \epsilon_{mn} \hat{e}_{mn}^a. \quad (\text{S20})$$

We use this decomposition in combination with the completeness of the band projectors $\sum_l \hat{P}_l(\mathbf{k}) = \mathbf{1}$ to obtain

$$\hat{P}_m(\partial^b \partial^c \hat{H}) \hat{P}_n = \sum_{l_1, l_2} \hat{P}_m(\partial^b [\hat{P}_{l_1}(\partial^c \hat{H}) \hat{P}_{l_2}]) \hat{P}_n \quad (\text{S21})$$

$$= \sum_{l_1, l_2} \hat{P}_m(\partial^b [\delta_{l_1, l_2} E_{l_1}^c \hat{P}_{l_1}]) \hat{P}_n + i \sum_{l_1, l_2} \hat{P}_m(\partial^b [\epsilon_{l_1 l_2} \hat{e}_{l_1 l_2}^c]) \hat{P}_n \quad (\text{S22})$$

$$= \sum_{l_1} E_{l_1}^{bc} \hat{P}_m \hat{P}_{l_1} \hat{P}_n + \sum_{l_1} E_{l_1}^c \hat{P}_m(\partial^b \hat{P}_{l_1}) \hat{P}_n + i \sum_{l_1, l_2} \epsilon_{l_1 l_2}^b \hat{P}_m \hat{e}_{l_1 l_2}^c \hat{P}_n + i \sum_{l_1, l_2} \epsilon_{l_1 l_2} \hat{P}_m(\partial^b \hat{e}_{l_1 l_2}^c) \hat{P}_n \quad (\text{S23})$$

$$= \delta_{mn} E_n^{bc} \hat{P}_n + i \epsilon_{mn}^c \hat{e}_{mn}^b + i \epsilon_{mn}^b \hat{e}_{mn}^c + i \sum_{l_1, l_2} \epsilon_{l_1 l_2} \hat{P}_m(\partial^b \hat{e}_{l_1 l_2}^c) \hat{P}_n. \quad (\text{S24})$$

using $\hat{P}_m(\partial^b \hat{P}_l) \hat{P}_n = 0$ for $l \neq n, m$. We introduced the short notation $E_n^{bc} = \partial^b \partial^c E_n$ and $\epsilon_{mn}^b = \partial^b \epsilon_{mn}$. The last term needs further consideration. We note that it vanishes if none of the indices l_1 and l_2 are m or n , since

$$\hat{P}_m(\partial^b \hat{e}_{l_1 l_2}^c) \hat{P}_n = i \hat{P}_m(\partial^b \hat{P}_{l_1})(\partial^c \hat{P}_{l_2}) \hat{P}_n + i \hat{P}_m \hat{P}_{l_1}(\partial^b \partial^c \hat{P}_{l_2}) \hat{P}_n + i \hat{P}_m \hat{P}_{l_1}(\partial^c \hat{P}_{l_2})(\partial^b \hat{P}_{l_2}) \hat{P}_n \quad (\text{S25})$$

$$= i \delta_{nl_2} \hat{P}_m(\partial^b \hat{P}_{l_1})(\partial^c \hat{P}_n) \hat{P}_n + i \delta_{ml_1} \delta_{nl_2} \hat{P}_m(\partial^b \partial^c \hat{P}_n) \hat{P}_n + i \delta_{ml_1} \hat{P}_m(\partial^c \hat{P}_{l_2})(\partial^b \hat{P}_{l_2}) \hat{P}_n. \quad (\text{S26})$$

Using $l_1 \neq l_2$ due to $\epsilon_{l_1 l_2}$, we obtain

$$\begin{aligned} \sum_{l_1, l_2} \epsilon_{l_1 l_2} \hat{P}_m(\partial^b \hat{e}_{l_1 l_2}^c) \hat{P}_n &= \epsilon_{mn} \hat{P}_m(\partial^b \hat{e}_{mn}^c) \hat{P}_n + \epsilon_{nm} \hat{P}_m(\partial^b \hat{e}_{nm}^c) \hat{P}_n \\ &+ \sum_{l \neq n, m} \epsilon_{lm} \hat{P}_m(\partial^b \hat{e}_{lm}^c) \hat{P}_n + \sum_{l \neq n, m} \epsilon_{ln} \hat{P}_m(\partial^b \hat{e}_{ln}^c) \hat{P}_n \\ &+ \sum_{l \neq n, m} \epsilon_{ml} \hat{P}_m(\partial^b \hat{e}_{ml}^c) \hat{P}_n + \sum_{l \neq n, m} \epsilon_{nl} \hat{P}_m(\partial^b \hat{e}_{nl}^c) \hat{P}_n \end{aligned} \quad (\text{S27})$$

$$= \epsilon_{mn} \hat{P}_m(\partial^b \hat{e}_{mn}^c) \hat{P}_n + \sum_{l \neq n, m} \epsilon_{ml} \hat{P}_m(\partial^b \hat{e}_{ml}^c) \hat{P}_n + \sum_{l \neq n, m} \epsilon_{ln} \hat{P}_m(\partial^b \hat{e}_{ln}^c) \hat{P}_n, \quad (\text{S28})$$

where we first considered the cases with either l_1 or l_2 are equal to n or m and took all constraints of Eq. (S26) into account in the second step. Now using Eq. (S26) and $l \neq m, n$, the contributions in the sums can be simplified into

$$\hat{P}_m(\partial^b \hat{e}_{ml}^c) \hat{P}_n = i \hat{P}_m(\partial^c \hat{P}_l)(\partial^b \hat{P}_l) \hat{P}_n = i \hat{P}_m(\partial^c \hat{P}_l) \hat{P}_l(\partial^b \hat{P}_l) \hat{P}_n = -i \hat{P}_m(\partial^c \hat{P}_l) \hat{P}_l(\partial^b \hat{P}_n) \hat{P}_n = i \hat{e}_{ml}^c \hat{e}_{ln}^b, \quad (\text{S29})$$

and

$$\hat{P}_m(\partial^b \hat{e}_{ln}^c) \hat{P}_n = i \hat{P}_m(\partial^b \hat{P}_l)(\partial^c \hat{P}_n) \hat{P}_n = i \hat{P}_m(\partial^b \hat{P}_l) \hat{P}_l(\partial^c \hat{P}_n) \hat{P}_n = -i \hat{e}_{ml}^c \hat{e}_{ln}^b. \quad (\text{S30})$$

Introducing the covariant derivative of the transition dipole moment defined by $\nabla^a \hat{e}_{mn}^b \equiv \hat{P}_m(\partial^a \hat{e}_{mn}^b) \hat{P}_n$ and combining the result with the other contributions in Eq. (S24), we conclude

$$\hat{P}_m(\partial^b \partial^c \hat{H}) \hat{P}_n = \delta_{mn} E_n^{bc} \hat{P}_n + i \epsilon_{mn}^c \hat{e}_{mn}^b + i \epsilon_{mn}^b \hat{e}_{mn}^c + i \epsilon_{mn} \nabla^b \hat{e}_{mn}^c - \sum_{l \neq m, n} \epsilon_{ml} \hat{e}_{ml}^c \hat{e}_{ln}^b + \sum_{l \neq m, n} \epsilon_{ln} \hat{e}_{ml}^b \hat{e}_{ln}^c, \quad (\text{S31})$$

For completeness, we also provide an alternate form, symmetrized in the indices b and c . First note that

$$- \sum_{l \neq n, m} \epsilon_{ml} \hat{e}_{ml}^c \hat{e}_{ln}^b + \sum_{l \neq n, m} \epsilon_{ln} \hat{e}_{ml}^b \hat{e}_{ln}^c = \hat{P}_m(\partial^c \hat{P}_m)(\hat{H} - E_m)(\partial^b \hat{P}_n) \hat{P}_n + \hat{P}_m(\partial^b \hat{P}_m)(\hat{H} - E_n)(\partial^c \hat{P}_n) \hat{P}_n, \quad (\text{S32})$$

using the projector decomposition of the Bloch Hamiltonian. Also symmetrizing $i \epsilon_{mn} \nabla^b \hat{e}_{mn}^c$, one obtains

$$\begin{aligned} \hat{P}_m(\partial^b \partial^c \hat{H}) \hat{P}_n &= \delta_{mn} E_n^{bc} \hat{P}_n + i \epsilon_{mn}^c \hat{e}_{mn}^b + i \epsilon_{mn}^b \hat{e}_{mn}^c \\ &+ \frac{i}{2} \epsilon_{mn} \nabla^b \hat{e}_{mn}^c + \frac{i}{2} \epsilon_{mn} \nabla^c \hat{e}_{mn}^b \\ \hat{P}_m(\partial^c \hat{P}_m)(\hat{H} - \frac{1}{2}[E_n + E_m])(\partial^b \hat{P}_n) \hat{P}_n &+ \hat{P}_m(\partial^b \hat{P}_m)(\hat{H} - \frac{1}{2}[E_n + E_m])(\partial^c \hat{P}_n) \hat{P}_n, \end{aligned} \quad (\text{S33})$$

generalizing a gauge-invariant separation for single-degenerate bands [112].

To proceed with the calculation at hand, we now combine Eq. (S31) with Eq. (S20), to calculate the other trace appearing in the conductivity Eq. (S8) :

$$\begin{aligned} \text{tr}[\hat{P}_m(\partial^a \hat{H}) \hat{P}_n(\partial^b \partial^c \hat{H})] &= \delta_{mn} E_n^a E_n^{bc} \text{tr}[\hat{P}_n] \\ &- \delta_{mn} E_n^a \sum_{l \neq m, n} \epsilon_{nl} \text{tr}[\hat{P}_n \hat{e}_{nl}^c \hat{e}_{ln}^b] + \delta_{mn} E_n^a \sum_{l \neq m, n} \epsilon_{ln} \text{tr}[\hat{P}_n \hat{e}_{nl}^b \hat{e}_{ln}^c] \\ &- \epsilon_{mn} \epsilon_{nm}^c \text{tr}[\hat{e}_{mn}^a \hat{e}_{nm}^b] - \epsilon_{mn} \epsilon_{nm}^b \text{tr}[\hat{e}_{mn}^a \hat{e}_{nm}^c] \\ &- \epsilon_{mn} \epsilon_{nm} \text{tr}[\hat{e}_{mn}^a \nabla^b \hat{e}_{nm}^c] \\ &- i \epsilon_{mn} \sum_{l \neq m, n} \epsilon_{nl} \text{tr}[\hat{e}_{mn}^a \hat{e}_{nl}^c \hat{e}_{lm}^b] + i \epsilon_{mn} \sum_{l \neq m, n} \epsilon_{lm} \text{tr}[\hat{e}_{mn}^a \hat{e}_{nl}^b \hat{e}_{lm}^c]. \end{aligned} \quad (\text{S34})$$

Now $\hat{P}_n \hat{e}_{nl}^b = \hat{e}_{nl}^b$, and we also identify the quantum geometric tensor Eq. (S10), expressed as $Q_{nm}^{ab} = -\text{tr}[\hat{e}_{mn}^a \hat{e}_{nm}^b]$:

$$\begin{aligned} \text{tr}[\hat{P}_m(\partial^a \hat{H}) \hat{P}_n(\partial^b \partial^c \hat{H})] &= \delta_{mn} E_n^a E_n^{bc} \text{tr}[\hat{P}_n] \\ &+ \delta_{mn} E_n^a \sum_{l \neq m, n} \epsilon_{nl} Q_{ln}^{cb} - \delta_{mn} E_n^a \sum_{l \neq m, n} \epsilon_{ln} Q_{ln}^{bc} \\ &+ \epsilon_{mn} \epsilon_{nm}^c Q_{nm}^{ab} + \epsilon_{mn} \epsilon_{nm}^b Q_{nm}^{ac} \\ &- \epsilon_{mn} \epsilon_{nm} \text{tr}[\hat{e}_{mn}^a \nabla^b \hat{e}_{nm}^c] \\ &- i \epsilon_{mn} \sum_{l \neq m, n} \epsilon_{nl} \text{tr}[\hat{e}_{mn}^a \hat{e}_{nl}^c \hat{e}_{lm}^b] + i \epsilon_{mn} \sum_{l \neq m, n} \epsilon_{lm} \text{tr}[\hat{e}_{mn}^a \hat{e}_{nl}^b \hat{e}_{lm}^c]. \end{aligned} \quad (\text{S35})$$

The quantum geometric connection Eq. (S11) is also given by $C_{mn}^{a;bc} = -\text{tr}[\hat{e}_{nm}^b \nabla^a \hat{e}_{mn}^c]$ for $n \neq m$. We also reorder indices in the ϵ :

$$\begin{aligned} \text{tr}[\hat{P}_m(\partial^a \hat{H}) \hat{P}_n(\partial^b \partial^c \hat{H})] &= \delta_{mn} E_n^a E_n^{bc} \text{tr}[\hat{P}_n] \\ &- \delta_{mn} E_n^a \sum_{l \neq m, n} \epsilon_{ln} (Q_{ln}^{bc} + Q_{ln}^{cb}) \\ &- \epsilon_{nm} \epsilon_{nm}^c Q_{nm}^{ab} - \epsilon_{nm} \epsilon_{nm}^b Q_{nm}^{ac} \\ &- \epsilon_{nm}^2 C_{nm}^{b;ac} \\ &+ i \epsilon_{nm} \sum_{l \neq m, n} \epsilon_{nl} \text{tr}[\hat{e}_{mn}^a \hat{e}_{nl}^c \hat{e}_{lm}^b] - i \epsilon_{nm} \sum_{l \neq m, n} \epsilon_{lm} \text{tr}[\hat{e}_{mn}^a \hat{e}_{nl}^b \hat{e}_{lm}^c]. \end{aligned} \quad (\text{S36})$$

Finally, we symmetrize in b, c , since the initial trace has this symmetry:

$$\begin{aligned} \text{tr}[\hat{P}_m(\partial^a \hat{H}) \hat{P}_n(\partial^b \partial^c \hat{H})] &= \delta_{mn} E_n^a E_n^{bc} \text{tr}[\hat{P}_n] \\ &- 2 \delta_{mn} E_n^a \sum_{l \neq n} \epsilon_{ln} Q_{(ln)}^{bc} \\ &- \epsilon_{nm} \epsilon_{nm}^c Q_{nm}^{ab} - \epsilon_{nm} \epsilon_{nm}^b Q_{nm}^{ac} \\ &- \frac{1}{2} \epsilon_{nm}^2 C_{nm}^{b;ac} - \frac{1}{2} \epsilon_{nm}^2 C_{nm}^{c;ab} \\ &+ \frac{i}{2} \epsilon_{nm} \sum_{l \neq m, n} (\epsilon_{nl} - \epsilon_{lm}) (\text{tr}[\hat{e}_{mn}^a \hat{e}_{nl}^c \hat{e}_{lm}^b] + \text{tr}[\hat{e}_{mn}^a \hat{e}_{nl}^b \hat{e}_{lm}^c]). \end{aligned} \quad (\text{S37})$$

Here, $(a_1 \dots a_n)$ indicates symmetrization of a tensor:

$$T_{(i_1 i_2 \dots i_n)} = \frac{1}{n!} \sum_{\sigma \in \mathfrak{S}_n} T_{i_{\sigma 1} i_{\sigma 2} \dots i_{\sigma n}}, \quad (\text{S38})$$

where the summation extends over the symmetric group on n symbols, and a conventional prefactor of $1/(n!)$ was included. We define antisymmetrization, denoted by $T_{[a_1 \dots a_n]}$, similarly:

$$T_{[i_1 i_2 \dots i_n]} = \frac{1}{n!} \sum_{\sigma \in \mathfrak{S}_n} \text{sgn}(\sigma) T_{i_{\sigma 1} i_{\sigma 2} \dots i_{\sigma n}}, \quad (\text{S39})$$

where $\text{sgn}(\sigma)$ denotes the signature of the permutation σ . Note also that $Q_{(mn)}^{bc} = Q_{(mn)}^{(bc)} = Q_{mn}^{(bc)}$.

B. Collecting contributions to quantum geometric quantities

Having expanded the traces containing the Hamiltonian into quantum geometric quantities in the previous section, we now return to Eq. (S8) and collect the coefficient in front of each independent geometric quantity (those that appeared in Eqs. (S18), (S37)) in the conductivity. Recall that the functions w^{nm}, u^{lmn} are defined in Eqs. (S5), (S6). To streamline the calculation

and clarify notation, we absorb the prefactor and momentum integral $\frac{e^3}{\hbar} \int \frac{d^d \mathbf{k}}{(2\pi)^d}$ into a compact notation $\int_{\mathbf{k}}$, and decompose the conductivity into five distinct contributions:

$$\sigma^{a;bc} = \underbrace{\int_{\mathbf{k}} (\dots) \text{tr}[\hat{P}_n]}_A + \underbrace{\int_{\mathbf{k}} (\dots) (Q_{nm}^{ab} + Q_{nm}^{ac})}_B + \underbrace{\int_{\mathbf{k}} (\dots) Q_{nm}^{bc}}_C \quad (\text{S40})$$

$$+ \underbrace{\int_{\mathbf{k}} (\dots) (C_{nm}^{b;ac} + C_{nm}^{c;ab})}_D + \underbrace{\int_{\mathbf{k}} (\dots) (\text{tr}[e_{mn}^a e_{nl}^b e_{lm}^c] + \text{tr}[e_{mn}^a e_{nl}^c e_{lm}^b])}_E, \quad (\text{S41})$$

where each term represents an integral over a band-structure-dependent prefactor (indicated by (\dots)), multiplied by a distinct quantum geometric invariant. We used the $b \leftrightarrow c$ symmetry to collect the quantum geometric tensors Q_{nm}^{ab} , Q_{nm}^{ac} , the connections $C_{nm}^{b;ac}$, $C_{nm}^{c;ab}$, and the three-band traces $\text{tr}[e_{mn}^a e_{nl}^b e_{lm}^c]$, $\text{tr}[e_{mn}^a e_{nl}^c e_{lm}^b]$ into one term each. We collect the quantities A , B , C , D , and E in what follows. We continue treating the general case $b \neq c$, which will reduce to the result shown in the main text upon setting $c = b$.

1. Contribution A: trivial geometry $\text{tr}[\hat{P}_n]$

All three traces contribute a diagonal (in the band indices) term:

$$A = \int_{\mathbf{k}} \left(\sum_n \frac{u^{nnn}}{2} E_n^a E_n^b E_n^c \text{tr}[\hat{P}_n] + \sum_n \frac{u^{nnn}}{2} E_n^a E_n^c E_n^b \text{tr}[\hat{P}_n] + \sum_n w^{nn} E_n^a E_n^b \text{tr}[\hat{P}_n] \right). \quad (\text{S42})$$

By integrating by parts in momentum, we may combine these contributions. The main technique is to use momentum derivatives of the energy as internal derivatives (since u^{nnn} , w^{nn} are functions of E_n), i.e.,

$$\partial^a f(E_n) = f'(E_n) E_n^a. \quad (\text{S43})$$

Denoting indefinite integrals in E_n by $\int \dots dE_n$, the above can be manipulated into

$$A = \int_{\mathbf{k}} \sum_n [u^{nnn} E_n^a E_n^b E_n^c + w^{nn} E_n^a E_n^b] \text{tr}[\hat{P}_n] \quad (\text{S44})$$

$$= \int_{\mathbf{k}} \sum_n \left[- \left(\int u^{nnn} dE_n \right) \partial^a (E_n^b E_n^c) - \left(\int w^{nn} dE_n \right) E_n^{abc} \right] \text{tr}[\hat{P}_n] \quad (\text{S45})$$

$$= \int_{\mathbf{k}} \sum_n \left[- \left(\int u^{nnn} dE_n \right) (E_n^c E_n^{ab} + E_n^b E_n^{ac}) - \left(\int w^{nn} dE_n \right) E_n^{abc} \right] \text{tr}[\hat{P}_n] \quad (\text{S46})$$

$$= \int_{\mathbf{k}} \sum_n \left[\left(\iint u^{nnn} dE_n dE_n \right) - \left(\int w^{nn} dE_n \right) \right] E_n^{abc} \text{tr}[\hat{P}_n]. \quad (\text{S47})$$

2. Contribution B: quantum geometric tensors Q_{nm}^{ab} and Q_{nm}^{ac}

Again all traces contribute a term proportional to Q_{nm}^{ab} (or equivalently to Q_{nm}^{ac}):

$$B = \int_{\mathbf{k}} \left(- \sum_{n \neq m} w^{nm} \epsilon_{nm} \epsilon_{nm}^c Q_{nm}^{ab} - \sum_{n \neq m} \left(\frac{u^{mnm}}{2} E_m^c + \frac{u^{mnn}}{2} E_n^c \right) \epsilon_{nm}^2 Q_{nm}^{ab} \right) + (b \leftrightarrow c). \quad (\text{S48})$$

It is convenient to separate Q_{nm}^{ab} into its symmetric and antisymmetric part in n, m , which also correspond to the real and imaginary part respectively:

$$B = \int_{\mathbf{k}} \left(- \sum_{n \neq m} w^{nm} \epsilon_{nm} \epsilon_{nm}^c Q_{(nm)}^{ab} - \sum_{n \neq m} \left(\frac{u^{mnm}}{2} E_m^c + \frac{u^{mnn}}{2} E_n^c \right) \epsilon_{nm}^2 Q_{(nm)}^{ab} \right. \\ \left. - \sum_{n \neq m} w^{nm} \epsilon_{nm} \epsilon_{nm}^c Q_{[nm]}^{ab} - \sum_{n \neq m} \left(\frac{u^{mnm}}{2} E_m^c + \frac{u^{mnn}}{2} E_n^c \right) \epsilon_{nm}^2 Q_{[nm]}^{ab} \right) + (b \leftrightarrow c). \quad (\text{S49})$$

Expanding $\epsilon_{nm}^c = E_n^c - E_m^c$:

$$\begin{aligned}
B = \int_{\mathbf{k}} & \left(- \sum_{n \neq m} w^{nm} \epsilon_{nm} E_n^c Q_{(nm)}^{ab} - \sum_{n \neq m} \left(\frac{u^{nmn}}{2} E_n^c + \frac{u^{mnn}}{2} E_n^c \right) \epsilon_{nm}^2 Q_{(nm)}^{ab} \right. \\
& + \sum_{n \neq m} w^{nm} \epsilon_{nm} E_m^c Q_{(nm)}^{ab} - \sum_{n \neq m} \left(-\frac{u^{nmn}}{2} E_n^c + \frac{u^{mnn}}{2} E_n^c \right) \epsilon_{nm}^2 Q_{[nm]}^{ab} \\
& \left. + \sum_{n \neq m} -w^{nm} \epsilon_{nm} E_n^c Q_{[nm]}^{ab} + \sum_{n \neq m} w^{nm} \epsilon_{nm} E_m^c Q_{[nm]}^{ab} \right) + (b \leftrightarrow c). \tag{S50}
\end{aligned}$$

We continue by relabeling sums so that all E^c are in band n :

$$\begin{aligned}
B = \int_{\mathbf{k}} & \left(- \sum_{n \neq m} w^{nm} \epsilon_{nm} E_n^c Q_{(nm)}^{ab} - \sum_{n \neq m} \left(\frac{u^{nmn}}{2} E_n^c + \frac{u^{mnn}}{2} E_n^c \right) \epsilon_{nm}^2 Q_{(nm)}^{ab} \right. \\
& - \sum_{n \neq m} w^{mn} \epsilon_{nm} E_n^c Q_{(nm)}^{ab} - \sum_{n \neq m} \left(-\frac{u^{nmn}}{2} E_n^c + \frac{u^{mnn}}{2} E_n^c \right) \epsilon_{nm}^2 Q_{[nm]}^{ab} \\
& \left. - \sum_{n \neq m} w^{nm} \epsilon_{nm} E_n^c Q_{[nm]}^{ab} + \sum_{n \neq m} w^{mn} \epsilon_{nm} E_n^c Q_{[nm]}^{ab} \right) + (b \leftrightarrow c). \tag{S51}
\end{aligned}$$

Collecting identical contributions finally gives

$$B = \int_{\mathbf{k}} \left(- \sum_{n \neq m} \left(2w^{(nm)} + \frac{u^{nmn}}{2} \epsilon_{nm} + \frac{u^{mnn}}{2} \epsilon_{nm} \right) \epsilon_{nm} E_n^c Q_{(nm)}^{ab} \right) \tag{S52}$$

$$- \sum_{n \neq m} \left(2w^{[nm]} - \frac{u^{nmn}}{2} \epsilon_{nm} + \frac{u^{mnn}}{2} \epsilon_{nm} \right) \epsilon_{nm} E_n^c Q_{[nm]}^{ab} \Big) + (b \leftrightarrow c). \tag{S53}$$

3. Contribution C: quantum geometric tensor Q_{nm}^{bc}

The last quantum geometric tensor contribution is Q_{nm}^{bc} . Collecting all coefficients yields

$$C = \int_{\mathbf{k}} \left(\sum_{n \neq m} 2w^{nn} \epsilon_{nm} E_n^a Q_{(nm)}^{bc} - \sum_{n \neq m} \left(\frac{u^{mnm}}{2} E_m^a + \frac{u^{nmm}}{2} E_n^a \right) \epsilon_{nm}^2 Q_{nm}^{bc} \right). \tag{S54}$$

As previously, we separate into symmetric and antisymmetric components:

$$\begin{aligned}
C = \int_{\mathbf{k}} & \left(\sum_{n \neq m} 2w^{nn} \epsilon_{nm} E_n^a Q_{(nm)}^{bc} - \sum_{n \neq m} \left(\frac{u^{nmm}}{2} E_n^a + \frac{u^{mnm}}{2} E_n^a \right) \epsilon_{nm}^2 Q_{(nm)}^{bc} \right. \\
& \left. - \sum_{n \neq m} \left(-\frac{u^{nmm}}{2} E_n^a + \frac{u^{mnm}}{2} E_n^a \right) \epsilon_{nm}^2 Q_{[nm]}^{bc} \right). \tag{S55}
\end{aligned}$$

The third sum is evidently 0, and the result simplifies to

$$C = \int_{\mathbf{k}} \left(\sum_{n \neq m} 2w^{nn} \epsilon_{nm} E_n^a Q_{(nm)}^{bc} - \sum_{n \neq m} u^{nmm} E_n^a \epsilon_{nm}^2 Q_{(nm)}^{bc} \right) \tag{S56}$$

$$= \int_{\mathbf{k}} \left(\sum_{n \neq m} (2w^{nn} - u^{nmm} \epsilon_{nm}) \epsilon_{nm} E_n^a Q_{(nm)}^{bc} \right). \tag{S57}$$

4. *Contribution D: connections $C_{nm}^{b;ac}$, $C_{nm}^{c;ab}$*

The total contribution from connections is

$$D = \int_{\mathbf{k}} \left(- \sum_{m,n} \frac{1}{2} w^{nm} \epsilon_{nm}^2 C_{nm}^{b;ac} - \sum_{m,n} \frac{1}{2} w^{nm} \epsilon_{nm}^2 C_{nm}^{c;ab} \right). \quad (\text{S58})$$

5. *Contribution E: three-band traces $\text{tr}[e_{mn}^a e_{nl}^b e_{lm}^c]$, $\text{tr}[e_{mn}^a e_{nl}^c e_{lm}^b]$*

The contribution to the three-band traces $\text{tr}[e_{mn}^a e_{nl}^b e_{lm}^c]$, $\text{tr}[e_{mn}^a e_{nl}^c e_{lm}^b]$ is given by

$$E = \int_{\mathbf{k}} \left(\sum_{m,n} \frac{i}{2} w^{nm} \epsilon_{nm} \sum_{l \neq m,n} (\epsilon_{nl} - \epsilon_{lm}) \text{tr}[e_{mn}^a e_{nl}^b e_{lm}^c] - i \sum_{l,m,n} \frac{u^{mnl}}{2} \epsilon_{mn} \epsilon_{nl} \epsilon_{lm} \text{tr}[\hat{e}_{mn}^a \hat{e}_{nl}^b \hat{e}_{lm}^c] \right) + (b \leftrightarrow c), \quad (\text{S59})$$

which we combine into a single sum:

$$E = \int_{\mathbf{k}} \left(\frac{i}{2} \sum_{(l,m,n)} \left(w^{nm} \epsilon_{nm} (\epsilon_{nl} - \epsilon_{lm}) - u^{mnl} \epsilon_{mn} \epsilon_{nl} \epsilon_{lm} \right) \left(\text{tr}[e_{mn}^a e_{nl}^b e_{lm}^c] + \text{tr}[e_{mn}^a e_{nl}^c e_{lm}^b] \right) \right). \quad (\text{S60})$$

We indicate summing only over different band indices with the notation (l, m, n) (i.e. $l \neq m, l \neq n, m \neq n$). Now

$$\text{tr}[e_{mn}^a e_{nl}^b e_{lm}^c]^* = \text{tr}[e_{ml}^c e_{ln}^b e_{nm}^a] = \text{tr}[e_{nm}^a e_{ml}^c e_{ln}^b], \quad (\text{S61})$$

effectively permuting b, c and n, m at the same time. The contribution may then be written as

$$E = \int_{\mathbf{k}} \left(\frac{i}{2} \sum_{(l,m,n)} \left(w^{nm} \epsilon_{nm} (\epsilon_{nl} - \epsilon_{lm}) - u^{mnl} \epsilon_{mn} \epsilon_{nl} \epsilon_{lm} \right) \left(\text{tr}[e_{mn}^a e_{nl}^b e_{lm}^c] + \text{tr}[e_{nm}^a e_{ml}^c e_{ln}^b]^* \right) \right). \quad (\text{S62})$$

We now separate the functions w, u into symmetric and antisymmetric parts in n, m :

$$E = \int_{\mathbf{k}} \left(\frac{i}{2} \sum_{(l,m,n)} \left(w^{(nm)} \epsilon_{nm} (\epsilon_{nl} - \epsilon_{lm}) - u^{(mn)l} \epsilon_{mn} \epsilon_{nl} \epsilon_{lm} \right) \left(\text{tr}[e_{mn}^a e_{nl}^b e_{lm}^c] + \text{tr}[e_{nm}^a e_{ml}^c e_{ln}^b]^* \right) \right. \\ \left. + \frac{i}{2} \sum_{(l,m,n)} \left(w^{[nm]} \epsilon_{nm} (\epsilon_{nl} - \epsilon_{lm}) - u^{[mn]l} \epsilon_{mn} \epsilon_{nl} \epsilon_{lm} \right) \left(\text{tr}[e_{mn}^a e_{nl}^b e_{lm}^c] + \text{tr}[e_{nm}^a e_{ml}^c e_{ln}^b]^* \right) \right). \quad (\text{S63})$$

Taking the antisymmetry of the ϵ combinations multiplying w, u into consideration, we reindex sums to permute the indices n, m of $\text{tr}[e_{nm}^a e_{ml}^c e_{ln}^b]^*$:

$$E = \int_{\mathbf{k}} \left(\frac{i}{2} \sum_{(l,m,n)} \left(w^{(nm)} \epsilon_{nm} (\epsilon_{nl} - \epsilon_{lm}) - u^{(mn)l} \epsilon_{mn} \epsilon_{nl} \epsilon_{lm} \right) \left(\text{tr}[e_{mn}^a e_{nl}^b e_{lm}^c] - \text{tr}[e_{mn}^a e_{nl}^c e_{lm}^b]^* \right) \right. \\ \left. + \frac{i}{2} \sum_{(l,m,n)} \left(w^{[nm]} \epsilon_{nm} (\epsilon_{nl} - \epsilon_{lm}) - u^{[mn]l} \epsilon_{mn} \epsilon_{nl} \epsilon_{lm} \right) \left(\text{tr}[e_{mn}^a e_{nl}^b e_{lm}^c] + \text{tr}[e_{mn}^a e_{nl}^c e_{lm}^b]^* \right) \right). \quad (\text{S64})$$

Identifying the real and imaginary parts of $\text{tr}[e_{mn}^a e_{nl}^b e_{lm}^c]$, we finally obtain

$$E = \int_{\mathbf{k}} \left(- \sum_{(l,m,n)} \left(w^{(nm)} \epsilon_{nm} (\epsilon_{nl} - \epsilon_{lm}) - u^{(mn)l} \epsilon_{mn} \epsilon_{nl} \epsilon_{lm} \right) \text{Im} \text{tr}[e_{mn}^a e_{nl}^b e_{lm}^c] \right. \\ \left. + i \sum_{(l,m,n)} \left(w^{[nm]} \epsilon_{nm} (\epsilon_{nl} - \epsilon_{lm}) - u^{[mn]l} \epsilon_{mn} \epsilon_{nl} \epsilon_{lm} \right) \text{Re} \text{tr}[e_{mn}^a e_{nl}^b e_{lm}^c] \right). \quad (\text{S65})$$

C. How to perform the Γ expansion

Now that we have collected the coefficient in front of each geometric contribution, we describe the way the Γ expansion mentioned in the main text is done. Indeed, the functions in Eqs. (S47), (S52), (S56), (S58), (S65) are in general complicated functions of the band energies and Γ . As an example, the coefficient of trivial geometry is given by

$$\frac{3E_n^3\Gamma + 5E_n\Gamma^3 + 3E_n^4 \arctan\left(\frac{E_n}{\Gamma}\right) + 6E_n^2\Gamma^2 \arctan\left(\frac{E_n}{\Gamma}\right) + 3\Gamma^4 \arctan\left(\frac{E_n}{\Gamma}\right)}{12\pi\Gamma^2(E_n^2 + \Gamma^2)^2}. \quad (\text{S66})$$

Other coefficients are in general more complicated, and depend on the energies of multiple bands. However, it is physically reasonable to assume that Γ is smaller than the bandwidth, and we would like to make use of this fact to “expand” these functions in Γ . Schematically, the previous calculations reduce the conductivity to a sum of terms of the type

$$\propto \int \frac{d^d\mathbf{k}}{(2\pi)^d} f(\Gamma, E_n, E_m, \dots) (\text{quantum geometric quantity}), \quad (\text{S67})$$

where f is one of the coefficients found in the previous subsection, and we explicitly highlighted its Γ dependence. We want to Taylor expand this expression (the result after integration) in Γ around zero by replacing f by a suitable simpler function, to collect the (perturbatively) most significant contributions. As we show now it is, however, incorrect to simply Taylor expand f in Γ .

To illustrate the problem we begin with the simple example of a Lorentzian:

$$f(x, \Gamma) = \frac{\Gamma}{\pi(\Gamma^2 + x^2)}. \quad (\text{S68})$$

A Taylor expansion $\forall x \neq 0$ yields that the first contribution is of order $\mathcal{O}(\Gamma^1)$. However, for $x = 0$ the function reduces to $1/(\pi\Gamma)$, which has a pole in Γ around zero (in other words it is of order $\mathcal{O}(\Gamma^{-1})$). The resolution of this conundrum resides in taking the limit in the *distributional* sense. Indeed, it is a well-known fact that

$$\frac{\Gamma}{\pi(\Gamma^2 + x^2)} \xrightarrow{\Gamma \rightarrow 0} \delta(x) \quad (\text{S69})$$

in the space of distributions. Since we are calculating the conductivity by integrating over momentum space (effectively also integrating over energies ξ_n), this distributional expansion is the appropriate one to expand the final result in orders of Γ .

The coefficients Eqs. (S47), (S52), (S56), (S58), (S65) of the geometric quantities are more complicated than Lorentzians, and a systematic approach is required.

Conveniently, the distributional limit above is a continuous limit of functions in Fourier space. Indeed, the Fourier transform of the Lorentzian above (in x) is given by

$$f(x, \Gamma) \xrightarrow{\mathcal{F}} \widehat{f}(\xi, \Gamma) = \frac{1}{\sqrt{2\pi}} (e^{\Gamma\xi}\theta(-\xi) + e^{-\Gamma\xi}\theta(\xi)). \quad (\text{S70})$$

Now the limit $\Gamma \rightarrow 0$ (or Taylor expansion in Γ) is defined everywhere, and performing the inverse Fourier transform yields

$$\widehat{f}(\xi, \Gamma) \xrightarrow{\Gamma \rightarrow 0} \frac{1}{\sqrt{2\pi}} \xleftarrow{\mathcal{F}^{-1}} \delta(x), \quad (\text{S71})$$

that is, if we perform the inverse Fourier transform of the limit we now recover a Dirac delta function. This is the method we use for the functions appearing in Eq. (S2 B): We

1. Fourier transform in all relevant energies appearing (there can be multiple if multiple bands are involved)
2. Taylor expand in Γ up to order $\mathcal{O}(\Gamma^0)$ (check if this is defined everywhere in Fourier space)
3. perform the inverse Fourier transform back.

For this paper we choose to expand in Γ up to order $\mathcal{O}(\Gamma^0)$, but this can be chosen entirely differently in another context. In particular, there is no constraint to collecting terms of order $\mathcal{O}(\Gamma^1)$ or higher. Clearly we are able to recover a delta distribution from a Lorentzian, but, in general, what types of functions (or distributions) can we recover using this method? First, we require our input functions $f(\Gamma, E_n, E_m, \dots)$ to have a Fourier transform. Note that many functions that don't have a well-defined Fourier transform (like Heaviside's step function) do have a well-defined *distributional* Fourier transform. In our case,

a sufficient definition of being well-defined is that the inverse Fourier transform of the Fourier transform recovers the original function. The second condition is that the Taylor expansion in Γ must be defined everywhere in Fourier space. Effectively, this procedure transforms a complicated function $f(\Gamma, E_n, E_m, \dots)$ into a simpler function $f_s(\Gamma, E_n, E_m, \dots)$ such that the schematic expression Eq. (S67) is expanded:

$$\int \frac{d^d \mathbf{k}}{(2\pi)^d} f(\Gamma, E_n, E_m, \dots)(\text{QG quantity}) = \int \frac{d^d \mathbf{k}}{(2\pi)^d} f_s(\Gamma, E_n, E_m, \dots)(\text{QG quantity}) + \mathcal{O}(\Gamma^1). \quad (\text{S72})$$

As an example, for Eq. (S66) (the explicit form of the coefficient of trivial geometry Eq. (S47)), these steps work out to be

1. $\frac{ie^{\Gamma\xi_n}(\Gamma^2\xi_n^2-3\Gamma\xi_n+3)\theta(-\xi_n)}{12\sqrt{2\pi}\Gamma^2\xi_n} + \frac{ie^{\Gamma(-\xi_n)}(\Gamma^2\xi_n^2+3\Gamma\xi_n+3)\theta(\xi_n)}{12\sqrt{2\pi}\Gamma^2\xi_n},$
2. $-\frac{i(\Gamma^2\xi_n^2-6)}{24\sqrt{2\pi}\Gamma^2\xi_n},$
3. $\frac{1-2\theta(-E_n)}{8\Gamma^2} + \frac{1}{24}\delta'(E_n),$

where ξ_n denotes the Fourier space variable corresponding to E_n . For the other cases, the explicit functions as well as their Fourier transforms become too complicated to show explicitly, but as will be shown in the next section the final results are indeed simple. When the function depends on multiple energies E_n, E_m, \dots , each one needs to be Fourier transformed, introducing Fourier space variables ξ_n, ξ_m, \dots . Explicitly, we perform Fourier transforms using MATHEMATICA [113].

D. Performing the Γ expansion

Having found a procedure for the expansion in Γ , we now apply it to each coefficient of a geometric quantity Eqs. (S47), (S52), (S56), (S58), (S65), keeping terms of order $\mathcal{O}(\Gamma^{-2})$, $\mathcal{O}(\Gamma^{-1})$ and $\mathcal{O}(\Gamma^0)$. The Γ -expanded versions of contributions A–E are denoted by \bar{A} through \bar{E} .

1. Contribution \bar{A} : trivial geometry $\text{tr}[\hat{P}_n]$

As shown in the previous subsection, in the Γ expansion contribution A (shown in Eq. (S47)) is simply

$$\bar{A} = \int_{\mathbf{k}} \sum_n \frac{1-2\theta(-E_n)}{8\Gamma^2} E_n^{abc} \text{tr}[\hat{P}_n] = -\frac{1}{4\Gamma^2} \int_{\mathbf{k}} \sum_n \theta(-E_n) E_n^{abc} \text{tr}[\hat{P}_n]. \quad (\text{S73})$$

We neglected the part proportional to $\delta'(E_n)$, as it is two orders higher in Γ than the first and will not mix with any other geometric quantity later on. The equality follows from the momentum integration over \mathbf{k} , since $\int \frac{d^d \mathbf{k}}{(2\pi)^d} E_n^{abc} = 0$.

2. Contribution \bar{B} : quantum geometric tensors Q_{nm}^{ab} and Q_{nm}^{ac}

In the Γ expansion, contribution B (shown in Eq. (S52)) reduces to

$$\bar{B} = \int_{\mathbf{k}} \left(\sum_{m \neq n} \left(\frac{\delta(E_n)}{E_m} + \frac{1}{2} \delta'(E_n) \right) E_n^c Q_{(nm)}^{ab} + \sum_{m \neq n} \frac{i}{2\Gamma} \delta(E_n) E_n^c Q_{[nm]}^{ab} \right) + (b \leftrightarrow c). \quad (\text{S74})$$

3. Contribution \bar{C} : quantum geometric tensor Q_{nm}^{bc}

In the Γ expansion, contribution C (shown in Eq. (S56)) becomes

$$\bar{C} = \int_{\mathbf{k}} \sum_{m \neq n} \left(-\frac{2\delta(E_n)}{E_m} - \delta'(E_n) \right) E_n^a Q_{(nm)}^{bc}. \quad (\text{S75})$$

4. Contribution \bar{D} : connections $C_{nm}^{b;ac}$, $C_{nm}^{c;ab}$

In the Γ expansion, contribution D (shown in Eq. (S58)) simplifies to

$$\bar{D} = \int_{\mathbf{k}} \sum_{m,n} \frac{1}{4} (\delta(E_m) + \delta(E_n)) \left(C_{(nm)}^{b;ac} + C_{(nm)}^{c;ab} \right) \quad (\text{S76})$$

$$= \int_{\mathbf{k}} \sum_{m,n} \frac{1}{2} \delta(E_n) \left(C_{(nm)}^{b;ac} + C_{(nm)}^{c;ab} \right). \quad (\text{S77})$$

We utilized the n, m symmetry of $\delta(E_m) + \delta(E_n)$ in the last equality.

5. Contribution \bar{E} : to three-band traces $\text{tr}[e_{mn}^a e_{nl}^b e_{lm}^c]$, $\text{tr}[e_{mn}^a e_{nl}^c e_{lm}^b]$

In the Γ expansion of the final contribution, E (shown in Eq. (S65)), only the term proportional to $\text{Im} \text{tr}[e_{mn}^a e_{nl}^b e_{lm}^c]$ survives, and we obtain

$$\bar{E} = \int_{\mathbf{k}} \sum_{(l,m,n)} \left(\frac{\delta(E_n)}{2} - \frac{\delta(E_m)}{2} \right) \text{Im} \text{tr}[e_{mn}^a e_{nl}^b e_{lm}^c]. \quad (\text{S78})$$

Now that the coefficient does not depend on the l band, simplifications are possible. Indeed, explicitly writing out the trace yields

$$\bar{E} = \int_{\mathbf{k}} \sum_{(l,m,n)} \left(\frac{\delta(E_n)}{2} - \frac{\delta(E_m)}{2} \right) \text{Im} \left\{ -i \text{tr}[\hat{P}_m(\partial^a \hat{P}_n) \hat{P}_n(\partial^b \hat{P}_l) \hat{P}_l(\partial^c \hat{P}_m)] \right\}, \quad (\text{S79})$$

which we split into

$$\bar{E} = \int_{\mathbf{k}} \left(- \sum_{(l,m,n)} \frac{\delta(E_n)}{2} \text{Re} \left\{ \text{tr}[\hat{P}_m(\partial^a \hat{P}_n) \hat{P}_n(\partial^b \hat{P}_l) \hat{P}_l(\partial^c \hat{P}_m)] \right\} \right. \quad (\text{S80})$$

$$\left. + \sum_{(l,m,n)} \frac{\delta(E_m)}{2} \text{Re} \left\{ \text{tr}[\hat{P}_m(\partial^a \hat{P}_n) \hat{P}_n(\partial^b \hat{P}_l) \hat{P}_l(\partial^c \hat{P}_m)] \right\} \right). \quad (\text{S81})$$

Now by definition of projectors,

$$\sum_n \hat{P}_n = \mathbb{1} \Rightarrow \sum_n \hat{P}_n^2 = \mathbb{1}. \quad (\text{S82})$$

Applying a derivative yields

$$\sum_n (\partial^a \hat{P}_n) \hat{P}_n = - \sum_n \hat{P}_n (\partial^a \hat{P}_n). \quad (\text{S83})$$

Using this identity to reduce Eq. (S80) yields (remember l, m, n are necessarily all different in this sum)

$$\bar{E} = \int_{\mathbf{k}} \sum_n \frac{\delta(E_n)}{2} \text{Re} \left\{ \sum_{m \neq n} \text{tr}[\hat{P}_m(\partial^a \hat{P}_n) \hat{P}_n(\partial^b \hat{P}_n)(\partial^c \hat{P}_m)] \right\} \quad (\text{S84})$$

$$- \int_{\mathbf{k}} \sum_{m \neq n} \frac{\delta(E_m)}{2} \text{Re} \left\{ \sum_n \text{tr}[\hat{P}_m(\partial^a \hat{P}_n) \hat{P}_n(\partial^b \hat{P}_n)(\partial^c \hat{P}_m)] \right\}, \quad (\text{S85})$$

which, since $\hat{P}_m(\partial^a \hat{P}_n) \hat{P}_n = \hat{P}_m(\partial^a \hat{P}_n)$ for $m \neq n$, reduces to

$$\bar{E} = \int_{\mathbf{k}} \left(\sum_{n \neq m} \frac{\delta(E_n)}{2} \text{Re} \left\{ \text{tr}[\hat{P}_m(\partial^a \hat{P}_n)(\partial^b \hat{P}_n)(\partial^c \hat{P}_m)] \right\} - \sum_{n \neq m} \frac{\delta(E_m)}{2} \text{Re} \left\{ \text{tr}[\hat{P}_m(\partial^a \hat{P}_n)(\partial^b \hat{P}_n)(\partial^c \hat{P}_m)] \right\} \right). \quad (\text{S86})$$

We now relabel the second sum and combine both parts:

$$\bar{E} = \int_{\mathbf{k}} \sum_{n \neq m} \frac{\delta(E_n)}{2} \operatorname{Re} \left\{ \operatorname{tr}[\hat{P}_m(\partial^a \hat{P}_n)(\partial^b \hat{P}_n)(\partial^c \hat{P}_m)] - \operatorname{tr}[\hat{P}_n(\partial^a \hat{P}_m)(\partial^b \hat{P}_m)(\partial^c \hat{P}_n)] \right\}. \quad (\text{S87})$$

Now $\operatorname{Re} \left\{ \operatorname{tr}[\hat{P}_m(\partial^a \hat{P}_n)(\partial^b \hat{P}_n)(\partial^c \hat{P}_m)] \right\} = \operatorname{Re} \left\{ \operatorname{tr}[\hat{P}_m(\partial^a \hat{P}_n)(\partial^b \hat{P}_n)(\partial^c \hat{P}_m)]^\dagger \right\}$, which we use to transform the first trace:

$$\begin{aligned} \bar{E} &= \int_{\mathbf{k}} \sum_{n \neq m} \frac{\delta(E_n)}{2} \operatorname{Re} \left\{ \operatorname{tr}[(\partial^c \hat{P}_m)(\partial^b \hat{P}_n)(\partial^a \hat{P}_n) \hat{P}_m] - \operatorname{tr}[\hat{P}_n(\partial^a \hat{P}_m)(\partial^b \hat{P}_m)(\partial^c \hat{P}_n)] \right\} \\ &= - \int_{\mathbf{k}} \sum_{n \neq m} \frac{\delta(E_n)}{2} \operatorname{Re} \left\{ \operatorname{tr}[\hat{P}_n(\partial^a \hat{P}_m)(\partial^c \hat{P}_m)(\partial^b \hat{P}_n)] + \operatorname{tr}[\hat{P}_n(\partial^a \hat{P}_m)(\partial^b \hat{P}_m)(\partial^c \hat{P}_n)] \right\}. \end{aligned} \quad (\text{S88})$$

It is proven in Eq. (33) of Ref. [48] that

$$\sum_{m \neq n} C_{mn}^{a;bc} = -Q_n^{b;ac} + \operatorname{tr} \left[\hat{P}_n \left(\sum_{m \neq n} (\partial^b \hat{P}_m)(\partial^a \hat{P}_m) \right) (\partial^c \hat{P}_n) \right], \quad (\text{S89})$$

where $Q_n^{a;bc}$ is the skewness tensor Eq. (S12).

Using this equation and $\operatorname{Re} C_{nm}^{a;bc} = C_{(nm)}^{a;bc}$, the contribution finally simplifies to

$$\bar{E} = - \int_{\mathbf{k}} \left(\sum_{n \neq m} \frac{\delta(E_n)}{2} C_{(nm)}^{c;ab} + \sum_{n \neq m} \frac{\delta(E_n)}{2} C_{(nm)}^{b;ac} + \sum_n \delta(E_n) \operatorname{Re} Q_n^{a;bc} \right). \quad (\text{S90})$$

Interestingly, these connections exactly cancel with the connections explicitly obtained before in Eq. (S76).

E. Combining all contributions

We may now combine all previously isolated contributions \bar{A} through \bar{E} , and use integration by parts and quantum geometric identities to simplify the total result. The starting point is the sum of all results of the previous section, given by

$$\sigma^{a;bc} = \frac{e^3}{\hbar} \int \frac{d^d \mathbf{k}}{(2\pi)^d} \left(- \sum_n \theta(-E_n) \frac{1}{4\Gamma^2} E_n^{abc} \operatorname{tr}[\hat{P}_n] \right) \quad (\text{S91})$$

$$+ \sum_{m \neq n} \left(-\frac{2\delta(E_n)}{E_m} - \delta'(E_n) \right) E_n^a Q_{(nm)}^{bc} \quad (\text{S92})$$

$$+ \sum_{m \neq n} \left(\frac{\delta(E_n)}{E_m} + \frac{1}{2} \delta'(E_n) \right) E_n^c Q_{(nm)}^{ab} + \sum_{m \neq n} \frac{i}{2\Gamma} \delta(E_n) E_n^c Q_{[nm]}^{ab} \quad (\text{S93})$$

$$+ \sum_{m \neq n} \left(\frac{\delta(E_n)}{E_m} + \frac{1}{2} \delta'(E_n) \right) E_n^b Q_{(nm)}^{ac} + \sum_{m \neq n} \frac{i}{2\Gamma} \delta(E_n) E_n^b Q_{[nm]}^{ac} \quad (\text{S94})$$

$$- \sum_n \delta(E_n) \operatorname{Re} Q_n^{a;bc} \Big). \quad (\text{S95})$$

Where possible, we will use the factor of E_n^a to perform integration by parts since $\delta'(E_n) E_n^a = \partial_a \delta(E_n)$. Symmetric and antisymmetric parts are identified as real and imaginary, respectively. We begin by splitting up sums to simplify contributions

individually

$$\sigma^{a;bc} = \frac{e^3}{\hbar} \int \frac{d^d \mathbf{k}}{(2\pi)^d} \left(- \sum_n \theta(-E_n) \frac{1}{4\Gamma^2} E_n^{abc} \text{tr}[\hat{P}_n] \right. \quad (\text{S96})$$

$$- \sum_{m \neq n} \frac{2\delta(E_n)}{E_m} E_n^a \text{Re} Q_{nm}^{bc} - \sum_{m \neq n} \delta'(E_n) E_n^a \text{Re} Q_{nm}^{bc} \quad (\text{S97})$$

$$+ \sum_{m \neq n} \frac{\delta(E_n)}{E_m} E_n^c \text{Re} Q_{nm}^{ab} + \sum_{m \neq n} \frac{1}{2} \delta'(E_n) E_n^c \text{Re} Q_{nm}^{ab} - \sum_{m \neq n} \frac{1}{2\Gamma} \delta(E_n) E_n^c \text{Im} Q_{nm}^{ab} \quad (\text{S98})$$

$$+ \sum_{m \neq n} \frac{\delta(E_n)}{E_m} E_n^b \text{Re} Q_{nm}^{ac} + \sum_{m \neq n} \frac{1}{2} \delta'(E_n) E_n^b \text{Re} Q_{nm}^{ac} - \sum_{m \neq n} \frac{1}{2\Gamma} \delta(E_n) E_n^b \text{Im} Q_{nm}^{ac} \quad (\text{S99})$$

$$\left. - \sum_n \delta(E_n) \text{Re} Q_n^{a;bc} \right). \quad (\text{S100})$$

We begin integrating by parts using E_n^a as an internal derivative, and additionally use $\frac{\delta(E_n)}{E_m} = \frac{\delta(E_n)}{E_m - E_n}$:

$$\sigma^{a;bc} = \frac{e^3}{\hbar} \int \frac{d^d \mathbf{k}}{(2\pi)^d} \left(- \sum_n \theta(-E_n) \frac{1}{4\Gamma^2} E_n^{abc} \text{tr}[\hat{P}_n] \right. \quad (\text{S101})$$

$$- \sum_{m \neq n} 2\delta(E_n) E_n^a \frac{\text{Re} Q_{nm}^{bc}}{E_m - E_n} + \sum_{m \neq n} \delta(E_n) \text{Re} \partial^a Q_{nm}^{bc} \quad (\text{S102})$$

$$+ \sum_{m \neq n} \delta(E_n) E_n^c \frac{\text{Re} Q_{nm}^{ab}}{E_m - E_n} - \sum_{m \neq n} \frac{1}{2} \delta(E_n) \text{Re} \partial^c Q_{nm}^{ab} - \sum_{m \neq n} \frac{1}{2\Gamma} \delta(E_n) E_n^c \text{Im} Q_{nm}^{ab} \quad (\text{S103})$$

$$+ \sum_{m \neq n} \delta(E_n) E_n^b \frac{\text{Re} Q_{nm}^{ac}}{E_m - E_n} - \sum_{m \neq n} \frac{1}{2} \delta(E_n) \text{Re} \partial^b Q_{nm}^{ac} - \sum_{m \neq n} \frac{1}{2\Gamma} \delta(E_n) E_n^b \text{Im} Q_{nm}^{ac} \quad (\text{S104})$$

$$\left. - \sum_n \delta(E_n) \text{Re} Q_n^{a;bc} \right). \quad (\text{S105})$$

Now there are convenient relations between the single-band and multiband QGTs (defined in Eqs. (S9), (S10))

$$\sum_{m \neq n} \text{Re} Q_{nm}^{ab} = \sum_{m \neq n} \text{Re} (Q_{mn}^{ab})^\dagger = -\text{Re} Q_n^{ab}, \quad (\text{S106})$$

$$\sum_{m \neq n} \text{Im} Q_{nm}^{ab} = \sum_{m \neq n} \text{Im} (Q_{mn}^{ab})^\dagger = \text{Im} Q_n^{ab}. \quad (\text{S107})$$

The sums are only over m in this case. We may then transform the conductivity to

$$\sigma^{a;bc} = \frac{e^3}{\hbar} \int \frac{d^d \mathbf{k}}{(2\pi)^d} \left(- \sum_n \theta(-E_n) \frac{1}{4\Gamma^2} E_n^{abc} \text{tr}[\hat{P}_n] \right. \quad (\text{S108})$$

$$- \sum_{m \neq n} 2\delta(E_n) E_n^a \frac{\text{Re} Q_{mn}^{bc}}{E_m - E_n} - \sum_{m \neq n} \delta(E_n) \text{Re} \partial^a Q_n^{bc} \quad (\text{S109})$$

$$+ \sum_{m \neq n} \delta(E_n) E_n^c \frac{\text{Re} Q_{mn}^{ab}}{E_m - E_n} + \sum_n \frac{1}{2} \delta(E_n) \text{Re} \partial^c Q_n^{ab} - \sum_n \frac{1}{2\Gamma} \delta(E_n) E_n^c \text{Im} Q_n^{ab} \quad (\text{S110})$$

$$+ \sum_{m \neq n} \delta(E_n) E_n^b \frac{\text{Re} Q_{mn}^{ac}}{E_m - E_n} + \sum_n \frac{1}{2} \delta(E_n) \text{Re} \partial^b Q_n^{ac} - \sum_n \frac{1}{2\Gamma} \delta(E_n) E_n^b \text{Im} Q_n^{ac} \quad (\text{S111})$$

$$\left. - \sum_n \delta(E_n) \text{Re} Q_n^{a;bc} \right). \quad (\text{S112})$$

Using the identity

$$\partial^a Q_n^{bc} = (Q_n^{c;ab})^\dagger + Q_n^{b;ac} \Rightarrow \text{Re } \partial^a Q_n^{bc} = \text{Re } Q_n^{c;ab} + \text{Re } Q_n^{b;ac} \quad (\text{S113})$$

leads to the following relation, reminiscent of Christoffel symbols in terms of the metric:

$$Q_n^{a;bc} = \frac{1}{2} (\partial^b Q_n^{ac} + \partial^c Q_n^{ab} - \partial^a Q_n^{bc}) . \quad (\text{S114})$$

We insert this relation for the last term:

$$\sigma^{a;bc} = \frac{e^3}{\hbar} \int \frac{d^d \mathbf{k}}{(2\pi)^d} \left(- \sum_n \theta(-E_n) \frac{1}{4\Gamma^2} E_n^{abc} \text{tr}[\hat{P}_n] \right. \quad (\text{S115})$$

$$\left. - \sum_{m \neq n} 2\delta(E_n) E_n^a \frac{\text{Re } Q_{mn}^{bc}}{E_m - E_n} \right. \quad (\text{S116})$$

$$\left. + \sum_{m \neq n} \delta(E_n) E_n^c \frac{\text{Re } Q_{mn}^{ab}}{E_m - E_n} - \sum_n \frac{1}{2\Gamma} \delta(E_n) E_n^c \text{Im } Q_n^{ab} \right. \quad (\text{S117})$$

$$\left. + \sum_{m \neq n} \delta(E_n) E_n^b \frac{\text{Re } Q_{mn}^{ac}}{E_m - E_n} - \sum_n \frac{1}{2\Gamma} \delta(E_n) E_n^b \text{Im } Q_n^{ac} \right. \quad (\text{S118})$$

$$\left. - \sum_n \frac{1}{2} \delta(E_n) \text{Re } \partial^a Q_n^{bc} \right) . \quad (\text{S119})$$

As is apparent, the first term (the NLD contribution) is completely symmetric in a, b, c . Accordingly, it is classified as an Ohmic (as opposed to Hall, i.e. non-dissipative) contribution according to [71]. We may now reorder terms and integrate the first term by parts to isolate a Fermi surface delta function everywhere:

$$\sigma^{a;bc} = \frac{e^3}{\hbar} \int \frac{d^d \mathbf{k}}{(2\pi)^d} \sum_n \delta(E_n) \left(- \frac{1}{(2\Gamma)^2} E_n^a E_n^{bc} \text{tr}[\hat{P}_n] \right. \quad (\text{S120})$$

$$\left. - \frac{1}{2\Gamma} (E_n^c \text{Im } Q_n^{ab} + E_n^b \text{Im } Q_n^{ac}) \right. \quad (\text{S121})$$

$$\left. - \sum_{m \neq n} \left(2E_n^a \frac{\text{Re } Q_{mn}^{bc}}{E_m - E_n} - E_n^c \frac{\text{Re } Q_{mn}^{ab}}{E_m - E_n} - E_n^b \frac{\text{Re } Q_{mn}^{ac}}{E_m - E_n} \right) \right. \quad (\text{S122})$$

$$\left. - \frac{1}{2} \text{Re } \partial^a Q_n^{bc} \right) . \quad (\text{S123})$$

Using the decomposition of Q_n^{ab} into the familiar quantum metric and Berry curvature

$$Q_n^{ab} = g_n^{ab} - \frac{i}{2} \Omega_n^{ab} , \quad (\text{S124})$$

as well as the (symmetric) two-state metric $\text{Re } Q_{mn}^{ab} = g_{mn}^{ab}$, the conductivity is finally given by

$$\sigma^{a;bc} = \frac{e^3}{\hbar} \int \frac{d^d \mathbf{k}}{(2\pi)^d} \sum_n \delta(E_n) \left(- \frac{1}{(2\Gamma)^2} E_n^a E_n^{bc} \text{tr}[\hat{P}_n] \right. \quad (\text{S125})$$

$$\left. + \frac{1}{4\Gamma} (E_n^c \Omega_n^{ab} + E_n^b \Omega_n^{ac}) \right. \quad (\text{S126})$$

$$\left. - \sum_{m \neq n} \left(2E_n^a \frac{g_{mn}^{bc}}{E_m - E_n} - E_n^c \frac{g_{mn}^{ab}}{E_m - E_n} - E_n^b \frac{g_{mn}^{ac}}{E_m - E_n} \right) \right. \quad (\text{S127})$$

$$\left. - \frac{1}{2} \partial^a g_n^{bc} \right) . \quad (\text{S128})$$

Setting $b = c$, this expression yields the NLD, BCD, interQMD, and intraQMD contributions in the main text. The third line is the interQMD term, found with varying coefficients throughout the literature [31, 32, 56, 70], depending on the approach used and how the scattering is introduced (see Sec. S1). In Sec. S6, we discuss what would have changed if Γ had been band-dependent, and whether such an approach is consistent.

S3. SYMMETRY DECOMPOSITION OF THE NONLINEAR CONDUCTIVITY TENSOR

A. Symmetry transformation of band projectors and quantum geometric invariants

A Bloch Hamiltonian $\hat{H}(\mathbf{k})$ is symmetric under a transformation \mathcal{U} if

$$\mathcal{U}^\dagger \hat{H}(D_U \mathbf{k}) \mathcal{U} = \hat{H}(\mathbf{k}). \quad (\text{S129})$$

Here, D_U is a representation of \mathcal{U} in momentum space, which belongs to $O(3)$. Importantly, \mathcal{U} may be either unitary or antiunitary. We assume that \mathcal{U} is \mathbf{k} -independent, up to a possible \mathbf{k} -dependent overall phase. For a lattice Hamiltonian, affine symmetries (consisting of a linear part and a translation) and time-reversal \mathcal{T} can always be represented in a \mathbf{k} -independent way for an adequate Fourier basis choice [114, 115]. Indeed, in the so-called convention I Bloch-like basis functions are defined by [115]

$$|\chi_j^{\mathbf{k}}\rangle = \sum_{\mathbf{R}} e^{i\mathbf{k}\cdot(\mathbf{R}+\boldsymbol{\tau}_j)} |\phi_{\mathbf{R}j}\rangle, \quad (\text{S130})$$

where \mathbf{R} is a lattice vector which specifies the unit cell, and the index j runs over the orbitals, located at $\boldsymbol{\tau}_j$, in the cell. The wavefunction of the tight binding orbital j in the unit cell located at \mathbf{R} is denoted by $|\phi_{\mathbf{R}j}\rangle$. Affine symmetries and \mathcal{T} can then be represented in a \mathbf{k} -independent way up to a \mathbf{k} -dependent phase [114]. These symmetries suffice to generate all magnetic space groups. Furthermore, only this Fourier convention is consistent with coupling to the electromagnetic potential \mathbf{A} via [64]

$$\hat{H}(\mathbf{k}) \rightarrow \hat{H}(\mathbf{k} - q\mathbf{A}). \quad (\text{S131})$$

If $|\psi_n(\mathbf{k})\rangle$ is an eigenstate of $\hat{H}(\mathbf{k})$, we see from Eq. (S129) that

$$\hat{H}(D_U \mathbf{k}) \mathcal{U} |\psi_n(\mathbf{k})\rangle = \mathcal{U} \hat{H}(\mathbf{k}) |\psi_n(\mathbf{k})\rangle = E_n \mathcal{U} |\psi_n(\mathbf{k})\rangle. \quad (\text{S132})$$

Thus, we find

$$|\psi_n(D_U \mathbf{k})\rangle = \mathcal{U} |\psi_n(\mathbf{k})\rangle, \quad (\text{S133})$$

up to gauge choice of eigenbasis. This implies that the projectors transform as

$$\hat{P}_n(D_U \mathbf{k}) = |\psi_n(D_U \mathbf{k})\rangle \langle \psi_n(D_U \mathbf{k})| = \mathcal{U} \hat{P}_n(\mathbf{k}) \mathcal{U}^\dagger. \quad (\text{S134})$$

Note that any \mathbf{k} -dependent overall phase in \mathcal{U} cancels in the projector, so that \mathcal{U} can be assumed to be momentum independent without loss of generality. The transformation of the band projectors under symmetries Eq. (S134) allows us to deduce transformation rules for quantum geometric invariants. We illustrate this for the multiband QGT Eq. (S10)

$$Q_{mn}^{ab}(\mathbf{k}) = \text{tr} \left[\hat{P}_n(\mathbf{k}) [(\partial^a \hat{P}_m)(\mathbf{k})] [(\partial^b \hat{P}_n)(\mathbf{k})] \right]. \quad (\text{S135})$$

Its real part is the two-state quantum metric g_{nm}^{ab} defined in the main text, see Eq. (5c). We start by considering a unitary \mathcal{U} . We evaluate it at $D_U \mathbf{k}$ leading to

$$Q_{mn}^{ab}(D_U \mathbf{k}) = \text{tr} \left[\hat{P}_n(D_U \mathbf{k}) [(\partial^a \hat{P}_m)(D_U \mathbf{k})] [(\partial^b \hat{P}_n)(D_U \mathbf{k})] \right]. \quad (\text{S136})$$

The chain rule implies $\partial^{a'} (\hat{P}_n(D_U \mathbf{k})) = (\partial^b \hat{P}_n)(D_U \mathbf{k}) \partial^{a'} (D_U \mathbf{k})^b = D_U^{ba'} (\partial^b \hat{P}_n)(D_U \mathbf{k}) = (D_U^{-1})^{a'b} (\partial^b \hat{P}_n)(D_U \mathbf{k})$ leading to $(\partial^a \hat{P}_n)(D_U \mathbf{k}) = D_U^{aa'} \partial^{a'} (\hat{P}_n(D_U \mathbf{k}))$, where we sum over repeated indices. Inserting Eq. (S134) leads to

$$Q_{mn}^{ab}(D_U \mathbf{k}) = D_U^{aa'} D_U^{bb'} \text{tr} \left[\hat{P}_n(D_U \mathbf{k}) [\partial^{a'} (\hat{P}_m(D_U \mathbf{k}))] [\partial^{b'} (\hat{P}_n(D_U \mathbf{k}))] \right] \quad (\text{S137})$$

$$= D_U^{aa'} D_U^{bb'} \text{tr} \left[(\mathcal{U} \hat{P}_n(\mathbf{k}) \mathcal{U}^\dagger) [\partial^{a'} (\mathcal{U} \hat{P}_m(\mathbf{k}) \mathcal{U}^\dagger)] [\partial^{b'} (\mathcal{U} \hat{P}_n(\mathbf{k}) \mathcal{U}^\dagger)] \right] \quad (\text{S138})$$

$$= D_U^{aa'} D_U^{bb'} \text{tr} \left[\hat{P}_n(\mathbf{k}) (\partial^{a'} \hat{P}_m(\mathbf{k})) (\partial^{b'} \hat{P}_n(\mathbf{k})) \right] \quad (\text{S139})$$

$$= D_U^{aa'} D_U^{bb'} Q_{mn}^{a'b'}(\mathbf{k}) \quad (\text{unitary transformation}), \quad (\text{S140})$$

using the \mathbf{k} -independence of \mathcal{U} and $\mathcal{U}^\dagger\mathcal{U} = \mathbb{1}$. The multiband QGT thus transforms as a tensor. Any higher-order trace of projectors, i.e., higher-order quantum geometric invariants such as the quantum geometric connection, will also transform as tensors. In particular, $Q_n^{ab} = Q_{nn}^{ab}$ will equally transform in the same way.

If the symmetry transformation \mathcal{U} is antiunitary, we have $\mathcal{U} = \mathcal{D}\mathcal{K}$, where \mathcal{D} is unitary and \mathcal{K} represents complex conjugation. Then $|\psi_n(D_U\mathbf{k})\rangle = \mathcal{D}\mathcal{K}|\psi_n(\mathbf{k})\rangle = \mathcal{D}(|\psi_n(\mathbf{k})\rangle)^*$, leading to

$$\hat{P}_n(D_U\mathbf{k}) = |\psi_n(D_U\mathbf{k})\rangle\langle\psi_n(D_U\mathbf{k})| = \mathcal{D} \left(\hat{P}_n(\mathbf{k}) \right)^* \mathcal{D}^\dagger. \quad (\text{S141})$$

Note that D_U does include the effect of time-reversal on momentum. We obtain

$$Q_{mn}^{ab}(D_U\mathbf{k}) = D_U^{aa'} D_U^{bb'} \left(Q_{mn}^{a'b'}(\mathbf{k}) \right)^* \quad (\text{antiunitary transformation}). \quad (\text{S142})$$

Antiunitary transformations imply that the Berry curvature $\Omega_n^{ab} = -\text{Im} Q_{nn}^{ab}$ yields an additional sign flip, while the two-state quantum metric $g_{nm}^{ab} = \text{Re} Q_{nm}^{ab}$ does not.

B. Symmetry transformation of nonlinear conductivity tensor

The implications of the symmetry transformations given via Eqs. (S140) and (S142) on the conductivity tensor $\sigma^{a;bc}$ are now almost immediate. The band energies are invariant under symmetry transformations: $E_n(D_U\mathbf{k}) = E_n(\mathbf{k})$. Similarly to projectors, the velocity and second derivative of the energy then transform as

$$v^a(D_U\mathbf{k}) = (\partial^a E)(D_U\mathbf{k}) = D_U^{aa'} \partial^{a'} (E(D_U\mathbf{k})) = D_U^{aa'} \partial^{a'} E(\mathbf{k}) = D_U^{aa'} v^{a'}(\mathbf{k}), \quad (\text{S143})$$

$$(\partial^a \partial^b E)(D_U\mathbf{k}) = D_U^{aa'} D_U^{bb'} (\partial^a \partial^b E(\mathbf{k})). \quad (\text{S144})$$

Starting with Eq. (S125) for the conductivity with general indices a, b, c and performing a change of variables $\mathbf{k} \rightarrow D_U\mathbf{k}$, the conductivity transforms as

$$\sigma^{a;bc} = \frac{e^3}{\hbar} \int \frac{d^d\mathbf{k}}{(2\pi)^d} \sum_n \delta(E_n(\mathbf{k}) - \mu) (\sigma_{\text{NLD}}^{a;bc}(\mathbf{k}) + \sigma_{\text{BCD}}^{a;bc}(\mathbf{k}) + \sigma_{\text{interQMD}}^{a;bc}(\mathbf{k}) + \sigma_{\text{intraQMD}}^{a;bc}(\mathbf{k})) \quad (\text{S145})$$

$$= \frac{e^3}{\hbar} \int \frac{d^d\mathbf{k}}{(2\pi)^d} \sum_n \delta(E_n(D_U\mathbf{k}) - \mu) (\sigma_{\text{NLD}}^{a;bc}(D_U\mathbf{k}) + \sigma_{\text{BCD}}^{a;bc}(D_U\mathbf{k}) + \sigma_{\text{interQMD}}^{a;bc}(D_U\mathbf{k}) + \sigma_{\text{intraQMD}}^{a;bc}(D_U\mathbf{k})) \quad (\text{S146})$$

$$= D_U^{aa'} D_U^{bb'} D_U^{cc'} \frac{e^3}{\hbar} \int \frac{d^d\mathbf{k}}{(2\pi)^d} \sum_n \delta(E_n(\mathbf{k}) - \mu) (\sigma_{\text{NLD}}^{a';b'c'}(\mathbf{k}) + \eta \sigma_{\text{BCD}}^{a';b'c'}(\mathbf{k}) + \sigma_{\text{interQMD}}^{a';b'c'}(\mathbf{k}) + \sigma_{\text{intraQMD}}^{a';b'c'}(\mathbf{k})), \quad (\text{S147})$$

where $\eta = 1$ ($\eta = -1$) for unitary (antiunitary) transformations.

The equation above reduces to the constraint

$$\sigma^{a;bc} = D_U^{aa'} D_U^{bb'} D_U^{cc'} \sigma_{\text{NLD}}^{a';b'c'} + \eta D_U^{aa'} D_U^{bb'} D_U^{cc'} \sigma_{\text{BCD}}^{a';b'c'} + D_U^{aa'} D_U^{bb'} D_U^{cc'} \sigma_{\text{interQMD}}^{a';b'c'} + D_U^{aa'} D_U^{bb'} D_U^{cc'} \sigma_{\text{intraQMD}}^{a';b'c'}. \quad (\text{S148})$$

This tensorial equation yields a system of 27 individual equations (one for each of the tensor components).

Additionally, further constraints for each of the contributions appear due to their specific form (see Eq. (S125)). Indeed,

$$\sigma_{\text{NLD}}^{a;bc} = \sigma_{\text{NLD}}^{(a;bc)}, \quad (\text{S149})$$

$$\sigma_{\text{BCD}}^{a;aa} = \sigma_{\text{interQMD}}^{a;aa} = 0. \quad (\text{S150})$$

(...) indicates symmetrization here. Finally, the entire tensor is symmetric in its last two indices: $\sigma^{a;bc} = \sigma^{a;cb}$, which reduces the number of independent components from 27 to 18.

We begin by listing the result of these constraints for a few common symmetries in Table S1. We follow the syntax

$$\left(\begin{array}{ccc} \sigma^{x;xx} & \sigma^{x;yy} & \sigma^{x;zz} \\ \sigma^{y;xx} & \sigma^{y;yy} & \sigma^{y;zz} \\ \sigma^{z;xx} & \sigma^{z;yy} & \sigma^{z;zz} \end{array} \right), \quad (\text{S151})$$

Terms with electric-field direction, such as $\sigma^{x;xy}$, are also constrained. Here, we continue to focus on the experimentally most accessible case $\sigma^{a;bb}$. indicating by a zero that a symmetry prevents a certain conductivity, and maximally reduce the number of independent components of the conductivity tensor appearing.

In magnetic space groups (MSGs), however, multiple symmetries have to be taken into account simultaneously. We do this algorithmically, using data from [116]. A similar treatment was done in Ref. [72] for spin space groups, but with a different formula for the nonlinear conductivity, which changes results. Indeed, as mentioned above, the interQMD contribution is purely transverse, imposing further constraints. For each MSG, we simultaneously impose the constraints enforced by each symmetry to obtain the nonzero tensor components of $\sigma^{a;bc}$ for each of the four contributions. This allows us to sort through all 1651 MSGs, imposing certain conditions, of which we present relevant choices below.

The first three cases are designed to isolate contributions from NLD, inter- and intraQMD together, or intraQMD and NLD alone. In the fourth case, we additionally impose a MSG which enforces a nodal plane [45]. In all cases shown below, the NLD contribution has the same constraints as the intraQMD contribution. Finally, the MAGNDATA database [98, 99] is used to find experimentally verified materials belonging to the obtained MSGs. In general, the database does not provide information as to whether a material is metallic or an insulator (and thus does or does not have an NLHE). Therefore, in this SM we show all materials from the database regardless of whether they are insulating or not. In the following, we indicate by $\sigma_{\dots} \neq 0$ that a certain contribution is not constrained to be zero by magnetic symmetries.

TABLE S1. Observable components of the conductivity tensor $\sigma^{a;bc}$, separated into the 4 components NLD, BCD, interQMD and intraQMD (see S3). We also show the representation D_U of the symmetry used. See Eq. S151 for the definition of matrix components.

Name	D_U	σ_{NLD}	σ_{BCD}	σ_{interQMD}	σ_{intraQMD}
C_2^z	$\begin{pmatrix} -1 & 0 & 0 \\ 0 & -1 & 0 \\ 0 & 0 & 1 \end{pmatrix}$	$\begin{pmatrix} 0 & 0 & 0 \\ 0 & 0 & 0 \\ \sigma^{z;xx} & \sigma^{z;yy} & \sigma^{z;zz} \end{pmatrix}$	$\begin{pmatrix} 0 & 0 & 0 \\ 0 & 0 & 0 \\ \sigma^{z;xx} & \sigma^{z;yy} & 0 \end{pmatrix}$	$\begin{pmatrix} 0 & 0 & 0 \\ 0 & 0 & 0 \\ \sigma^{z;xx} & \sigma^{z;yy} & 0 \end{pmatrix}$	$\begin{pmatrix} 0 & 0 & 0 \\ 0 & 0 & 0 \\ \sigma^{z;xx} & \sigma^{z;yy} & \sigma^{z;zz} \end{pmatrix}$
$C_2^z \mathcal{T}$	$\begin{pmatrix} 1 & 0 & 0 \\ 0 & 1 & 0 \\ 0 & 0 & -1 \end{pmatrix}$	$\begin{pmatrix} \sigma^{x;xx} & \sigma^{x;yy} & \sigma^{x;zz} \\ \sigma^{y;xx} & \sigma^{y;yy} & \sigma^{y;zz} \\ 0 & 0 & 0 \end{pmatrix}$	$\begin{pmatrix} 0 & 0 & 0 \\ 0 & 0 & 0 \\ \sigma^{z;xx} & \sigma^{z;yy} & 0 \end{pmatrix}$	$\begin{pmatrix} 0 & \sigma^{x;yy} & \sigma^{x;zz} \\ \sigma^{y;xx} & 0 & \sigma^{y;zz} \\ 0 & 0 & 0 \end{pmatrix}$	$\begin{pmatrix} \sigma^{x;xx} & \sigma^{x;yy} & \sigma^{x;zz} \\ \sigma^{y;xx} & \sigma^{y;yy} & \sigma^{y;zz} \\ 0 & 0 & 0 \end{pmatrix}$
C_3^z	$\begin{pmatrix} -\frac{1}{2} & -\frac{\sqrt{3}}{2} & 0 \\ \frac{\sqrt{3}}{2} & -\frac{1}{2} & 0 \\ 0 & 0 & 1 \end{pmatrix}$	$\begin{pmatrix} -\sigma^{x;yy} & \sigma^{x;yy} & 0 \\ -\sigma^{y;yy} & \sigma^{y;yy} & 0 \\ \sigma^{z;yy} & \sigma^{z;yy} & \sigma^{z;zz} \end{pmatrix}$	$\begin{pmatrix} 0 & 0 & 0 \\ 0 & 0 & 0 \\ \sigma^{z;yy} & \sigma^{z;yy} & 0 \end{pmatrix}$	$\begin{pmatrix} 0 & 0 & 0 \\ 0 & 0 & 0 \\ \sigma^{z;yy} & \sigma^{z;yy} & 0 \end{pmatrix}$	$\begin{pmatrix} -\sigma^{x;yy} & \sigma^{x;yy} & 0 \\ -\sigma^{y;yy} & \sigma^{y;yy} & 0 \\ \sigma^{z;yy} & \sigma^{z;yy} & \sigma^{z;zz} \end{pmatrix}$
$C_3^z \mathcal{T}$	$\begin{pmatrix} \frac{1}{2} & \frac{\sqrt{3}}{2} & 0 \\ -\frac{\sqrt{3}}{2} & \frac{1}{2} & 0 \\ 0 & 0 & -1 \end{pmatrix}$	$\begin{pmatrix} 0 & 0 & 0 \\ 0 & 0 & 0 \\ 0 & 0 & 0 \end{pmatrix}$	$\begin{pmatrix} 0 & 0 & 0 \\ 0 & 0 & 0 \\ \sigma^{z;yy} & \sigma^{z;yy} & 0 \end{pmatrix}$	$\begin{pmatrix} 0 & 0 & 0 \\ 0 & 0 & 0 \\ 0 & 0 & 0 \end{pmatrix}$	$\begin{pmatrix} 0 & 0 & 0 \\ 0 & 0 & 0 \\ 0 & 0 & 0 \end{pmatrix}$
C_4^z	$\begin{pmatrix} 0 & -1 & 0 \\ 1 & 0 & 0 \\ 0 & 0 & 1 \end{pmatrix}$	$\begin{pmatrix} 0 & 0 & 0 \\ 0 & 0 & 0 \\ \sigma^{z;yy} & \sigma^{z;yy} & \sigma^{z;zz} \end{pmatrix}$	$\begin{pmatrix} 0 & 0 & 0 \\ 0 & 0 & 0 \\ \sigma^{z;yy} & \sigma^{z;yy} & 0 \end{pmatrix}$	$\begin{pmatrix} 0 & 0 & 0 \\ 0 & 0 & 0 \\ \sigma^{z;yy} & \sigma^{z;yy} & 0 \end{pmatrix}$	$\begin{pmatrix} 0 & 0 & 0 \\ 0 & 0 & 0 \\ \sigma^{z;yy} & \sigma^{z;yy} & \sigma^{z;zz} \end{pmatrix}$
$C_4^z \mathcal{T}$	$\begin{pmatrix} 0 & 1 & 0 \\ -1 & 0 & 0 \\ 0 & 0 & -1 \end{pmatrix}$	$\begin{pmatrix} 0 & 0 & 0 \\ 0 & 0 & 0 \\ -\sigma^{z;yy} & \sigma^{z;yy} & 0 \end{pmatrix}$	$\begin{pmatrix} 0 & 0 & 0 \\ 0 & 0 & 0 \\ \sigma^{z;yy} & \sigma^{z;yy} & 0 \end{pmatrix}$	$\begin{pmatrix} 0 & 0 & 0 \\ 0 & 0 & 0 \\ -\sigma^{z;yy} & \sigma^{z;yy} & 0 \end{pmatrix}$	$\begin{pmatrix} 0 & 0 & 0 \\ 0 & 0 & 0 \\ -\sigma^{z;yy} & \sigma^{z;yy} & 0 \end{pmatrix}$
\mathcal{M}_x	$\begin{pmatrix} -1 & 0 & 0 \\ 0 & 1 & 0 \\ 0 & 0 & 1 \end{pmatrix}$	$\begin{pmatrix} 0 & 0 & 0 \\ \sigma^{y;xx} & \sigma^{y;yy} & \sigma^{y;zz} \\ \sigma^{z;xx} & \sigma^{z;yy} & \sigma^{z;zz} \end{pmatrix}$	$\begin{pmatrix} 0 & 0 & 0 \\ \sigma^{y;xx} & 0 & \sigma^{y;zz} \\ \sigma^{z;xx} & \sigma^{z;yy} & 0 \end{pmatrix}$	$\begin{pmatrix} 0 & 0 & 0 \\ \sigma^{y;xx} & 0 & \sigma^{y;zz} \\ \sigma^{z;xx} & \sigma^{z;yy} & 0 \end{pmatrix}$	$\begin{pmatrix} 0 & 0 & 0 \\ \sigma^{y;xx} & \sigma^{y;yy} & \sigma^{y;zz} \\ \sigma^{z;xx} & \sigma^{z;yy} & \sigma^{z;zz} \end{pmatrix}$
$\mathcal{M}_x \mathcal{T}$	$\begin{pmatrix} 1 & 0 & 0 \\ 0 & -1 & 0 \\ 0 & 0 & -1 \end{pmatrix}$	$\begin{pmatrix} \sigma^{x;xx} & \sigma^{x;yy} & \sigma^{x;zz} \\ 0 & 0 & 0 \\ 0 & 0 & 0 \end{pmatrix}$	$\begin{pmatrix} 0 & 0 & 0 \\ \sigma^{y;xx} & 0 & \sigma^{y;zz} \\ \sigma^{z;xx} & \sigma^{z;yy} & 0 \end{pmatrix}$	$\begin{pmatrix} 0 & \sigma^{x;yy} & \sigma^{x;zz} \\ 0 & 0 & 0 \\ 0 & 0 & 0 \end{pmatrix}$	$\begin{pmatrix} \sigma^{x;xx} & \sigma^{x;yy} & \sigma^{x;zz} \\ 0 & 0 & 0 \\ 0 & 0 & 0 \end{pmatrix}$
\mathcal{PT}	$\begin{pmatrix} 1 & 0 & 0 \\ 0 & 1 & 0 \\ 0 & 0 & 1 \end{pmatrix}$	$\begin{pmatrix} \sigma^{x;xx} & \sigma^{x;yy} & \sigma^{x;zz} \\ \sigma^{y;xx} & \sigma^{y;yy} & \sigma^{y;zz} \\ \sigma^{z;xx} & \sigma^{z;yy} & \sigma^{z;zz} \end{pmatrix}$	$\begin{pmatrix} 0 & 0 & 0 \\ 0 & 0 & 0 \\ 0 & 0 & 0 \end{pmatrix}$	$\begin{pmatrix} 0 & \sigma^{x;yy} & \sigma^{x;zz} \\ \sigma^{y;xx} & 0 & \sigma^{y;zz} \\ \sigma^{z;xx} & \sigma^{z;yy} & 0 \end{pmatrix}$	$\begin{pmatrix} \sigma^{x;xx} & \sigma^{x;yy} & \sigma^{x;zz} \\ \sigma^{y;xx} & \sigma^{y;yy} & \sigma^{y;zz} \\ \sigma^{z;xx} & \sigma^{z;yy} & \sigma^{z;zz} \end{pmatrix}$

C. Magnetic space groups with no BCD

We begin by simply imposing that the BCD is zero. To avoid MSGs which have no nonlinear conductivity at all, we also impose a nonzero intraQMD:

$$\sigma_{\text{BCD}} = 0, \quad \sigma_{\text{intraQMD}} \neq 0. \quad (\text{S152})$$

208 MSGs, shown in Table S2, are compatible with this constraint. In all cases the NLD is also nonzero, and in most cases the interQMD is as well (see below). Many materials (175 as of writing) in the MAGNDATA [98, 99] database have phases belonging to one of these MSGs. Some examples are EuTiO_3 , MnTiO_3 , Mn_2Au , MnPS_3 , $\text{Co}_4\text{Nb}_2\text{O}_9$, Ca_2MnO_4 , CuMnAs , MgMnO_3 , EuMnSb_2 , $\text{Fe}_4\text{Nb}_2\text{O}_9$, KFeO_2 , $\text{Co}_4\text{Ta}_2\text{O}_9$, KFeS_2 , MnNb_3S_6 , VNb_3S_6 , MnPd_2 , MnNb_2O_6 , MnTa_2O_6 , SrMnO_3 , ThMn_2 , FeSn_2 , FeGe_2 and CoNb_3S_6 . Recently, the material MnBi_2Te_4 was connected to NLHE contributions beyond the BCD [35, 76]. This material, however, breaks inversion symmetry only in the thin even-layered case [117].

TABLE S2. List of MSGs enforcing the conditions $\sigma_{\text{BCD}} = 0$, and $\sigma_{\text{intraQMD}} \neq 0$ on the nonlinear conductivity.

2.6	10.44	10.45	11.52	11.53	12.60	12.61	13.67	13.68
14.77	14.78	15.87	15.88	16.3	17.9	17.10	18.18	18.19
19.27	20.33	20.34	21.40	21.41	22.47	23.51	24.55	47.251
48.259	49.267	49.268	50.279	50.280	51.291	51.292	51.293	52.307
52.308	52.309	53.323	53.324	53.325	54.339	54.340	54.341	55.355
55.356	56.367	56.368	57.379	57.380	57.381	58.395	58.396	59.407
59.408	60.419	60.420	60.421	61.435	62.443	62.444	62.445	63.459
63.460	63.461	64.471	64.472	64.473	65.483	65.484	66.493	66.494
67.503	67.504	68.513	68.514	69.523	70.529	71.535	72.541	72.542
73.550	74.556	74.557	83.46	83.47	84.54	84.55	85.62	85.63
86.70	86.71	87.78	87.79	88.84	88.85	89.90	89.91	90.98
90.99	91.106	91.107	92.114	92.115	93.122	93.123	94.130	94.131
95.138	95.139	96.146	96.147	97.154	97.155	98.160	98.161	111.253
111.255	112.261	112.263	113.269	113.271	114.277	114.279	121.329	121.331
122.335	122.337	123.341	123.346	124.353	124.358	125.365	125.370	126.377
126.382	127.389	127.394	128.401	128.406	129.413	129.418	130.425	130.430
131.437	131.442	132.449	132.454	133.461	133.466	134.473	134.478	135.485
135.490	136.497	136.502	137.509	137.514	138.521	138.526	139.533	139.538
140.543	140.548	141.553	141.558	142.563	142.568	147.15	148.19	149.21
149.23	150.27	151.29	151.31	152.35	153.37	153.39	154.43	155.47
162.75	162.76	163.81	163.82	164.87	165.93	166.99	167.105	174.133
174.135	175.139	175.140	176.145	176.146	177.153	178.159	179.165	180.171
181.177	182.183	187.212	188.218	189.223	190.229	191.235	192.245	193.255

D. Magnetic space groups with no BCD and no interQMD

To isolate the new intraQMD contribution, one can impose the stronger condition

$$\sigma_{\text{BCD}} = 0, \quad \sigma_{\text{interQMD}} = 0, \quad \sigma_{\text{intraQMD}} \neq 0. \quad (\text{S153})$$

Only the following MSGs are compatible: 149.21, 151.29, 153.37, 162.76, 163.82, 174.133, 175.139, 176.145.

In all cases, $\sigma_{\text{NLD}} = 0$ is not constrained to be zero. The only material candidates from the MAGNDATA database [98, 99] that have phases belonging to one of these MSGs are $\text{U}_{14}\text{Au}_{51}$ and $\text{K}_2\text{Mn}_3(\text{VO}_4)_2\text{CO}_3$.

E. Magnetic space groups with no BCD and no interQMD in a plane

For the intraQMD (and NLD) contributions to be theoretically distinguishable, the previous condition can be relaxed to be true only in a plane:

$$\sigma_{\text{BCD}} = 0 \text{ in } xy \text{ plane,} \quad \sigma_{\text{interQMD}} = 0 \text{ in } xy \text{ plane,} \quad \sigma_{\text{intraQMD}} \neq 0 \text{ in } xy \text{ plane.} \quad (\text{S154})$$

Now the following longer list of MSGs is compatible: 147.15, 148.19, 149.21, 149.23, 151.29, 151.31, 153.37, 153.39, 162.75, 162.76, 163.81, 163.82, 174.133, 175.139, 176.145.

Material candidates from the MAGNDATA database [98, 99] with phases in these MSGs are MnTiO_3 , MnGeO_3 , MgMnO_3 , $\text{U}_{14}\text{Au}_{51}$, Yb_3Pt_4 , $\text{CoTe}_6\text{O}_{13}$, $[\text{Na}(\text{OH}_2)_3]\text{Mn}(\text{NCS})_3$ and $\text{K}_2\text{Mn}_3(\text{VO}_4)_2\text{CO}_3$.

Constraining to the xz or yz plane instead does not yield any new MSGs. $\text{U}_{14}\text{Au}_{51}$ and $\text{K}_2\text{Mn}_3(\text{VO}_4)_2\text{CO}_3$ verify the constraint in all planes.

F. Nodal planes and QMD-driven NLHE

In [45], a list of MSGs that enforce nodal planes is provided. Of these groups, the following enforce $\sigma_{\text{BCD}} = 0$ while being compatible with $\sigma_{\text{intraQMD}} \neq 0$: 147.15, 148.19, 149.21, 149.23, 151.29, 151.31, 153.37, 153.39, 162.75, 162.76, 163.81, 163.82, 174.133, 175.139, 176.145.

All of them also do not constrain σ_{interQMD} . Material candidates from the MAGNDATA database [98, 99] that belong to these MSGs are $\text{Cu}_3\text{Mo}_2\text{O}_9$, $\text{Ca}_2\text{CoSi}_2\text{O}_7$, Nd_5Si_4 , BaCrF_5 , TbFeO_3 , MnNb_3S_6 , $\text{C}_7\text{H}_{14}\text{NFeCl}_4$, $\text{Yb}_2\text{Ge}_2\text{O}_7$, SrMnO_3 , SrMnO_3 , CsNiCl_3 , RbNiCl_3 and CsNiCl_3 .

S4. PARTICLE-HOLE AND \mathcal{CPT} SYMMETRY

In this section, we discuss the implications of particle-hole (PH) \mathcal{C} as well as \mathcal{CPT} symmetry on the contributions to the nonlinear conductivity. Topological semimetals, with band crossings close to the Fermi level, in general, exhibit an approximate PH and/or \mathcal{CPT} symmetry. We discuss below that the nonlinear Hall conductivity of these materials must then be odd in μ with respect to the charge neutrality point, except for the BCD in \mathcal{CPT} symmetric systems, which is even.

A. PH Symmetry

A system has PH symmetry (\mathcal{C}) if the Hamiltonian transforms as

$$\mathcal{C}_U^\dagger H^*(-\mathbf{k}) \mathcal{C}_U = -H(\mathbf{k}), \quad (\text{S155})$$

where \mathcal{C}_U is a unitary operator such that $\mathcal{C} = \mathcal{C}_U \mathcal{K}$, taken to be independent of \mathbf{k} (see S3). Consequently, if $|\psi_n(\mathbf{k})\rangle$ is an eigenstate of $H(\mathbf{k})$ with eigenvalue E_n , $\mathcal{C}_U |\psi_n(\mathbf{k})\rangle$ is an eigenstate of $H^*(-\mathbf{k})$

$$H^*(-\mathbf{k}) \mathcal{C}_U |\psi_n(\mathbf{k})\rangle = -\mathcal{C}_U H |\psi_n(\mathbf{k})\rangle = -E_n \mathcal{C}_U |\psi_n(\mathbf{k})\rangle, \quad (\text{S156})$$

with opposite eigenvalue $E_{-n} := -E_n$. Thus, $H(-\mathbf{k}) (\mathcal{C}_U |\psi_n(\mathbf{k})\rangle)^* = E_{-n} (\mathcal{C}_U |\psi_n(\mathbf{k})\rangle)^*$, and up to gauge $|\psi_{-n}(-\mathbf{k})\rangle = (\mathcal{C}_U |\psi_n(\mathbf{k})\rangle)^*$. It follows that projectors transform as

$$\mathcal{C}_U \hat{P}_n(\mathbf{k}) \mathcal{C}_U^\dagger = \hat{P}_{-n}^*(-\mathbf{k}). \quad (\text{S157})$$

With these properties in hand, we now make the change of variables $\mathbf{k} \rightarrow -\mathbf{k}$ in the equation for conductivity:

$$\begin{aligned} \sigma^{a;bb} &= \frac{e^3}{\hbar} \int \frac{d^d \mathbf{k}}{(2\pi)^d} \sum_n \delta(E_n(\mathbf{k}) - \mu) \left(-\frac{1}{(2\Gamma)^2} \frac{v_n^a(\mathbf{k})}{m_n^{bb}(\mathbf{k})} \text{tr}[\hat{P}_n(\mathbf{k})] + \frac{1}{2\Gamma} v_n^b(\mathbf{k}) \Omega_n^{ab}(\mathbf{k}) \right. \\ &\quad \left. + 2 \sum_{m \neq n} \frac{v_n^b(\mathbf{k}) g_{mn}^{ab}(\mathbf{k}) - v_n^a(\mathbf{k}) g_{mn}^{bb}(\mathbf{k})}{\epsilon_{mn}(\mathbf{k})} - \frac{1}{2} \partial^a g_n^{bb}(\mathbf{k}) \right) \end{aligned} \quad (\text{S158})$$

$$\begin{aligned} &= \frac{e^3}{\hbar} \int \frac{d^d \mathbf{k}}{(2\pi)^d} \sum_n \delta(E_{-n}(\mathbf{k}) - (-\mu)) \left(\frac{1}{(2\Gamma)^2} \frac{v_{-n}^a(\mathbf{k})}{m_{-n}^{bb}(\mathbf{k})} \text{tr}[\hat{P}_{-n}(\mathbf{k})] + \frac{1}{2\Gamma} v_{-n}^b(\mathbf{k}) (\Omega_{-n}^{ab}(\mathbf{k}))^* \right. \\ &\quad \left. + 2 \sum_{m \neq n} \frac{v_{-n}^b(\mathbf{k}) (g_{(-m)(-n)}^{ab}(\mathbf{k}))^* - v_{-n}^a(\mathbf{k}) (g_{(-m)(-n)}^{bb}(\mathbf{k}))^*}{-\epsilon_{(-m)(-n)}(\mathbf{k})} + \frac{1}{2} \partial^a (g_{-n}^{bb}(\mathbf{k}))^* \right). \end{aligned} \quad (\text{S159})$$

We used $v_n^a(-\mathbf{k}) = \partial^a E_n(-\mathbf{k}) = v_{-n}^a(\mathbf{k})$ and $m_n^{bb}(-\mathbf{k}) = -m_{-n}^{bb}(\mathbf{k})$ (the change of variables also applies to $\partial_{\mathbf{k}}$). Now, $g_{mn}(\mathbf{k})$, $g_n(\mathbf{k})$ are real and $\Omega_n^{ab}(\mathbf{k})$ is purely imaginary:

$$\begin{aligned} \sigma^{a;bb} = & \frac{e^3}{\hbar} \int \frac{d^d \mathbf{k}}{(2\pi)^d} \sum_n \delta(E_{-n}(\mathbf{k}) - (-\mu)) \left(\frac{1}{(2\Gamma)^2} \frac{v_{-n}^a(\mathbf{k})}{m_{-n}^{bb}(\mathbf{k})} \text{tr}[\hat{P}_{-n}(\mathbf{k})] - \frac{1}{2\Gamma} v_{-n}^b(\mathbf{k}) \Omega_{-n}^{ab}(\mathbf{k}) \right. \\ & \left. - 2 \sum_{m \neq n} \frac{v_{-n}^b(\mathbf{k}) (g_{(-m)(-n)}^{ab}(\mathbf{k}) - v_{-n}^a(\mathbf{k}) g_{(-m)(-n)}^{bb}(\mathbf{k}))}{\epsilon_{(-m)(-n)}(\mathbf{k})} + \frac{1}{2} \partial^a g_{-n}^{bb}(\mathbf{k}) \right). \end{aligned} \quad (\text{S160})$$

Finally, we relabel the sums by $-n \rightarrow n$, $-m \rightarrow m$ and extract the overall $-$ sign:

$$\begin{aligned} \sigma^{a;bb} = & -\frac{e^3}{\hbar} \int \frac{d^d \mathbf{k}}{(2\pi)^d} \sum_n \delta(E_n(\mathbf{k}) - (-\mu)) \left(-\frac{1}{(2\Gamma)^2} \frac{v_n^a(\mathbf{k})}{m_n^{bb}(\mathbf{k})} \text{tr}[\hat{P}_n(\mathbf{k})] + \frac{1}{2\Gamma} v_n^b(\mathbf{k}) \Omega_n^{ab}(\mathbf{k}) \right. \\ & \left. + 2 \sum_{m \neq n} \frac{v_n^b(\mathbf{k}) (g_{mn}^{ab}(\mathbf{k}) - v_n^a(\mathbf{k}) g_{mn}^{bb}(\mathbf{k}))}{\epsilon_{mn}(\mathbf{k})} - \frac{1}{2} \partial^a g_n^{bb}(\mathbf{k}) \right). \end{aligned} \quad (\text{S161})$$

We have thus effectively proven that with PH symmetry, the conductivity verifies

$$\sigma^{a;bb}(\mu) = -\sigma^{a;bb}(-\mu). \quad (\text{S162})$$

B. \mathcal{CPT} Symmetry

A closely related symmetry is what we refer to as \mathcal{CPT} symmetry (PH symmetry combined with \mathcal{PT}), where the Hamiltonian satisfies

$$\mathcal{S}^\dagger H(-\mathbf{k}) \mathcal{S} = -H(\mathbf{k}), \quad (\text{S163})$$

where \mathcal{S} is a *unitary* operator, as opposed to PH symmetry. The bands can be labeled in the same way, respecting

$$E_n(\mathbf{k}) = -E_{-n}(\mathbf{k}), \quad n \in \{0, \dots, N\}. \quad (\text{S164})$$

Projectors simply transform as

$$\mathcal{S}^\dagger \hat{P}_n(\mathbf{k}) \mathcal{S} = \hat{P}_{-n}(-\mathbf{k}). \quad (\text{S165})$$

The only difference compared to the PH symmetric case is that the BCD contribution now no longer flips sign, i.e. we obtain the relations

$$\sigma_{\text{NLD}}^{a;bb}(\mu) = -\sigma_{\text{NLD}}^{a;bb}(-\mu), \quad (\text{S166})$$

$$\sigma_{\text{BCD}}^{a;bb}(\mu) = \sigma_{\text{BCD}}^{a;bb}(-\mu), \quad (\text{S167})$$

$$\sigma_{\text{interQMD}}^{a;bb}(\mu) = -\sigma_{\text{interQMD}}^{a;bb}(-\mu), \quad (\text{S168})$$

$$\sigma_{\text{intraQMD}}^{a;bb}(\mu) = -\sigma_{\text{intraQMD}}^{a;bb}(-\mu). \quad (\text{S169})$$

S5. ANALYTIC RESULTS FOR LOW-ENERGY MODELS

In this section, we begin by showing how the contributions to the NLHE are calculated analytically in this work. We then present the various low-energy models for which these were obtained, and show plots when those were omitted in the main text.

A. Calculating the NLHE analytically for low-energy models

In this section, we describe how the analytic results for the conductivities were obtained. All low-energy models considered in this work have analytically diagonalizable Hamiltonians, yielding expressions for the energies and band projectors. Throughout this section, we use the 3D Dirac point as an example, the other cases being similar. From analytic expressions of the projectors,

one immediately obtains various quantum geometric quantities. For example, the quantum geometric tensor Q_{12}^{ab} (1, 2 are band indices) is given by

$$Q_{12}^{ab} = \frac{k_y k_z v^4}{2 (v^2 (k_x^2 + k_y^2 + k_z^2) + m^2)^2}. \quad (\text{S170})$$

From such expressions, all 4 contributions NLD, BCD, interQMD, and intraQMD before integration are obtained. For example, including the Dirac delta function and evaluating the sum over all bands, the intraQMD contribution $\sigma_{\text{intraQMD}}(\mathbf{k})$ is

$$\sigma_{\text{intraQMD}}^{y;xx}(\mathbf{k}) = \frac{k_y v^4 (v^2 (-k_x^2 + k_y^2 + k_z^2) + m^2) \delta(k_y t - \mu + \sqrt{m^2 + (k_x^2 + k_y^2 + k_z^2) v^2})}{2 (v^2 (k_x^2 + k_y^2 + k_z^2) + m^2)^3} \quad (\text{S171})$$

$$+ \frac{k_y v^4 (v^2 (-k_x^2 + k_y^2 + k_z^2) + m^2) \delta(-k_y t + \mu + \sqrt{m^2 + (k_x^2 + k_y^2 + k_z^2) v^2})}{2 (v^2 (k_x^2 + k_y^2 + k_z^2) + m^2)^3}. \quad (\text{S172})$$

We now treat the cases $\mu > 0$ and $\mu < 0$ separately, as in each case only one of the Dirac delta functions is nonzero. Assuming for the sake of the argument that $\mu > 0$, we resolve the first delta function by integrating over k_x , using the change of variable formula

$$\delta(g(x)) = \sum_i \frac{\delta(x - x_i)}{|g'(x_i)|}, \quad (\text{S173})$$

where the sum extends over all roots of $g(x)$. A solution for k_x exists as long as

$$-\frac{\sqrt{\mu^2 - k_y^2(v^2 - t^2) - 2k_y\mu t - m^2}}{v} < k_z < \frac{\sqrt{\mu^2 - k_y^2(v^2 - t^2) - 2k_y\mu t - m^2}}{v}, \quad (\text{S174})$$

$$-\frac{-\mu t - \sqrt{m^2 t^2 + (\mu^2 - m^2)v^2}}{v^2 - t^2} < k_y < \frac{\mu(-t) + \sqrt{m^2 t^2 + (\mu^2 - m^2)v^2}}{v^2 - t^2}.$$

By solution, we mean a k_x that is a root of the argument of the delta function. After this k_x integration, the result is

$$\frac{k_y v^3 (k_y^2 (t^2 - 2v^2) - 2k_y \mu t - 2k_z^2 v^2 + \mu^2 - 2m^2)}{(k_y t - \mu)^5 \sqrt{k_y^2 (t - v)(t + v) - 2k_y \mu t - k_z^2 v^2 + \mu^2 - m^2}}. \quad (\text{S175})$$

We now integrate this over k_y, k_z using Eq. (S174) as integration bounds. These integrals are performed using RUBI [118], a package for MATHEMATICA [113] for symbolic integration. Performing these steps for all contributions yields the results shown in the following sections as well as in the main text.

B. NLHE of a 3D tilted Dirac and Weyl point

We begin by showing how the Dirac Hamiltonian defined by Eq. (6) in the main text is derived. Defining a set of mutually anticommuting γ matrices

$$\gamma_1 = \sigma_z \otimes \sigma_x, \quad \gamma_2 = \sigma_0 \otimes \sigma_y, \quad \gamma_3 = \sigma_0 \otimes \sigma_z, \quad \gamma_4 = \sigma_x \otimes \sigma_x, \quad \gamma_5 = \sigma_y \otimes \sigma_x, \quad (\text{S176})$$

together with the identity matrix $\gamma_0 = \sigma_0 \otimes \sigma_0$, we may represent inversion symmetry by $\mathcal{P} = \gamma_3$ and time-reversal by $\mathcal{T} = (-i\sigma_y \otimes \sigma_0)\mathcal{K}$, where \mathcal{K} is the complex conjugation operator. The set of γ matrices above can be expanded by defining

$$\gamma_{ij} = \frac{1}{2i} [\gamma_i, \gamma_j]. \quad (\text{S177})$$

Together, the γ_{ij} and the γ matrices span the space of Hermitian 4×4 matrices. All γ_i are, in fact, \mathcal{PT} symmetric:

$$\mathcal{PT}\gamma_i(\mathcal{PT})^\dagger = \gamma_i. \quad (\text{S178})$$

From this, it follows (by antiunitarity of \mathcal{T}) that the γ_{ij} flip sign under \mathcal{PT} : $\mathcal{PT}\gamma_{ij}(\mathcal{PT})^\dagger = -\gamma_{ij}$. Up to rotations in k_i or γ_i , a \mathcal{PT} symmetric tilted gapped 3D Dirac point must then be given by

$$\hat{H} = tk_y\gamma_0 + k_x\gamma_1 + k_y\gamma_2 + k_z\gamma_3 + m\gamma_5, \quad (\text{S179})$$

which corresponds to Eq. (6) in the main text.

The model also retains PH symmetry (\mathcal{C} , see Sec. S4 A) represented by $\sigma_0 \otimes \sigma_x \mathcal{K}$. This enforces that all conductivities are *odd* functions of μ .

For the nonlinear conductivity to be nonzero, the chemical potential must be outside the gap, which corresponds to the condition $v^2\mu^2 > m^2(v^2 - t^2)$. Within this regime, the analytic results for the Hall conductivities $\sigma^{y;xx} = \sigma^{y;zz}$ are given by

$$\sigma_{\text{NLD}}^{y;xx} = \sigma(\mu) \frac{v^2 \left(\frac{2t\sqrt{m^2(t^2-v^2)+\mu^2v^2}(2m^2t^2+3\mu^2v^2)}{m^2t^2+\mu^2v^2} + \mu(t^2-3v^2) \log \left(\frac{\mu v^2 + t\sqrt{m^2(t^2-v^2)+\mu^2v^2}}{\mu v^2 - t\sqrt{m^2(t^2-v^2)+\mu^2v^2}} \right) \right)}{16\pi^2\Gamma^2t^4}, \quad (\text{S180})$$

$$\sigma_{\text{BCD}}^{y;xx} = 0, \quad (\text{S181})$$

$$\sigma_{\text{interQMD}}^{y;xx} = -\sigma(\mu) \frac{t(m^2(t-v)(t+v) + \mu^2v^2)^{3/2}}{6\pi^2(m^2t^2 + \mu^2v^2)^2}, \quad (\text{S182})$$

$$\sigma_{\text{intraQMD}}^{y;xx} = -\sigma(\mu) \frac{m^2tv^2\sqrt{m^2(t^2-v^2) + \mu^2v^2}(m^2(t^2+2v^2) + \mu^2v^2)}{12\pi^2(m^2t^2 + \mu^2v^2)^3}. \quad (\text{S183})$$

σ is the sign function here.

Now when the mass m is set to 0, the Hamiltonian can be block diagonalized by expressing it in the basis of eigenvectors of the \mathcal{CPT} symmetry. Indeed, in this basis the Hamiltonian is simply

$$\hat{H} = (tk_y\sigma_0 + v(-k_x\sigma_x - k_y\sigma_y + k_z\sigma_z)) \oplus (tk_y\sigma_0 + v(-k_x\sigma_x - k_y\sigma_y - k_z\sigma_z)) + m\gamma_{52}. \quad (\text{S184})$$

An additional change of basis $\hat{H} \rightarrow (\sigma_0 \otimes \sigma_z)^{-1}\hat{H}(\sigma_0 \otimes \sigma_z)$ then yields

$$\hat{H} = (tk_y\sigma_0 + v(k_x\sigma_x + k_y\sigma_y + k_z\sigma_z)) \oplus (tk_y\sigma_0 + v(k_x\sigma_x + k_y\sigma_y - k_z\sigma_z)) + m\gamma_{52}. \quad (\text{S185})$$

The sign preceding k_z in the second block is inconsequential, as it may be removed by sending $k_z \rightarrow -k_z$. Thus, this Hamiltonian describes two decoupled 3D tilted Weyl points when $m = 0$. We conclude that setting $m = 0$ in Eqs. (S180), (S181), (S182) and (S183) yields exactly twice the conductivity of a 3D Weyl point. The contributions to this conductivity are given by

$$\begin{aligned} \sigma_{\text{NLD}}^{y;xx} &= \frac{v^2\mu(3tv + (t^2 - 3v^2)\tanh^{-1}(\frac{t}{v}))}{16\pi^2t^4\Gamma^2}, \\ \sigma_{\text{BCD}}^{y;xx} &= 0, \\ \sigma_{\text{interQMD}}^{y;xx} &= -\frac{t}{12\pi^2v\mu}, \\ \sigma_{\text{intraQMD}}^{y;xx} &= 0. \end{aligned} \quad (\text{S186})$$

The intraQMD contribution to the 3D Dirac point is proportional to the mass and therefore vanishes in this limit. The Weyl point model preserves \mathcal{CPT} symmetry, while particle-hole (\mathcal{C}) and \mathcal{PT} symmetries are individually broken. As demonstrated in Sec. S4 B, this symmetry also enforces $\sigma^{a;bb}(-\mu) = -\sigma^{a;bb}(\mu)$ for all contributions except the BCD (which is zero in this case). Note that the NLD contribution $\sigma_{\text{NLD}}^{y;xx}$ for a nontilted ($t = 0$) 3D Weyl point vanishes. The interQMD contribution, $\sigma_{\text{interQMD}}^{y;xx}$ is proportional to $1/\mu$, and diverges at the band crossing point. We plot the obtained conductivities for the 3D Weyl point in Fig. S1.

C. Gapless limit of the nodal plane

The nodal plane model in the main text, for $m = 0$, recovers a $\mathcal{C}_2\mathcal{T}$ symmetry, forcing all contributions to $\sigma^{z;xx}$ to be zero (see Tab. S1). Analytically, however, the interQMD is not integrable in k_z in this limit, because the inverse band gap factor introduces a pole at $k_z = 0$. Because of this, the k_z integral and the $m \rightarrow 0$ do not commute. This explains why the expression shown for the interQMD does not vanish in the $m \rightarrow 0$ limit.

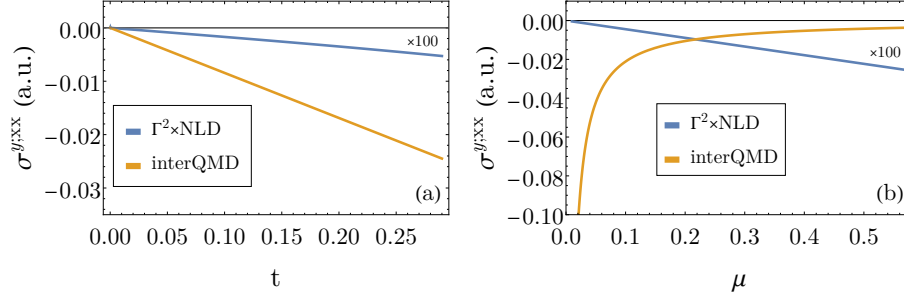


FIG. S1. The dependence of contributions to the NLHE for the tilted 3D Weyl model (See Sec. S5 B and Eq. (S185)) on (a) t and (b) μ . In both plots, $v = 1$. In (a) $\mu = 0.1$, while in (b) $t = 0.5$. The NLD contribution is proportional to $1/\Gamma^2$, depending on the material-dependent scattering rate Γ . We therefore multiply the NLD by Γ^2 to remove this factor, and multiply the result by 100 so that it is visible in the same figure. As we stated in the main text, the intraQMD contribution to the conductivity is zero.

D. NLHE of a 2D Dirac point

We now discuss the 2D case of the tilted Dirac point. Up to coordinate system rotations, the Hamiltonian is given by

$$H = tk_y\sigma_0 + vk_x\sigma_y - vk_y\sigma_x + m\sigma_z, \quad (\text{S187})$$

where t represents the tilt of the Dirac cone, and m the mass gap. The σ_i are Pauli matrices. We assume a type-I Dirac point, where $v > t$. The contribution is only non-zero when the chemical potential μ is above or below the gap, which is equivalent to $v^2\mu^2 > m^2(v^2 - t^2)$. This model was also used by Sodemann and Fu to calculate the Berry curvature dipole [55]. We note that the model described by Eq. (S187) retains a symmetry combining a mirror reflection and time-reversal, $\mathcal{M}_y\mathcal{T}$, represented in total by $\sigma_x\mathcal{K}$ where \mathcal{K} is complex conjugation. Focusing on Hall conductivities, we may apply Eq. (4) to obtain either $\sigma^{y;xx}$ or $\sigma^{x;yy}$ (one also finds nonzero $\sigma^{y;yy}$). Contributions to the former are found to be

$$\begin{aligned} \sigma_{\text{NLD}}^{y;xx} &= \frac{\mu m^2 t^2 (t^2 - 3v^2) + \mu^3 v^2 (t^2 - 2v^2)}{(m^2 t^2 + \mu^2 v^2)^{3/2}} + 2\sigma(\mu)\sqrt{v^2 - t^2}, \\ \sigma_{\text{BCD}}^{y;xx} &= 0, \\ \sigma_{\text{interQMD}}^{y;xx} &= \frac{\mu t v^3 (m^2 (v^2 - t^2) - \mu^2 v^2)}{8\pi (m^2 t^2 + \mu^2 v^2)^{5/2}}, \\ \sigma_{\text{intraQMD}}^{y;xx} &= \frac{\mu t v^3 (m^4 (t^4 - 5v^4) + 2\mu^2 m^2 t^2 v^2 + \mu^4 v^4)}{32\pi (m^2 t^2 + \mu^2 v^2)^{7/2}}, \end{aligned} \quad (\text{S188})$$

where $\sigma(x)$ is the sign function, while in the latter case we recover the BCD as the only non-zero contribution. This separation is consistent with the $\mathcal{M}_y\mathcal{T}$ symmetry, see Sec. S3. The contributions to $\sigma_{\text{NLD}}^{y;xx}$ are in fact non-zero even for $m = 0$, as opposed to $\sigma^{x;yy}$ [55]. These contributions are plotted as a function of m and μ in Fig. S2. The system also has particle-hole (PH) symmetry. As shown in Sec. S4 A this symmetry enforces $\sigma^{a;bb}(-\mu) = -\sigma^{a;bb}(\mu)$, which is indeed verified here.

Consistent with the symmetry analysis summarized in Table I in the main text, depending on the directions measured we either observe exclusively the BCD contribution, or everything except the BCD. Under time-reversal $t \rightarrow -t$ and $m \rightarrow -m$, and equations above make apparent that $\sigma^{y;xx}$ only contributes in time-reversal symmetry broken systems.

E. NLHE of a nodal line

A model closely related to the 2D tilted Dirac point is that of an open nodal line. Indeed, adding a dispersion depending on k_z to the Hamiltonian of the 2D (tilted) Dirac point Eq. (S187) leads to a nodal line on the k_z axis:

$$H = tk_y\sigma_0 + vk_x\sigma_y - vk_y\sigma_x + m\sigma_z + \epsilon(k_z)\sigma_0. \quad (\text{S189})$$

As the simplest possible model, we choose $\epsilon(k_z) = ak_z^2$ with $a > 0$, as using only a linear term results in no contribution to the NL conductivity, because the 2D Dirac point conductivities obtained are odd in μ . Conveniently, this new k_z -dependent term can

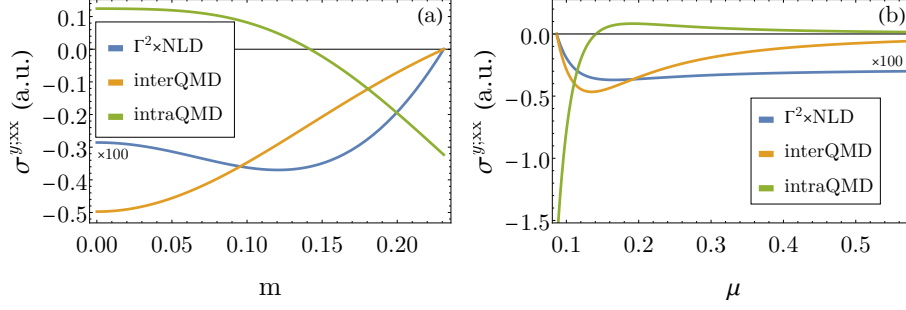


FIG. S2. The dependence of contributions to the NLHE for the 2D tilted Dirac point (see Sec. S5 D) on (a) m and (b) μ . In both plots, $v = 1$, $t = 1/2$. In (a) m is varied while fixing $\mu = 0.2$, while in (b) μ is varied fixing $m = 0.1$. The NLD contribution is proportional to $1/\Gamma^2$, depending on the material-dependent scattering rate Γ . We therefore multiply the NLD by Γ^2 to remove this factor, and multiply the result by 100 so that it is visible in the same figure. For (b) the chemical potential starts at the edge of the gap, $\mu \geq \frac{m}{v} \sqrt{v^2 - t^2}$. The BCD contribution to $\sigma_{\text{BCD}}^{y;xx}$ is 0 in this case. In both cases, the plot is cut off when μ enters the mass gap.

be treated as an effective chemical potential for the 2D Dirac point defined in Eq. (S187), $\mu_{\text{eff}} = \mu - ak_z^2$ [97]. In this way, the integral over k_z can be transformed into an integral over μ_{eff} , with integration bounds such that the chemical potential is outside the gap. For simplicity, we only consider $\mu = 0$. Furthermore, to obtain finite results for the NLD term, the integration in k_z must be limited to a range above and below the nodal line, $k_z \in [-L, L]$. A realistic choice of L is system dependent, so that for clarity we keep L arbitrary and consider only the leading order behavior as $L \rightarrow \infty$. Explicit expressions for the conductivities may then be obtained using elliptic integrals. For simplicity, we only show the leading order contributions in tilt t and gap m around 0 for each term. The resulting conductivities are

$$\begin{aligned} \sigma_{\text{NLD}}^{y;xx} &= \frac{Lt}{64\pi^2\Gamma^2}, & \sigma_{\text{interQMD}}^{y;xx} &= \frac{t}{42\pi^2 a^{1/2} m^{3/2}}, \\ \sigma_{\text{BCD}}^{y;xx} &= 0, & \sigma_{\text{intraQMD}}^{y;xx} &= \frac{t}{264\pi^2 a^{1/2} m^{3/2}}. \end{aligned} \quad (\text{S190})$$

Note that contrary to [97], which applies a formula from [32], we do not obtain any logarithmic divergence in the gap for $\sigma_{\text{interQMD}}^{y;xx}$, but rather a polynomial one. This is dependent on the dispersion $\epsilon(k_z)$ chosen, for which Ref. [97] used $\epsilon(k_z) = k_z + k_z^2$. The contributions are plotted in Fig. S5 E. As for the 2D tilted Dirac point, if we had calculated $\sigma^{x;yy}$ instead, only a BCD contribution would have appeared.

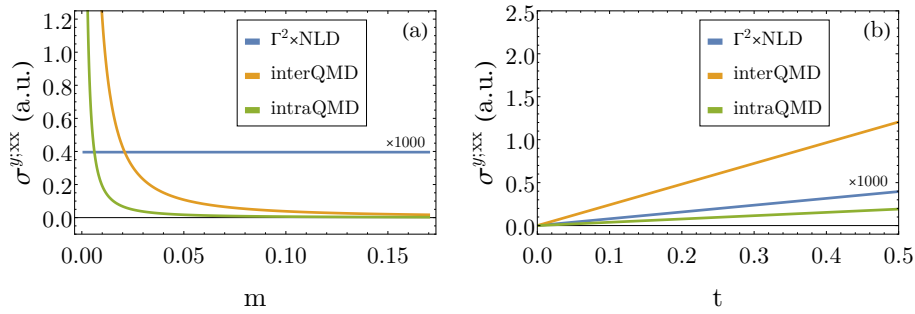


FIG. S3. The dependence of contributions to the NLHE for the tilted nodal line (S189) on (a) m and (b) t . In both plots, $a = 1$. For (a) $v = 1$, $t = 0.5$, while for (b) $v = 1/2$, $m = 0.01$. The NLD contribution is proportional to $1/\Gamma^2$, depending on the material-dependent scattering rate Γ . We therefore multiply the NLD by Γ^2 to remove this factor, and multiply the result by 1000 so that it is visible in the same figure. We also set $L = 0.5$.

As $a \rightarrow 0$ the two QMD terms diverge in an inverse square root law. That the nonlinear Drude term seems unaffected is an artifact of the expansion in t, m , and it equally diverges in an inverse square root law when the full expressions are taken into account. Since at $a = 0$ we recover a 2D (in k_x, k_y) Dirac point for all k_z , it is natural we obtain a divergent conductivity.

S6. A NOTE ON BAND-DEPENDENT SCATTERING RATES

To model a band-dependent scattering rate, in Sec. S2 A we could have introduced a scattering rate Γ that is diagonal in bands, with Green's functions given by

$$G^{R/A}(\epsilon, \mathbf{k}) = \frac{1}{\epsilon - \hat{H}(\mathbf{k}) \pm i\hat{\Gamma}} = \sum_n \frac{\hat{P}_n(\mathbf{k})}{\epsilon - E_n(\mathbf{k}) \pm i\Gamma_n}. \quad (\text{S191})$$

This was also motivated by the attempt to match approaches used in previous semiclassical results, where different lifetimes for on- and off-shell particles were used [5, 69]. The expansion in Γ works almost identically, setting $\Gamma_n = c_n\Gamma$ for some c_n and then expanding in Γ . The final result of this approach is given by

$$\begin{aligned} \sigma^{a;bc} &= \frac{e^3}{\hbar} \int \frac{d^d\mathbf{k}}{(2\pi)^d} \sum_n \delta(E_n) \left(-\frac{1}{(2\Gamma_n)^2} E_n^a E_n^{bc} \text{tr}[\hat{P}_n] \right. \\ &\quad + \frac{1}{4\Gamma_n} (E_n^c \Omega_n^{ab} + E_n^b \Omega_n^{ac}) \\ &\quad - \sum_{m \neq n} \left(\frac{(\Gamma_n + \Gamma_m)^2}{2\Gamma_n^2} E_n^a \frac{g_{mn}^{bc}}{E_m - E_n} - \frac{\Gamma_m}{\Gamma_n} E_n^c \frac{g_{mn}^{ab}}{E_m - E_n} - \frac{\Gamma_m}{\Gamma_n} E_n^b \frac{g_{mn}^{ac}}{E_m - E_n} \right) \\ &\quad \left. + \sum_{m \neq n} \frac{\Gamma_m}{2\Gamma_n} \partial^a g_{mn}^{bc} \right). \end{aligned} \quad (\text{S192})$$

Setting $\Gamma_n = \Gamma$ recovers the main result Eq. (S125). Since n is the on-shell band while m is (where it appears) necessarily off-shell, varying lifetimes could be introduced for each one, inspired by previous work [5, 69]. Indeed, setting the off-shell self-energies to 0, we find a vanishing intraQMD and modified interQMD. Ultimately, however, this approach does not allow matching results found with other methods.

Additionally, a band-dependent scattering rate is in general momentum-dependent in the orbital basis, since it is diagonal in the band basis. Such a self-energy necessarily breaks the Ward identity, and already at the linear level the well-known TKNN formula is not recovered [119]. Indeed, the antisymmetric contribution is found to be

$$\sigma^{[a;b]} = -\frac{e^2}{\hbar} \int \frac{d^d\mathbf{k}}{(2\pi)^d} \sum_n \theta(-E_n) \frac{\Gamma_m}{\Gamma_n} \text{Im} Q_{nm}^{ab}, \quad (\text{S193})$$

which only recovers the TKNN formula when $\Gamma_m = \Gamma_n$. To take a non-constant scattering rate Γ into account consistently, a full perturbative treatment of disorder including vertex corrections (and possibly crossing diagrams) should be done, which we leave to potential future work.

S7. EFFICIENT NUMERICAL EVALUATION OF NLHE

To avoid the numerical implementation of derivatives of projectors, which is computationally costly and potentially unstable, it is useful to have an expression for the NLHE where derivatives only act on the Hamiltonian (but not on the wave functions). These derivatives may be evaluated analytically beforehand, or using automatic differentiation methods. We obtain such expressions by expanding various traces containing only projectors (without derivatives) and derivatives of the Hamiltonian, generalizing the Hellmann-Feynman theorem. To begin, the derivative of the energy can simply be calculated as

$$v_n^a E_n^a = \text{tr}[\hat{P}_n(\partial^a \hat{H})]. \quad (\text{S194})$$

For $m \neq n$, the QGT can be calculated from derivatives of the Hamiltonian as

$$Q_{nm}^{ab} = -\frac{1}{\epsilon_{nm}^2} \text{tr}[\hat{P}_m(\partial^a \hat{H}) \hat{P}_n(\partial^b \hat{H})], \quad (m \neq n). \quad (\text{S195})$$

Both of these identities can easily be verified using Eq. (S13). From the latter, we immediately obtain the two-state quantum metric and the Berry curvature:

$$g_{mn}^{ab} = -\frac{1}{\epsilon_{nm}^2} \text{Re} \text{tr}[\hat{P}_n(\partial^a \hat{H}) \hat{P}_m(\partial^b \hat{H})], \quad (\text{S196})$$

and

$$\Omega_n^{ab} = 2 \operatorname{Im} \sum_{m \neq n} Q_{mn}^{ab} = 2 \operatorname{Im} \sum_{m \neq n} -\frac{1}{\epsilon_{mn}^2} \operatorname{tr}[\hat{P}_n(\partial^a \hat{H}) \hat{P}_m(\partial^b \hat{H})] = 2 \operatorname{Im} \sum_{m \neq n} \frac{1}{\epsilon_{mn}^2} \operatorname{tr}[\hat{P}_m(\partial^a \hat{H}) \hat{P}_n(\partial^b \hat{H})]. \quad (\text{S197})$$

These can be used to calculate the BCD and interQMD terms. A useful identity can be extracted from Eq. (S37) with $n = m$:

$$\operatorname{tr}[\hat{P}_n(\partial^a \hat{H}) \hat{P}_n(\partial^b \partial^c \hat{H})] = E_n^a E_n^{bc} \operatorname{tr}[\hat{P}_n] - E_n^a \sum_{l \neq n} \epsilon_{ln} (Q_{ln}^{bc} + Q_{ln}^{cb}) \quad (\text{S198})$$

$$= E_n^a E_n^{bc} \operatorname{tr}[\hat{P}_n] - 2 \operatorname{tr}[\hat{P}_n(\partial^a \hat{H})] \sum_{l \neq n} \epsilon_{ln} \operatorname{Re} Q_{ln}^{bc}. \quad (\text{S199})$$

Substituting one of the energy derivatives and the QGT by the traces above,

$$\operatorname{tr}[\hat{P}_n(\partial^a \hat{H}) \hat{P}_n(\partial^b \partial^c \hat{H})] = E_n^a E_n^{bc} \operatorname{tr}[\hat{P}_n] + 2 \operatorname{tr}[\hat{P}_n(\partial^a \hat{H})] \sum_{l \neq n} \frac{1}{\epsilon_{ln}} \operatorname{Re} \operatorname{tr}[\hat{P}_l(\partial^b \hat{H}) \hat{P}_n(\partial^c \hat{H})]. \quad (\text{S200})$$

We used that the real part of this trace is symmetric in l, n . Isolating the remaining energy derivatives, we obtain

$$E_n^a E_n^{bc} \operatorname{tr}[\hat{P}_n] = -\operatorname{tr}[\hat{P}_n(\partial^a \hat{H}) \hat{P}_n(\partial^b \partial^c \hat{H})] + 2 \operatorname{tr}[\hat{P}_n(\partial^a \hat{H})] \sum_{l \neq n} \frac{1}{\epsilon_{ln}} \operatorname{Re} \operatorname{tr}[\hat{P}_l(\partial^b \hat{H}) \hat{P}_n(\partial^c \hat{H})]. \quad (\text{S201})$$

This is the NLD term. Note that a sum over all bands is required in this calculation, which increases the numerical effort. However, it must be compared to performing a full diagonalization at multiple points to obtain a finite-difference approximation of this derivative, which is less accurate and possibly more resource-intensive.

Finally, we present a formula for the intraQMD contribution, proportional to the skewness tensor Eq. (S12)

$$\operatorname{Re} \partial^a Q_n^{bb} = 2 \operatorname{Re} Q_n^{b;ab}. \quad (\text{S202})$$

We focused on the most relevant case of $b = c$ as in the main text, and used Eq. (S113). We thus need to express

$$Q_n^{b;ab} = \operatorname{tr}[\hat{P}_n(\partial^b \hat{P}_n)(\partial^a \partial^b \hat{P}_n)] \quad (\text{S203})$$

using derivatives of the Hamiltonian only. This case is the most complicated, but the method used to find a formula can be generalized to more complex cases. To begin, we insert an identity matrix as a sum over projectors:

$$Q_n^{b;ab} = \operatorname{tr}[\hat{P}_n(\partial^b \hat{P}_n)(\partial^a \partial^b \hat{P}_n)] \quad (\text{S204})$$

$$= \sum_m \operatorname{tr}[\hat{P}_n(\partial^b \hat{P}_n) \hat{P}_m(\partial^a \partial^b \hat{P}_n)] \quad (\text{S205})$$

$$= \sum_{m \neq n} \operatorname{tr}[\hat{P}_n(\partial^b \hat{P}_n) \hat{P}_m(\partial^a \partial^b \hat{P}_n)]. \quad (\text{S206})$$

Now a lengthy but straightforward calculation leads to

$$\begin{aligned} \hat{P}_m(\partial^a \partial^b \hat{H}) \hat{P}_n &= \epsilon_{nm}^b \hat{P}_m(\partial^a \hat{P}_n) \hat{P}_n + \epsilon_{nm}^a \hat{P}_m(\partial^b \hat{P}_n) \hat{P}_n - \epsilon_{mn} \hat{P}_m(\partial^a \partial^b \hat{P}_n) \hat{P}_n \\ &+ \sum_{k \neq m, n} \epsilon_{mk} \hat{P}_m(\partial^a \hat{P}_k) \hat{P}_k(\partial^b \hat{P}_n) \hat{P}_n + \sum_{k \neq m, n} \epsilon_{mk} \hat{P}_m(\partial^b \hat{P}_k) \hat{P}_k(\partial^a \hat{P}_n) \hat{P}_n. \end{aligned} \quad (\text{S207})$$

Now for $m \neq n$ we may use Eq. (S13) to insert derivatives of the Hamiltonian, which yields

$$\begin{aligned} \hat{P}_m(\partial^a \partial^b \hat{H}) \hat{P}_n &= -\frac{\epsilon_{nm}^b}{\epsilon_{mn}} \hat{P}_m(\partial^a \hat{H}) \hat{P}_n - \frac{\epsilon_{nm}^a}{\epsilon_{mn}} \hat{P}_m(\partial^b \hat{H}) \hat{P}_n - \epsilon_{mn} \hat{P}_m(\partial^a \partial^b \hat{P}_n) \hat{P}_n \\ &+ \sum_{k \neq m, n} \frac{1}{\epsilon_{mn} \epsilon_{kn}} \hat{P}_m(\partial^a \hat{H}) \hat{P}_k(\partial^b \hat{H}) \hat{P}_n + \sum_{k \neq m, n} \frac{1}{\epsilon_{mn} \epsilon_{kn}} \hat{P}_m(\partial^b \hat{H}) \hat{P}_k(\partial^a \hat{H}) \hat{P}_n. \end{aligned} \quad (\text{S208})$$

We may isolate the second derivative of a projector in the above:

$$\begin{aligned} \hat{P}_m(\partial^a \partial^b \hat{P}_n) \hat{P}_n &= -\frac{1}{\epsilon_{mn}} \hat{P}_m(\partial^a \partial^b \hat{H}) \hat{P}_n - \frac{\epsilon_{nm}^b}{\epsilon_{mn}^2} \hat{P}_m(\partial^a \hat{H}) \hat{P}_n - \frac{\epsilon_{nm}^a}{\epsilon_{mn}^2} \hat{P}_m(\partial^b \hat{H}) \hat{P}_n \\ &+ \sum_{k \neq m, n} \frac{1}{\epsilon_{mn} \epsilon_{kn}} \hat{P}_m(\partial^a \hat{H}) \hat{P}_k(\partial^b \hat{H}) \hat{P}_n + \sum_{k \neq m, n} \frac{1}{\epsilon_{mn} \epsilon_{kn}} \hat{P}_m(\partial^b \hat{H}) \hat{P}_k(\partial^a \hat{H}) \hat{P}_n. \end{aligned} \quad (\text{S209})$$

We now insert this back into $Q_n^{b;ab}$, also using Eq. (S13) again:

$$Q_n^{b;ab} = \sum_{m \neq n} \text{tr}[\hat{P}_n(\partial^b \hat{P}_n) \hat{P}_m(\partial^a \partial^b \hat{P}_n)] \quad (\text{S210})$$

$$= \sum_{m \neq n} \frac{1}{\epsilon_{mn}} \text{tr}[\hat{P}_n(\partial^b \hat{H}) \hat{P}_m(\partial^a \partial^b \hat{P}_n)] \quad (\text{S211})$$

$$= - \sum_{m \neq n} \frac{1}{\epsilon_{mn}^2} \text{tr}[\hat{P}_n(\partial^b \hat{H}) \hat{P}_m(\partial^a \partial^b \hat{H})] - \sum_{m \neq n} \frac{\epsilon_{nm}^b}{\epsilon_{mn}^3} \text{tr}[\hat{P}_n(\partial^b \hat{H}) \hat{P}_m(\partial^a \hat{H})] - \sum_{m \neq n} \frac{\epsilon_{nm}^a}{\epsilon_{mn}^3} \text{tr}[\hat{P}_n(\partial^b \hat{H}) \hat{P}_m(\partial^b \hat{H})] \quad (\text{S212})$$

$$+ \sum_{m \neq n} \sum_{k \neq m, n} \frac{1}{\epsilon_{mn}^2 \epsilon_{kn}} \text{tr}[\hat{P}_n(\partial^b \hat{H}) \hat{P}_m(\partial^a \hat{H}) \hat{P}_k(\partial^b \hat{H})] + \sum_{m \neq n} \sum_{k \neq m, n} \frac{1}{\epsilon_{mn}^2 \epsilon_{kn}} \text{tr}[\hat{P}_n(\partial^b \hat{H}) \hat{P}_m(\partial^b \hat{H}) \hat{P}_k(\partial^a \hat{H})].$$

For Hamiltonians with many bands, the (multiple) sums over band indices may be costly numerically. However, due to the factors of $1/\epsilon_{mn}$ inside the sums, these may be truncated to only include bands which are close by in energy. For general more complicated quantum geometric quantities, one only needs to use formulas such as Eq. (S209) for the required order of derivatives, and compose them to form the tensor as we did here.